

# Measuring and scaling environmentally induced dynamics of solar-induced chlorophyll fluorescence (SIF) from the ground to the aircraft

**Dissertation**

zur Erlangung des Grades

Doktor (oder Doktorin) der Agrarwissenschaften (Dr. agr.)

der Landwirtschaftlichen Fakultät  
der Rheinischen Friedrich-Wilhelms-Universität Bonn

von

***Juan José Quirós Vargas***

aus

*San José, Costa Rica*

Bonn 2023

**Measuring and scaling environmentally induced  
dynamics of solar-induced chlorophyll fluorescence  
(SIF) from the ground to the aircraft**

**Dissertation**

zur Erlangung des Grades

Doktor (oder Doktorin) der Agrarwissenschaften (Dr. agr.)

der Landwirtschaftlichen Fakultät  
der Rheinischen Friedrich-Wilhelms-Universität Bonn

von

***Juan José Quirós Vargas***

aus

*San José, Costa Rica*

Bonn 2023

Referent: *Prof. Dr. Uwe Rascher*  
Korreferent: *Prof. Dr. Jürgen Kusche*

Tag der mündlichen Prüfung: September 12, 2023

Angefertigt mit Genehmigung der Landwirtschaftlichen Fakultät der Universität Bonn

*... “If you wish to improve, be content to appear clueless in extraneous matters; don’t wish to seem knowledgeable” ... (Epictetus).*

---

To my wife and my daughter...

## Abstract

Chlorophyll fluorescence is the absorbed photosynthetically active radiation (PAR) re-emitted as a faint red glow when the photosynthetic apparatus is not able to run photochemistry. This relation that Chlorophyll fluorescence has with photosynthesis makes it an indicator of plant physiological status. After half a century research the emission of solar-induced Chlorophyll fluorescence (SIF) from the canopy can be measured from ground up to satellite scales. Though the first models of ground sensors were created since the 90's, operational platforms for the remote sensing of SIF were only possible in the last decade. The increasing accessibility of SIF information has aroused the interest of ecology, forestry and agriculture scientists to use it as a reference of plants functioning response to varying environmental factors. Such a challenge demands integrated knowledge from diverse disciplines like biology, plant physiology, agronomy, geography and data analytics and specific sub-disciplines depending on the spatiotemporal scale of the plant process being studied. The knowledge network on each specific area and scale is woven by the interconnection of every single study published on the matter. In this regard, the present thesis aims to contribute with new knowledge about the use of SIF data on ground, aerial and satellite scales where a study addressing the spatial relation of airborne-SIF with the plant available water in the root zone (PAW) is considered as the main contribution of this doctoral work.

Further, applications of Chlorophyll fluorescence data for field phenotyping were addressed in a ground-level study, where lower photosynthetic efficiency at noon was found in bean genotypes cultivated in a free-air CO<sub>2</sub> enriched (FACE) experiment. In the same study, a significant relation between SIF and the Chlorophyll fluorescence measured from active sensors is reported. Moreover, the potential use of unmanned aerial vehicles (UAVs) for the retrieval of SIF was discussed in a 'state-of-the-arte' article. Despite its great potential, the UAV-based SIF retrieval is challenged mainly by the complex characterization of the sensor pose and therefore its projected footprint on the ground. A higher progress on the retrieval of SIF has been achieved through airborne-based methods; e.g., with the recent development of the high-Performance airborne Imaging spectrometer (HyPlant), as well as with the improvement of the spectral fitting method (SFM) to retrieve SIF from hyperspectral information. With these novel advances it is possible to monitor SIF in high spatial resolution, enabling e.g. a deeper analysis of

the water stress impact on the crop physiology at large scale. In this regard, the spatial relation between airborne-SIF and PAW was observed to be significant in non-irrigated sugar beet fields, whilst it was not detected in cases where there was enough natural or artificial water supply. In winter wheat, a stronger response of SIF to a low PAW zone was observed when compared with temperature- and reflectance-based information. Besides, in order to provide initial understandings about how the relation of SIF with the soil moisture may behave at satellite level, a SIF-soil moisture comparison was done in the context of the gross primary productivity (GPP). It was found that the positive SIF-GPP relation was decoupled in the lower soil moisture areas during a heat wave at European scale. Additionally, a new potential direction for SIF downscaling approaches (based on fractal theory) is introduced.

The contributions of this doctoral work serve to advance our knowledge concerning the use of SIF data for vegetation functioning assessment at multiple scales. This becomes possible when the studies herewith presented are analyzed as a complement with related investigations published nearly in the same time window. Details about the context and methodologies of each study published within the frame of this thesis will be presented in the following pages.

## Kurzfassung

Die Chlorophyllfluoreszenz ist die absorbierte photosynthetisch aktive Strahlung (PAR), die als schwaches rotes Leuchten zurückgegeben wird, wenn der photosynthetische Apparat keine Photochemie betreiben kann. Diese Beziehung zwischen der Chlorophyllfluoreszenz und der Photosynthese macht sie zu einem Indikator für den physiologischen Zustand der Pflanze. Nach einem halben Jahrhundert Forschung kann die Emission der solarinduzierten Chlorophyllfluoreszenz (SIF) aus dem Kronendach vom Boden aus bis hin zu Satelliten gemessen werden. Die zunehmende Zugänglichkeit von SIF-Informationen hat das Interesse von Ökologie-, Forst- und Agrarwissenschaftlern geweckt, sie als Referenz für die Reaktion von Pflanzen auf unterschiedliche Umweltfaktoren zu nutzen. Eine solche Herausforderung erfordert integriertes Wissen aus verschiedenen Disziplinen wie Biologie, Pflanzenphysiologie, Agronomie, Geografie und Datenanalyse sowie aus spezifischen Teildisziplinen, je nach dem räumlichen und zeitlichen Umfang des untersuchten Pflanzenprozesses.

Die Verknüpfung jeder einzelnen veröffentlichten Studie zu diesem Thema, egal auf welchem spezifischen Bereich und Maßstab angewandt, führt zu einem ständig sich erweiterndem Wissensnetzwerk. Hierbei wobei eine Studie, die sich mit der räumlichen Beziehung zwischen luftgestützter SIF und dem pflanzenverfügbaren Wasser in der Wurzelzone (PAW) befasst, als Hauptbeitrag dieser Doktorarbeit angesehen wird.

Darüber hinaus wurden Anwendungen von Chlorophyll-Fluoreszenzdaten für die Phänotypisierung im Feld untersucht. Dabei wurde bei Bohnengenotypen, die in einem Experiment mit CO<sub>2</sub>-Anreicherung unter Freiluftbedingungen (FACE) angebaut wurden, eine geringere photosynthetische Effizienz zur Mittagszeit festgestellt. In derselbigen Studie wurde ein signifikanter Zusammenhang zwischen der SIF und der von aktiven Sensoren gemessenen Chlorophyllfluoreszenz festgestellt. Darüber hinaus wurde der potenzielle Einsatz unbemannter Luftfahrzeuge (UAVs) für die Erfassung von SIF in einem "State-of-the-Art"-Artikel diskutiert. Trotz des großen Potenzials birgt die UAV-basierte SIF-Ermittlung vor allem durch die komplexe Charakterisierung der Sensorposition und des damit verbundenen projizierten Fußabdrucks auf dem Boden Herausforderungen. Ein größerer Fortschritt bei der Ermittlung von SIF wurde durch flugzeuggestützte Methoden erzielt, z. B. durch die jüngste Entwicklung des luftgestützten Hochleistungs-Bildspektrometers (HyPlant) sowie durch die Verbesserung der spektralen Anpassungsmethode (SFM) zur Messung von Hyperspektraldaten. Mit diesen neuen Methoden ist es möglich, SIF in hoher räumlicher Auflösung zu erfassen, was z.B. eine vertiefte Analyse der Auswirkungen von Wasserstress auf die Physiologie der Pflanzen auf regionaler Ebene ermöglicht. In diesem Zusammenhang wurde ein signifikanter räumlicher Zusammenhang zwischen luftgestützter SIF und PAW auf nicht bewässerten Zuckerrübenfeldern beobachtet, während dies in Fällen mit ausreichender natürlicher oder künstlicher Wasserversorgung nicht beobachtet wurde. Bei Winterweizen wurde im Vergleich zu temperatur- und reflexionsbasierten Informationen eine stärkere Reaktion der SIF auf eine niedrige PAW-Zone beobachtet. Um erste Erkenntnisse darüber zu gewinnen, wie sich die Beziehung zwischen SIF und Bodenfeuchte auf Satellitenebene verhalten könnte, wurde außerdem ein Vergleich zwischen SIF und Bodenfeuchte im Zusammenhang mit der Bruttonitrogenproduktivität (GPP) durchgeführt. Dabei wurde festgestellt, dass die positive Beziehung zwischen SIF

und GPP in den Gebieten mit niedrigerer Bodenfeuchte während einer Hitzewelle auf europäischer Ebene entkoppelt wurde. Zusätzlich, eine neue potenzielle Richtung für SIF-Downscaling-Ansätze (Basierend auf der Fraktaltheorie) wird eingeführt.

Die Beiträge dieser Doktorarbeit dienen dazu, unser Wissen über die Verwendung von SIF-Daten für die Bewertung der Vegetationsfunktion auf verschiedenen Ebenen zu erweitern. Dies wird möglich, wenn die hier vorgestellten Studien als Ergänzung zu verwandten Untersuchungen analysiert werden, die fast im gleichen Zeitfenster veröffentlicht wurden. Details über den Kontext und die Methodik der einzelnen Studien, die im Rahmen dieser Arbeit veröffentlicht wurden, werden auf den folgenden Seiten vorgestellt.

## Table of abbreviations

Abbreviation	Meaning
a[CO <sub>2</sub> ]	Ambient concentration of CO <sub>2</sub>
B-H	Before heat wave peak
CFIS	Chlorophyll fluorescence imaging spectrometer
[CO <sub>2</sub> ]	Concentration of carbon dioxide
CSIRO	Commonwealth Scientific and Industrial Research
DEM	Digital elevation models
D-H	During heat wave peak
e[CO <sub>2</sub> ]	Elevated concentration of CO <sub>2</sub>
ET	Evapotranspiration
ETH	Eidgenössische Technische Hochschule Zürich
ETR	Electron transport rate
EUMETSAT	European organization for the exploitation of meteorological satellites
EVI	Enhanced vegetation index
FACE	Free-air concentration [CO <sub>2</sub> ] enrichment
FAO	Food and Agricultural Organization of the United Nations
FLD	Fraunhofer line depth
FLEX	Fluorescence explorer
Flox	Fluorescence box
F <sub>m</sub> '	Maximum fluorescence yield in light
F <sub>m</sub> <sup>o</sup>	Maximum fluorescence yield in dark adapted leaf
F <sub>q</sub> '/F <sub>m</sub> '	Yield of photosystem II (from LIFT)
F <sub>r1</sub> /F <sub>v</sub>	Reoxidation efficiency of Quinone A
F <sub>t</sub>	Fluorescence yield in light
GOME-2	Global ozone monitoring experiment 2
GOSAT	Greenhouse gases observing satellite
GPP	Gross primary productivity
HyPlant	High-performance airborne imaging spectrometer
IBG-2	Institute of bio-geosciences 2
IBIS	High performance imaging spectrometer within the HyPlant
JAXA	Japan aerospace exploration agency
LIDAR	Laser imaging detection and ranging
LIFT	Light-induced fluorescence transient
LST	Land surface temperature
LUE	Light use efficiency
MERIS	Medium resolution imaging spectrometer
MTCI	MERIS terrestrial chlorophyll index
NDVI	Normalized difference vegetation index

NIR	Near-infrared radiation
NIRv	Near infrared reflectance of vegetation
nm	Nanometer
NPQ	Non-photochemical quenching
OCO-2	Orbiting carbon observatory 2
OECD	Organization for economic co-operation and development
O <sub>2</sub>	Oxygen
PAM	Pulse amplitude modulation
PAR	Photosynthetic active radiation
PAW	Plant available water in the root zone
PL	Power law
PQ	Photochemical quenching
PRI	Photochemical reflectance index
PS I & II	Photosystem I & II
QA	Quinone A
RTM	Radiative transfer model
R&D	Research and development
RE	Red edge
RGB	Red-green-blue
SFM	Spectral fitting method
SIF	Solar-induced chlorophyll fluorescence
SIF <sub>Far-red</sub>	Solar-induced chlorophyll fluorescence emitted in the far red spectrum
SIF <sub>red</sub>	Solar-induced chlorophyll fluorescence emitted in the red spectrum
SIF <sub>TOT</sub>	Total Solar-induced chlorophyll fluorescence
SNR	Signal to noise ratio
SSD	Sensor surface distance
TROPOMI	Tropospheric monitoring instrument
UAV	Unmanned aerial vehicle
VI	Vegetation index
VIS	Red, green and blue
WDRVI	Wide dynamic range vegetation index
Y <sub>II</sub>	Photosynthetic efficiency of photosystem II

---

# Table of contents

Abstract.....	IV
Kurzfassung .....	V
Table of abbreviations .....	VIII
1 General Introduction.....	1
1.1 Remote sensing of vegetation .....	2
1.2 Solar-induced chlorophyll fluorescence (SIF).....	7
1.3 Chlorophyll fluorescence assessments at ground scale .....	12
1.4 SIF assessments at unmanned aerial vehicle (UAV) scale .....	15
1.5 SIF assessments at airborne scale.....	19
1.6 SIF assessments at satellite scale.....	22
1.7 The SIF-scaling issue: importance of downscaling.....	27
2 Knowledge gain and outlook .....	31
3 References .....	35
4 Publications related to this thesis.....	46
4.1 First author peer-reviewed articles and book chapter .....	47
4.1.1 First publication [Quiros-Vargas et al., 2020a] .....	48
4.1.2 Second publication [Quiros-Vargas et al., in preparation].....	49
4.1.3 Third publication [Quiros-Vargas et al., 2022] .....	50
4.2 First author conference peer reviewed study (full text) and posters (only abstract) .....	51
4.2.1 Fourth publication, peer reviewed study [Quiros-Vargas et al., 2021] .....	52
4.2.2 Fifth publication, poster [Quiros-Vargas et al., AGU-2020] .....	53
4.2.3 Sixth publication, poster [Quiros-Vargas et al., EGU-2022].....	54
4.2.4 Seventh publication, poster [Quiros-Vargas et al., LPS-2022a] .....	55
4.2.5 Eighth publication, poster [Quiros-Vargas et al., LPS-2022b].....	56
4.2.6 Ninth publication, poster [Quiros-Vargas et al., EARSeL-2022] .....	57
4.2.7 Tenth publication, poster [Quiros-Vargas et al., EMS-2022] .....	58
4.3 Co-authored peer-reviewed articles (only listed) .....	59
4.4 Main not co-authored discussed studies (only listed) .....	59
5 Other publications (since 2019) not directly related to the topic of the thesis (only listed) .....	61
5.1 First author and co-authored articles .....	62
5.2 Co-authored conferences .....	62
6 Additional activities (deliverables, talks, proposals and field campaigns) .....	64

# 1 General Introduction

World's agriculture production has to increase ~50% by 2050 in order to meet the food demand of a population estimated to rise up to 10 billion, according to the Food and Agricultural Organization of the United Nations (FAO, 2018). Solving such a challenge merely through the increase of agriculture areas is unrealistic, since according to the World Resources Institute (WRI, 2018) it would require a cropland expansion by an area nearly twice the size of India. To meet the alarmingly increasing demand for food in the next decades, other practices like reducing food waste (Stangherlin and Barcellos, 2018), better distributing aliments across society (Akkerman et al., 2010), but first of all, improving agricultural production must be employed. For the latest, the use of remote sensing tools plays a key role do to its capability for monitoring vegetation health over large areas in short periods of time (Kogan, 2019). In that sense, the remote sensing of solar-induced chlorophyll fluorescence (SIF; Meroni et al., 2009; Mohammed et al., 2019) has gained great interest in the last years, since SIF is more closely related to plant physiological processes (Porcar-Castell et al., 2021) than reflectance- or thermal-based information (Damm et al., 2018).

Within that context, the global goal of this thesis was to provide new knowledge on the response of plants to varying environmental conditions, by analyzing the dynamics of SIF information from ground to aerial scales. That goal is addressed through ten scientific publications (two articles, one book chapter, one peer-reviewed conference paper, and six conference posters) in which SIF data is used to understand the vegetation response to different environments, specifically to an elevated [CO<sub>2</sub>] (as studied in a ground-level study, and briefly mentioned in an aerial-scale review paper) and varying levels of soil water content (as investigated on airborne- and satellite-scale studies). One additional study on the downscaling (increase of spatial resolution) of SIF data is provided, in which the main goal is to propose a potential new research line that could be consider in future SIF-downscaling approaches. It is worth mentioning that the studies conducted within the frame of this thesis were possible thanks to the cooperation of researchers from at least eight different disciplines (agronomy, biology, mathematics, soil science, plant physiology, geography, informatics and meteorology).

In the following pages the basics of remote sensing of vegetation (subsection 1.1) and SIF (subsection 1.2) are first introduced, since they are the pillars that all publications have in common. In subsections 1.3 to 1.6 the general background (state-of-the-art, research gap and objectives) of each topic developed at specific SIF assessment scales (ground, aerial and satellite) is presented. In subsection 1.7 the general background of the SIF scaling issue is provided, with focus on SIF downscaling (understood as the increase of spatial resolution). A synthesis and conclusions chapter is presented in section 2, where the knowledge gain with this thesis contributions is placed within the SIF research and development (R&D) general context. In section 4 the first author (full text studies and poster abstracts) and co-authored (only listed) publications are presented. Additional first author and coauthored publications not strictly related to this thesis, as well as some additional activities done while completing this doctoral work are listed in sections 5 and 6.

To avoid confusion by numerous section subdivisions, keywords inside the main text are highlighted with an underline and larger font size. Highlighted keywords guide the line of argumentation of each corresponding subsection. Additional clarifications on the text and the works published within the frame of this thesis are presented in footnotes.

## 1.1 Remote sensing of vegetation

Decades of remote sensing research have resulted in the development of the wide variety of platforms and sensors that are currently available. The platforms can be classified according to their distance from the surface, also known as sensor surface distance (SSD), in: ground (centimeters-m's SSD), aerial (UAV at  $\sim < 100$  m SSD), airborne ( $\sim < 3$  km SSD) and satellite ( $> 1 \times 10^3$  kilometers SSD; Fig. 1a) scale. The spatial resolution of the information provided at each level decreases from millimeters on the ground scale, to (generally)  $> 10$  m on the satellite level. At each scale sensors are able to detect different object sizes, processes and types of vegetation information (Gamon et al., 2019).

Remote sensors can be classified in passive and active devices, being passive when the measured energy is naturally reflected or emitted by an object, and active when an artificial source of energy is used (Khorram et al., 2012). Passive sensors are generally attached to aerial and satellite platforms, whereas active devices are generally used for ground applications. An exception to it are the radar and laser imaging detection and ranging (LIDAR) sensors, which are feasibly adapted to aerial and satellite platforms. The most used remote sensing approaches for functional vegetation functioning assessments are based on the reflectance properties of plants (Thenkabail et al., 2011). The typical spectral signature of vegetation is presented and compared to one of a bare soil surface in Fig. 1b.

Numerous broad band multispectral remote sensing sensors were developed to capture information in the so called visible (VIS), as well as red edge (RE) and near infrared (NIR) regions of the electromagnetic spectrum (Deng et al., 2018). This type of sensors are characterized by providing information in a limited amount of separated wavelengths or bands. Visible light is associated to changes in pigments concentration, whilst NIR reflectance shows alterations of structural properties of leaves. Moreover, vital green canopies stronger reflect NIR radiation at the mesophyll cell walls, while pigments, such as chlorophyll, absorb more red and blue radiation.

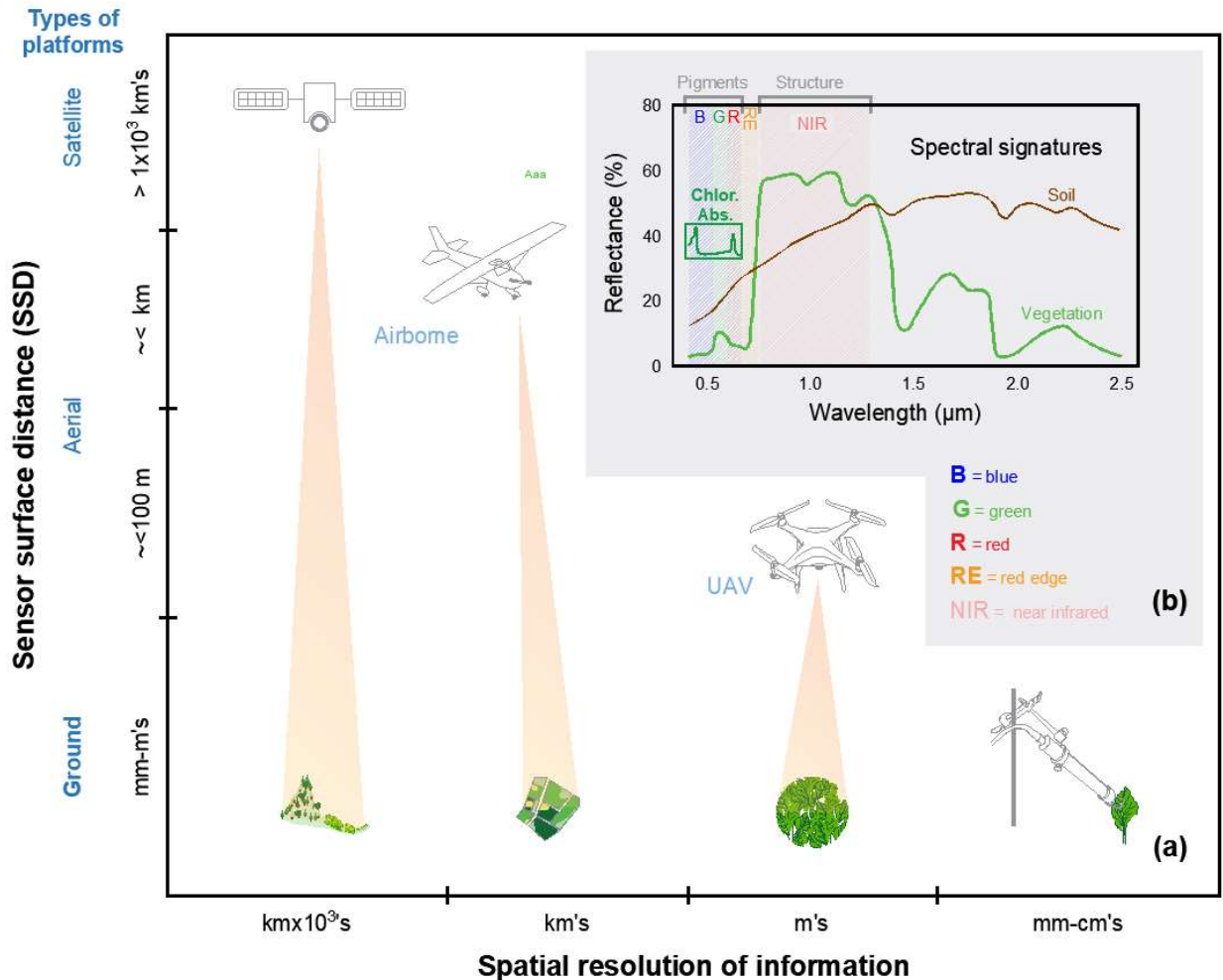


**Figure 1:** Sensor surface distance (SSD) and the spatial resolution of information provided by ground-, unmanned aerial vehicle (UAV)-, airborne- and satellite-platforms (a); and the typical spectral signature of green vegetation compared with the one of soil (b).

The translation of raw remote sensing data into quantitative information of plant traits relies in a wide variety of data processing techniques, ranging from statistical approaches to mathematical modeling and artificial intelligence routines (Verrelst et al., 2015). The most established parametric technique is the use of vegetation indices (VIs), which are the combination of two or more spectral bands into a specific mathematical expression, aiming for quantification of specific vegetation properties. A review of more than 115 VIs can be found in Xue and Su (2017). Table 1 shows the equations of the VIs used in the articles included within the present thesis.

**Table 1:** Equations of vegetation indices (VIs) used in the papers included within the present thesis.  $R_{<->}$  represents the reflectance at the specific wavelengths, and  $\alpha$  is a weighing coefficient ranging from 0.1 to 0.2 (more detailed information can be found in Quiros-Vargas et al., AGU-2020). \*Wavelengths on the formulas represent those used in the studies related to this thesis, they may differ from the specific wavelengths used in the original publications. <sup>1</sup>

Vegetation index (VI)	Formula*	Used in
Enhanced vegetation index (EVI; Liu and Huete, 1995)	$R_{<795-810>} - R_{<665-680>} \\ R_{<795-810>} + 6 * R_{<665-680>} - 7.5 * R_{<475-490>} + 1$	Quiros-Vargas et al. (2022a)
Wide dynamic range vegetation index (WDRVI; Gitelson, 2004)	$\frac{(\alpha * R_{<795-810>}) - R_{<665-680>}}{(\alpha * R_{<795-810>}) + R_{<665-680>}}$	Quiros-Vargas et al. (AGU-2020)
MERIS terrestrial chlorophyll index (MTCI; Dash and Curran, 2004)	$\frac{R_{<754\pm 7.5>} - R_{<709\pm 10>}}{R_{<709\pm 10>} - R_{<601\pm 10>}}$	Quiros-Vargas et al. (AGU-2020)
Photochemical reflectance index (PRI; Gamon et al., 1992)	$\frac{R_{<570\pm 2.5>} - R_{<531\pm 2.5>}}{R_{<570\pm 2.5>} + R_{<531\pm 2.5>}}$	Quiros-Vargas et al. (AGU-2020)
Normalized difference vegetation index (NDVI; Kriebler et al., 1969)	$\frac{R_{<795-810>} - R_{<665-680>}}{R_{<795-810>} + R_{<665-680>}}$	Quiros-Vargas et al. (AGU-2020, 2021)
Near infrared reflectance of vegetation (NIRv; Badgley et al., 2017)	$\frac{R_{<795-810>} - R_{<665-680>}}{R_{<795-810>} + R_{<665-680>}} * R_{<795-810>}$	Quiros-Vargas et al. (EGU-2022)

Reflectance-based methods succeeded in solving several issues in remote sensing of vegetation, especially those associated to existing above ground biomass-related parameters. Biomass and crop yield estimations, as well as plant counting algorithms were the basis for the development of commercially available automated tools with practical applications for farmers. Estimations of harvest loss for insurance purposes (Kenduiwo et al., 2021), the automatic detection of plants for tree inventory (White et al., 2016), crop row detection for auto steering guidance systems (Inforow, 2022), and biomass and yield (Quiros-Vargas et al., 2019) estimations are just a few of several practical applications that can be mentioned. Nevertheless, the low spectral resolution (20 nm band width) makes

<sup>1</sup> The references of conference posters associated to this thesis will be cited with the abbreviation of the conference before the year. This was done with two intentions: (i) to differentiate the posters from the main studies, and (ii) to ease the distinction between conference references, since most of them were presented in 2022.

such devices unable to track smooth changes in plant reflectance. A variety of imaging and non-imaging (point) spectrometers (instruments to separate and measure spectral features) were developed to tackle that limitation by providing higher spectral resolution (5 nm band width) over a continuous spectrum, opening what is known as hyperspectral remote sensing. The sensitivity given by such an amount of information makes it possible to detect smooth changes of early physiological processes activated in plants in response to biotic or abiotic stressors.

Besides VIs more advanced (non-parametric) methods have been widely explored for the calculation of vegetation products. For instance, machine learning processing chains imitate the way that humans analyze patterns and extract information of a specific problem. Some of the most common machine learning methods are based on the implementation of artificial neural network-, random forest-, decision tree- and nearest neighbor-based algorithms (Maxwell et al., 2017). Applied to remote sensing imagery, these techniques are used to calibrate algorithms to automatically solve simple (e.g., color-based image classification) as well as complex issues requiring structural learning methods (e.g., image classification with complex object geometries; Camps-Valls 2009). Nevertheless, the application of parametric (VIs) and non-parametric (machine learning) methods is often limited, as they work only under the specific conditions in which they were developed.

Alternatively, radiative transfer models (RTMs) can be employed to compute advanced vegetation products regardless of spatiotemporal characteristics of data acquisition and sensor characteristics (Chakhvashvili et al., 2022). With RTMs more realistic simulations of vegetation processes can be created by understanding the interaction between the radiation and a vegetation surface (Verrelst et al., 2015) from wide spectrum regions

## 1.2 Solar-induced chlorophyll fluorescence (SIF)

The solar light that reaches vegetation can be reflected, transmitted or absorbed (Fig. 2a). The absorbed solar light is captured by the pigments molecules located in the thylakoid membrane of chloroplasts (cellular organelles also composed by outer and inner membranes, stroma, granum, thylakoids and lamellae; Fig. 2b). The photons absorbed by chlorophyll molecules are transported to the reaction centers of photosystems II (PSII; Fig. 2c) producing what is known as photochemical quenching (PQ). After reaching the reaction center chlorophyll the electron passes to a series of protein complexes called the ‘electron transport chain’, which triggers several reactions leading (after several further steps) to the production of sugars. However, this ideal condition might not always occur, and depending on environmental conditions (e.g., light intensity or plant stress) the absorbed light can be dissipated as heat before reaching the reaction center (non-photochemical quenching -NPQ-), or re-emitted as chlorophyll fluorescence in the electron transport chain. Thus, the magnitude on which a plant emits more, or less, chlorophyll fluorescence compared with the heat dissipation and photochemistry depends on numerous factors, e.g.: the species, phenology, time point within the day (Siegmann et al., 2021) and the season (Mengistu et al., 2021), and the stress/health status as well (Zeng et al., 2022).

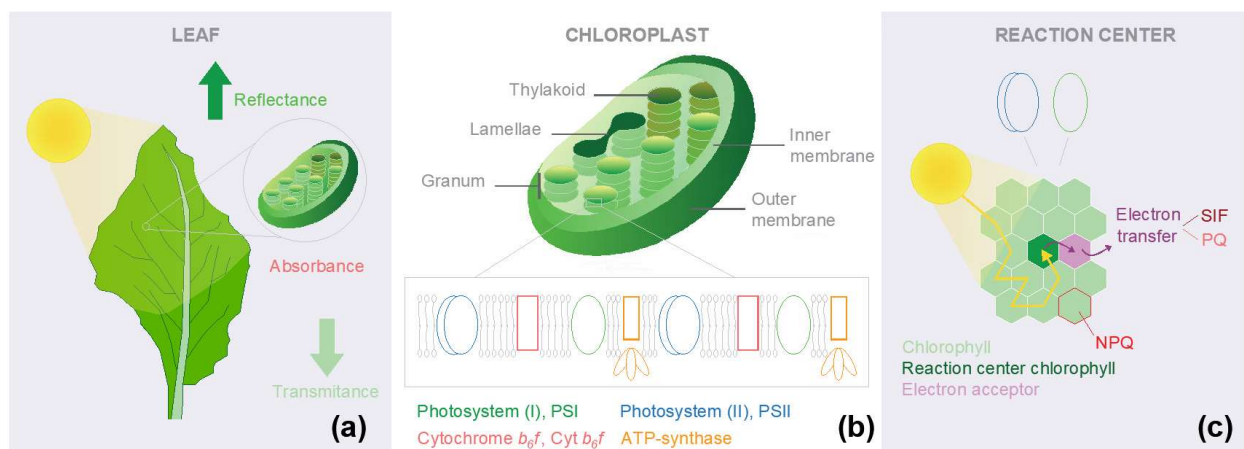


**Figure 2:** Interaction of light with vegetation at leaf (a), chloroplast (b; based on Biswal and Pandey, 2016) and reaction center (c) levels. The three paths that the energy can follow after being absorbed are represented in (c).

SIF is a low intensity signal (1-5 % of the reflected radiance; Meroni et al., 2009) emitted from the core of the photosynthetic apparatus under 400-700 nm (Photosynthetic Active Radiation, PAR) radiations, with a spectrum characterized by two crests at 690 nm ( $F_{\text{Red}}$ ) and 740 nm ( $F_{\text{Far-red}}$ ; Mohammed et al., 2019)<sup>2</sup>. Based on its connection to the functional status of photosynthesis, SIF has been used as an indicator of physiological changes caused by biotic (Zarco-Tejada et al., 2018) or abiotic (Panigada et al., 2014) stressors, as well as a GPP tracker (Martini et al., 2021). However, it is difficult to disentangle SIF from the reflected radiance, since it is attenuated by the reflected light. Moreover, the SIF signal intensity is distinctly decreasing with increasing distance from the molecular (PS) level due to scattering and re-absorption processes (Fig. 3a). At canopy level it can be reabsorbed by other canopy constituents (Porcar-Castell et al., 2014), and additionally the SIF signal leaving the canopy is weakened by the scattering caused by atmosphere molecules (Fig. 3b; Porcar-Castell et al., 2021).

The retrieval of SIF is complicated due to the combination of two factors: the by-nature low intensity of the signal and the strong background light that hinders the detection of such a faint glow. To overcome the second factor, SIF retrieval methods approach the attenuation of the background light through the use of solar or atmospheric absorption bands. Solar absorption bands are also called Fraunhofer lines (FLs), which are dark lines in the spectrum caused by the absorption of specific wavelengths by chemical elements in the sun. Assuming constancy in the reflectance and fluorescence signals, Fraunhofer line depth (FLD) methods were developed to retrieve SIF by calculating the ratio between the incoming solar radiance inside and outside a FL (within the Chlorophyll fluorescence emission spectrum), and the apparent reflectance (including the contribution of SIF) inside and outside the same FL (Theisen, 2002, and Plascyk 1975; cited by Meroni et al., 2009). The result shows a slightly higher apparent reflectance inside the FL, which is proportional to the emitted SIF signal. Besides, other retrieval methods exploit the absorption of solar light by elements in the Earth atmosphere through the so called ‘telluric bands’. In particular for the retrieval of SIF, Oxygen ( $O_2$ ) telluric bands are used since they absorb the solar light

---

<sup>2</sup> In the publications associated to this thesis only SIF- $O_2A$  (also called ‘SIF<sub>Far-red</sub>’ or ‘SIF’) data used, which is in general more often investigated by the SIF research community. Based on such information, further parameters like SIF yield (SIF/PAR) and SIF downscaled to leaf level were calculated.

at  $\sim 759$  nm ( $O_2$ -A) and  $\sim 687$  nm ( $O_2$ -B; Tubuxin et al., 2015; Fig. 3b) from where  $SIF_{Far-red}$  (hereinafter referred to as SIF) and  $SIF_{Red}$  can be measured, respectively.

Novel spectral fitting methods (SFM) were developed to retrieve SIF either from the  $O_2$  absorption bands or from the full Chlorophyll fluorescence spectrum (Cogliati et al., 2015; Cogliati et al., 2019) by using high resolution spectral data from contiguous bands within the spectral region of interest. SFM approaches offer some advantages over the FLD-based approaches, since they overcome the assumption of a constant reflectance and fluorescence signal (Meroni et al., 2010), they are based on the principles of the radiative transfer theory, and they allow for the correction of interferences of the atmosphere (e.g., aerosols, surface pressure, water vapor, etc.). A detailed revision of approaches to retrieve SIF can be found in Bandopadhyay et al. (2020).

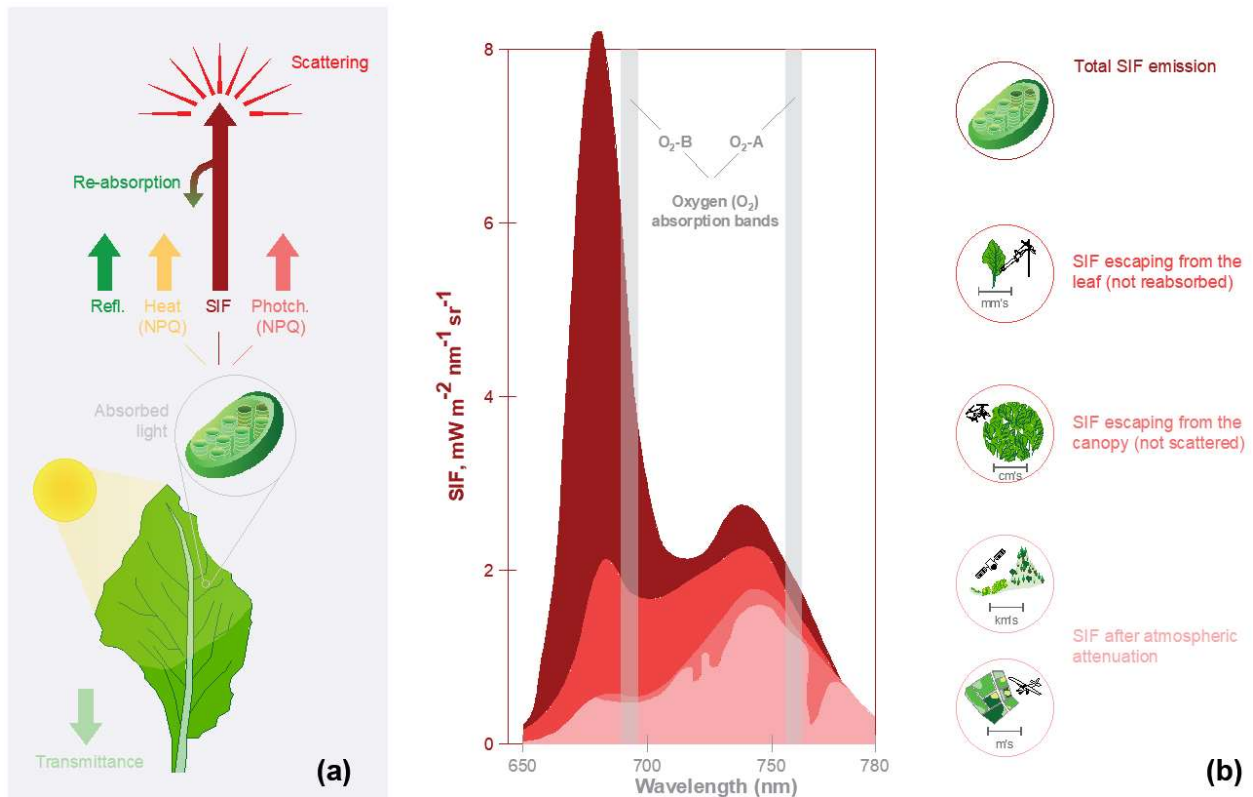


**Figure 3:** Possible ways followed by the absorbed light (a), and a detailed illustration of the attenuation of the solar-induced chlorophyll fluorescence (SIF) signal from the molecular-, to the ground-and aerial- (unmanned aerial vehicle -UAV- and airborne) and satellite-scales (b). Based on Porcar-Castell et al. (2021).

Imaging and non-imaging (point) spectrometers are employed to measure the high (sub-nm) spectral resolution reflectance used to retrieve SIF. At ground scale, point spectrometers like the fluorescence box (Flox; JB Hyperspectral) are used to monitor SIF with high temporal resolution, but low spatial coverage. On the other hand, a higher spatial coverage, but low temporal resolution, can be provided by imaging spectrometers mounted on airborne platforms, e.g., the imaging fluorimeter (IBIS, the high performance imaging spectrometer within the HyPlant; Gamon et al., 2018), the chlorophyll fluorescence imaging spectrometer (CFIS; Frankenberg et al., 2018) and the high-performance airborne imaging spectrometer (HyPlant; Rascher et al., 2015; Siegmann et al., 2019).

Despite of the great advances achieved during the last decades, the retrieval of SIF carries instrument- and retrieval-associated uncertainties, which are yet matter of investigation to be solved. Specific sensor characteristics like the detector and fore optics used, as well as the type of calibration used for one specific device, makes it difficult to standardize and compare SIF measurements across spatiotemporal scales and sensors. Moreover, the major source of uncertainty associated to the retrieval comes from the atmospheric interference, since it is sensitive to variations in factors like water vapor, terrain elevation, aerosol optical thickness and surface pressure. Thus, the method used (either empirical corrections or those based on radiative transfer models) to correct for the interference of atmosphere will have a strong impact on the output data (European Space Agency, ESA, 2022a; Photoproxy, report No. 3). Here, numeric inaccuracies in the atmospheric correction algorithms, and the use of atmospheric transfer models with an erroneous parameterization are probably the main sources of uncertainty (ESA, 2022c, and ESA, 2022d; corresponding to Flexsense campaigns final reports 2018 and 2019, respectively).

Besides the passive sensing of SIF, the active Chlorophyll fluorescence sensing has been possible for decades by using the pulse amplitude modulation (PAM; Schreiber, 2004) principle. PAM-based instruments measure the fluorescence yield provoked by saturating (blue or red light) pulses followed by intervals of exposure to actinic light, and use this information to estimate other photosynthesis-related traits, e.g., quantum efficiency of photosystem II ( $Y_{II}$ ), electron transport rate (ETR) and NPQ (Fig. 4a; Maxwell and Johnson, 2000). The

$Y_{II}$  is calculated as the difference between the maximum fluorescence yield ( $F_m'$ ) and the fluorescence yield ( $F_t$ ) in a light adapted photosynthetic tissue, divided by  $F_m'$ ; whilst ETR is calculated as the  $Y_{II}$  multiplied by the absorbed PAR, 0.5 (assuming equal distribution of the absorbed PAR between photosystems I and II) and 0.84 (as the leaf absorption coefficient). NPQ is in turn measured as the difference between the maximum fluorescence yield in dark adapted leaf ( $F_m^\circ$ ) and  $F_m'$ . Two of the main PAM-based instruments for field measurements can be mentioned: the MoniPAM (Fig. 4b) and the MiniPAM (Fig. 4c). The MoniPAM can be installed in a fixed location, thus allowing to collect data with high temporal resolution, while the MiniPAM is a mobile device and therefore allows to collect information at higher spatial resolution.

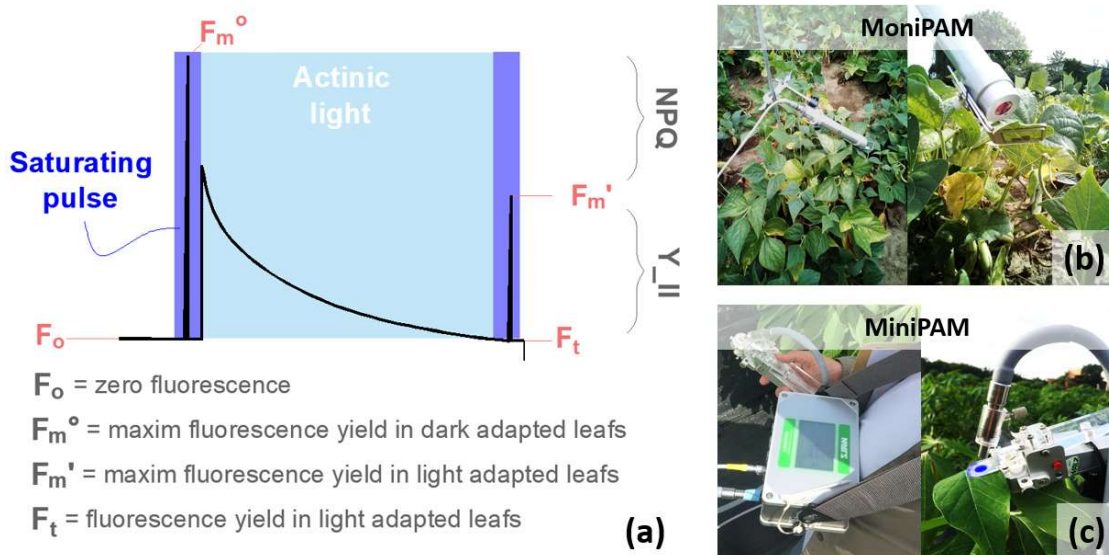


**Figure 4.** Typical fluorescence trace produced during the leaf exposure to saturating and actinic light pulses and the respective derived parameters ( $F_0$ ,  $F_m^\circ$ ,  $F_m'$  and  $F_t$ ; a; based on Maxwell and Johnson, 2000) used for the calculation of photosynthetic traits (non-photochemical quenching, NPQ, efficiency of photosystem II,  $Y_{II}$ , and the derived electron transport chain, ETR). In panels (b) and (c) images of the MoniPAM and MiniPAM instruments are respectively shown.

Another method available for the active sensing of chlorophyll fluorescence is the light-induced fluorescence transient (LIFT; Kolber et al., 1998) principle, based on the stimulation of chlorophyll fluorescence throughout fast repetition rate emissions of blue flashlets (Keller et al.; 2019). First, the closest possible to the

maximum reduction state of Quinone A ( $Q_A$ , primary electron acceptor of the photosystem II) is reached with the emission of faster flashlets. Subsequently, an interval with slower flashlets, in the order of ms, is emitted to analyze the re-oxidation of  $Q_A$  during the 'relaxation' phase after the excitation (Osmond et al., 2017). Among the main LIFT-derived Chlorophyll fluorescence traits are the  $Y_{II}$  and the reoxidation efficiency of  $Q_A$  ( $Fr1/Fv$ ). The results presented on Quiros-Vargas et al. (2021) derived from LIFT data were preceded mainly by Keller et al. (2019), a study about photosynthesis phenotyping in which a software was developed required for further LIFT data processing. In addition, Soares et al. (2021) and Zendonadi dos Santos et al. (2021) provided deeper analyses on the use of LIFT data for the phenotypic characterization of soybean (in a FACE environment) and wheat genotypes, respectively.

It is worth mentioning that remote sensing studies often require the integration of data from several methods (parametric, non-parametric, radiative transfer, etc.; Gerhards et al., 2019). This is due to the complexity of the vegetation processes being measured, which can be caused by several factors that at the same produce different responses in the plant. For instance, the several functions that water has in the plant physiology (turgor, thermal regulation, photolysis, etc.) can cause many responses at the root, leaf and canopy structure levels (Jonard et al., 2020). While VIs can be used to monitor changes in the canopy pigments composition, thermal data and SIF can be used to analyze alterations in canopy temperature and photosynthetic activity, respectively. <sup>3</sup>

### 1.3 Chlorophyll fluorescence assessments at ground scale

Since the second half of the 20<sup>th</sup> century, the demand for more productive and stress resistant varieties has greatly increased, and thereby the need of more efficient plant phenotyping techniques as well. In that sense, multiple platforms have been developed in order to make the assessment of varieties in the field more

---

<sup>3</sup> With this introduction about RS of SIF, the following subsections will a more detailed description of the SIF assessments at specific spatial scales, from the ground over the aerial (UAV and airborne) to the satellite scale. The main results of the studies reported in this thesis are presented within each subsection, aiming to contextualize where they are located within the general research status of each scale.

efficient. For example, the first mobile ground systems for plant phenotyping were pulled by walk and consisted of a horizontal platform with manually triggered sensors installed over bike wheels (White and Conley, 2013). Researchers rapidly realized the necessity to include mechanical and electrical components to reduce labor. Andrade-Sanchez et al. (2014), e.g., mounted three sensors on a horizontal axis installed in the front of a commercial sprayer with close to 2 m of maximum height clearance, thus improving performance. More efficient automated platforms were developed in the last three years by research institutions (Muller et al., 2018) and companies (Lemnatec, 2019), aiming at more accurate and less labor demanding field phenotyping campaigns. Ground sensing platforms (mentioned in section 1.1) stands, therefore, as the most robust and reliable technique to accurately assess key crop traits for plant phenotyping. The following six platforms are the main ones developed in the last five years:

- i. Phenomobile lite, from the Commonwealth Scientific and Industrial Research (CSIRO), Australia (Rebetzke et al., 2016).
- ii. Characterisation through Kinetic Observati (Gecko), from CSIRO, Australia (Potgieter et al., 2018).
- iii. Field-Scanalyzer<sup>®</sup>, from Lemnatec, Germany (Lemnatec, 2019)
- iv. Field-Scan<sup>®</sup>, from Phenospex, Netherlands (Phenospex, 2019)
- v. Field Phenotyping Platform (FIP), from the Eidgenössische Technische Hochschule (ETH), Switzerland (Kirchgessner et al., 2016).
- vi. Field-snake, from the Institute of Bio- and Geosciences (IBG-2), of the Julich Forschungszentrum, Germany.

The advent of platforms like the field-snake (Fig. 5a) has advanced the use of chlorophyll fluorescence information for plant phenotyping. The field snake is a mobile (up to 7 km h<sup>-1</sup> speed) platform equipped with a hydraulic system capable of moving a sensors box in the X-Y-Z directions. The sensors box slides at 0.18 m s<sup>-1</sup> along the 20 m X-axis and can be elevated up to 3.5 m over the X-axis level to create the Z-axis. The system payload is 100 kg, therefore it is capable to carry VIS, multispectral, hyperspectral and thermal cameras, as well as the abovementioned Flox and LIFT instruments for passive and active chlorophyll fluorescence measurements. The versatility of the field-snake combined with the accurate chlorophyll fluorescence information provided by instruments like Flox

and LIFT, makes it a suitable system to investigate the response of genotypes in free-air CO<sub>2</sub> enrichment (FACE) experiments (Quiros-Vargas et al., 2021). The latest constitutes a topic of high interest, since chlorophyll fluorescence information measured from active (Flexas et al., 2002) and passive (Jablonski et al., 2017) sensors has been reported as a good indicator to track the photosynthetic response of plants to varying levels of [CO<sub>2</sub>]. Yet, specific crop responses to higher atmospheric CO<sub>2</sub> concentration have to be further investigated, since the e[CO<sub>2</sub>] effect on a plant might vary according to the species, genotype and phenological stage.

The contribution of the present doctoral work in this (ground scale) context was about the chlorophyll fluorescence assessment in the late phenology (pod filling stage) of three bean genotypes cultivated in a FACE experiment (Quiros-Vargas et al., 2021). The lower noon SIF (Flox-derived) observed at the end of the pod filling stage under e[CO<sub>2</sub>], alongside the lower yield of photosystem II measured with the LIFT ( $Fq'/Fm'$ ) and the MoniPAM (YII; Fig. 5b), suggest a faster senescence effect in the three analyzed bean genotypes. This result may however differ in other crops and phenological stages; e.g., in an ongoing study Knopf et al. (in progress) did not find effects of e[CO<sub>2</sub>] in winter wheat senescence. In the same study, this observation was also supported by a faster seasonal NDVI decay in the e[CO<sub>2</sub>] experiment. Moreover, chlorophyll fluorescence estimations from the three instruments were compared since this was unclear in literature at the publication time (Fig. 5c). A correlation of Flox SIF with MoniPAM ( $R^2 = 0.62$ ) and LIFT chlorophyll fluorescence estimations was found. In the first case the significance ( $p = 0.03$ ) in the relation was influenced by the contrasting low and high chlorophyll fluorescence values at the beginning and end of pod filling stage, respectively. <sup>4</sup>

---

<sup>4</sup> In sections 1.3-1.7 figures with the main results obtained from scale specific studies are presented. In each figure a time line is included to better contextualize where this thesis contributions are located within the respective research area.

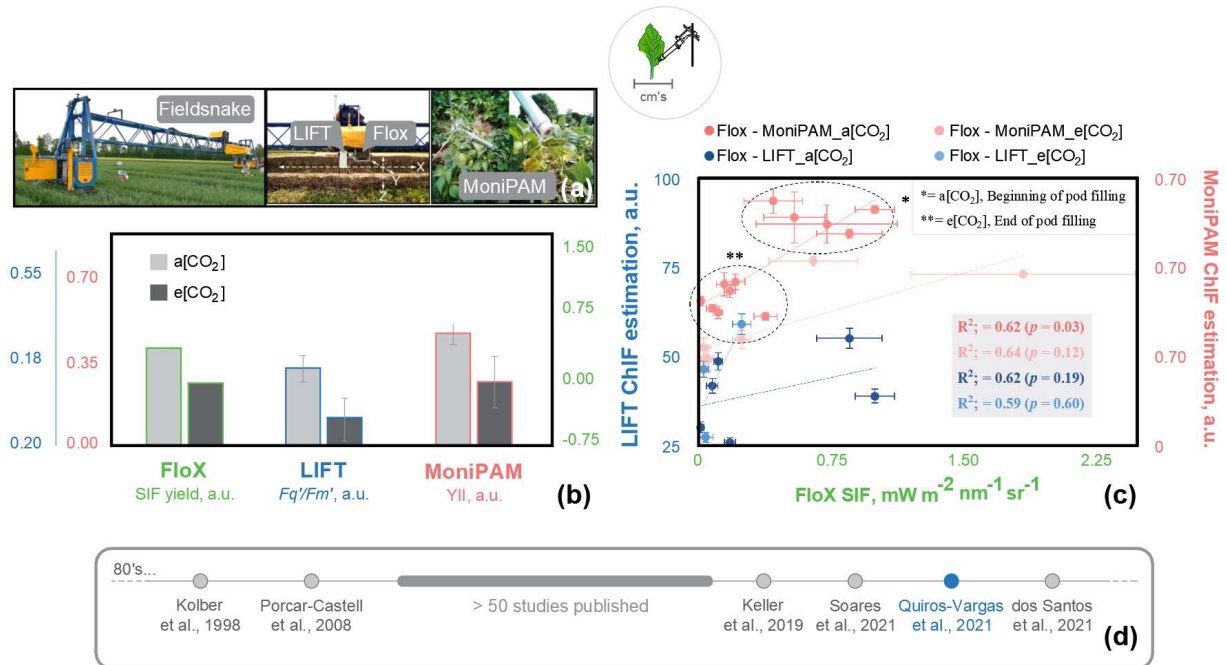


**Figure 5:** Platform (field-snake) and active (light-induced fluorescence transients -LIFT- and the moni Pulse-amplitude modulated –MoniPAM-) and passive (fluorescence box –Flox-) sensors used in the Quiros-Vargas et al. (2021) ground scale study (a). Different responses in solar-induced chlorophyll fluorescence (SIF) yield, and the yield of photosystem II from LIFT ( $Fq'/Fm'$ ) and MoniPAM (YII) in the ambient ( $a[CO_2]$ ) and elevated ( $e[CO_2]$ ) CO<sub>2</sub> concentration experiments (b). The relation between chlorophyll fluorescence estimations from the three sensors is presented in (c). Panel (d) shows where the Quiros-Vargas et al. (2021) study is located within research field of Chlorophyll fluorescence assessment from the ground scale.

#### 1.4 SIF assessments at unmanned aerial vehicle (UAV) scale

Vegetation in open fields is always heterogeneous due to edaphic and micro-climatic variations. The assessment of spatial variability in vegetation surfaces is necessary to improve management practices in agriculture fields, and to understand ecosystem dynamics. In the past, the assessment of vegetation status was carried by sparse and tedious field observations prone to inaccuracies and misinterpretations. At present, the advance of remote sensing technologies brought options to map large areas in short lapses of time with high spatial and temporal resolutions. Among those options, some authors identified the use of unmanned aerial vehicles (UAVs) as the most cost-effective technology in areas of

≤ 20 ha (Matese et al., 2015) in forestry (Torresan et al., 2017), environment (Manfreda et al., 2018), and in several branches of agronomy, e.g., crop protection (Psirofonio et al., 2017), site specific management and field phenotyping (Sankaran et al., 2015).

UAV platforms such as multicopters and fixed-wing gliders (Norasma et al., 2019; Ziliani et al., 2018) are the most used UAVs for vegetation monitoring, and its selection criteria relies on the needs of the specific research. Multicopters are generally intended to map smaller areas at lower altitude and higher spatial resolution, which is especially important to assess breeding research experiments, (Sankaran et al., 2015). Conversely, fixed-wing UAVs match the requirements for a larger scale monitoring (Chung et al., 2016), with applications in commercial farms. Besides the platform, the characteristics of the sensors and data processing methods are the essential aspects to focus in the planning and development of research. UAV sensors capturing data in red-green-blue (RGB) channels are the simplest sensors to use in low altitude imagery research, yet, useful to calculate parameters like the percentage of colors and band ratios like the Green-Red Vegetation Index (GRVI; Quiros-Vargas et al., 2020b). Furthermore, the high spatial resolution normally presented by RGB sensors make the suitable to compute detailed digital elevation models (DEM; Chu et al., 2017) of fields, useful to assess key agricultural information like crop lodging (Wilke et al., 2019). Despite the mentioned uses of RGB data, their application in remote sensing of vegetation is limited by the lack of information in the red edge (RE) and near Infrared (NIR) spectral windows. Indeed, this triggered the development of RGB altered cameras to make them sensitive to detect reflected light in the NIR spectrum. These kind of sensors were popular for several years due to their low cost and user-friendly characteristics (Quiros and Khot, 2016), however, the demand for more accurate NIR information by the remote sensing research community stimulated the development of multispectral camera capable to measure RGB, NIR and RE information simultaneously (Lum et al., 2016).

The further development of UAV-based hyperspectral sensors (Mäkynen et al., 2012) permitted more detailed remote sensing studies, e.g., for the classification of infested (with bark beetle; Näsi et al., 2015) and asymptomatic (infected with *Xylella fastidiosa*; Zarco-Tejada et al., 2018) plants, the estimation of leaf chlorophyll (Aasen et al., 2015) and carotenoids (Zarco-Tejada et al., 2013), the

individual tree crown detection (Nevalainen et al., 2017) and the assessment of water stress (Zarco-Tejada et al., 2012). Nevertheless, compared with RGB- and multispectral-based studies, there is a limited number of publications addressing hyperspectral low altitude sensing due the expensive cost of the sensors and the complexity in data processing (Adão et al., 2017). The use of UAV-hyperspectral systems for the retrieval of SIF sensors is nowadays a topic of utmost interest, due to the close relation that SIF has with the physiological status of photosynthesis, especially if integrated with thermal data (Gerhards et al., 2019). However, the retrieval of SIF requires high (sub-nm) spectral information and therefore all the studies published in this direction have worked with spectrometers mounted on the UAV platforms, which add complexity to the data collection and analysis. One of the major difficulties of working with spectrometers data collected form UAV platforms is the location and characterization of the sensor footprint, which has been addressed in some studies (Gautam et al., 2020), yet it has not been solved. A plausible solution can be the development of an imaging sensor, i.e. a multi-channel camera or scanning spectroradiometer, which is currently being investigated at the IBG-2 as well.

The state-of-the-art of UAV-based SIF assessments is still in an experimental stage, where different sensor and platform developments are being carried by researchers from several groups in the world. Therefore, a publication summarizing the main of those developments was missing in the literature. This is why the contribution of the present doctoral work in the (UAV-scale) context was a review of the available UAV-based methods for SIF retrieval with non-imaging spectrometers (Quiros-Vargas et al., 2020a). In the study three systems were reported, the so called Floxplane, Piccolo-Doppio and AirSIF. The first consisted of a fixed wing platform aimed to characterize the interference of the (multiple km) atmosphere column on the retrieval of SIF; whereas the Piccolo-Doppio and AirSIF share the same principle of the bifurcation of the spectroradiometer optical path. Preliminary results were presented, e.g., those obtained by researchers from the University of Edinburgh-GeoSciences, who installed a Piccolo-Doppio system on an UAV to retrieve SIF of a FACE experiment with oak trees (Fig. 6a). They found a high correlation ( $R^2 = 0.88$ ) of SIF with incoming radiation (Fig. 6b). Further, the authors found SIF be useful as indicator of treatment effects and their relation with environmental factors.

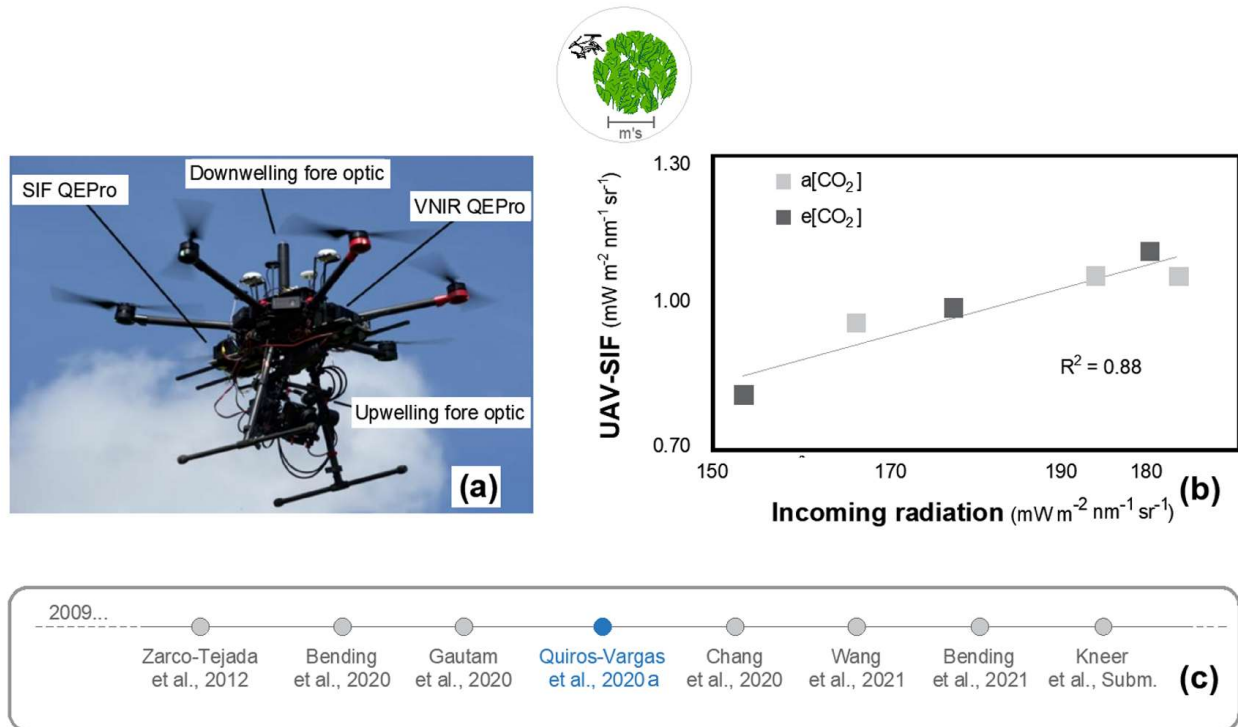


**Figure 6:** Unmanned aerial vehicle (UAV) platform (a; source: Dr. Andrew Reville, BBSRC/NERC ATEC project at the University of Edinburgh-GeoSciences) and the correlation of solar-induced chlorophyll fluorescence (SIF) retrieved from it with incoming radiation (b), extracted from Quiros-Vargas et al. (2020a). Light and dark gray squares correspond to data points from the ambient ( $a[\text{CO}_2]$ ) and elevated ( $e[\text{CO}_2]$ )  $\text{CO}_2$  concentration experiments, respectively, measured in a mature oak forest at the BIFoR FACE site in the UK. Panel (c) shows where the publication Quiros-Vargas et al. (2020a) is located within the research field focused on the retrieval of SIF from the aerial (UAV) scale.

After Quiros-Vargas et al. (2020a), two new SIF measurement system for drones have been developed (Fig. 6c). Chang et al. (2020) further developed a new system implementing a mechanical arm to alternate between upwelling and downwelling measurements, in order to avoid light loss from the fiber entrance. Additionally, Wang et al. (2021) reported the feasibility of retrieving SIF from the UAV-based FluorSpec system. These two platforms are mentioned by Bendig et al. (2021), who provided an updated overview about the reliability of UAV-based SIF measurements for applications in plant phenotyping and precision agriculture.

## 1.5 SIF assessments at airborne scale

Vegetation surfaces (i.e., agriculture fields, forest, wetlands, shrubs, etc.) are not isolated points in an inert space. Spatial patterns in agriculture areas reflect dynamic processes linking plant populations of different fields. The abovementioned UAV-based systems are generally able to just provide information about intra-field patterns, which may hinder the understanding of a certain larger scale phenomenon. This limitation can be overcome with airborne-based remote sensing systems due to its capacity to cover larger areas. For instance, since its first results capturing airborne SIF (Rascher et al., 2015), data from the HyPlant imaging spectrometer (Siegmann et al., 2019) has pushed forward for the understanding of large scale vegetation processes. There are numerous studies using HyPlant data since then: Wieneke et al. (2016) analyzed HyPlant SIF usefulness to improve GPP estimations, while Tagliabue et al. (2020) proposed the use of HyPlant SIF for the assessment of the functional diversity as a reference of ecosystems functioning and stability. Recently, Siegmann et al. (2021) used HyPlant data to downscale the canopy SIF to the SIF emission efficiency ( $E_f$ ) at the leaf level, following the approach suggested by (Yang et al., 2020).

The larger spatial coverage enabled by airborne sensors becomes important for the assessment of water stress, since the soil water content will be strongly determined by the topography and soil physical characteristics of a whole landscape. Indeed, the use of SIF for water stress assessment is the subject for our contribution at airborne scale, and it is also related to two of the main emerging SIF applications mentioned by Porcar-Castell et al. (2021): (i) the pre-visual stress detection, and (ii) the water cycle studies. Besides, understanding the SIF response to varying soil water content levels have applications on climate modeling, since it can help to elucidate the mechanistic basis of SIF towards better constraining transpiration and photosynthetic dynamics.

The state-of-the-art of airborne-based SIF measurements is, in general, in a 'prove of concepts' stage. Namely, airborne SIF information (in most of the cases from HyPlant) is being used to prove research concepts in agriculture (Siegmann et al., 2021) and environmental (Tagliabue et al., 2016) study areas. In agriculture, investigations about the use of airborne SIF data for water stress assessment in particular are currently gaining relevance. In this sense, Damm et al. (2022) recently

published the first study showing how SIF data detected an early physiological plant response to drought effects, which previously was just theoretically known. In addition to the Damm et al. (2022) study, this year two additional studies following a similar direction have been published: “Remote Sensing of Instantaneous Drought Stress at Canopy Level Using Sun-Induced Chlorophyll fluorescence and Canopy Reflectance” (De Cannière et al., 2022) and “Stress detection in agriculture with focus on the synergistic use of different optical domains: a review” (Berger et al., 2022). As common factor, those studies try to contribute in elucidating how the soil water availability can be related to the emission of SIF. Such knowledge gap is addressed as well in this thesis through the studies commented below.

The contributions of the present doctoral work in this (airborne-scale) context were mainly two. First, in Quiros-Vargas et al. (AGU-2020) we found HyPlant SIF (Fig. 7a and 6b) to be more sensitive than VIs to the effect of heat in lower soil water retention capacity areas. In the same study, we report a significant match (that was not observed with NDVI) between the spatial patterns of SIF and soil homogeneous units similarly as it was reported by von Hebel et al. (2018). Subsequently, in Quiros-Vargas et al. (in revision at PNAS-Nexus) we report on the spatial relation between SIF and the plant available water in the root zone (PAW) over several irrigated potato, and non-irrigated sugar beet and winter wheat fields. Based on airborne data from three consecutive growing seasons our results showed for the first time the relation between SIF and PAW, which was strongly positive in non-irrigated sugar beet (Fig. 7c) in the late morning (~11:00 h). Remarkably, no relations were found in irrigated potato fields (Fig. 7d). These findings constitute the latest study published using airborne SIF information (Fig. 7e), and are intended to set a first step towards the development of SIF-based precision irrigation techniques. When interpreting these data, however, it is essential to take into account that the SIF-PAW relation can vary, for instance, according to the stress severity and the spatiotemporal scale of data. Both topics are addressed in the following subsections 1.6 (where the SIF-soil moisture relation in an upscaled, satellite-level, scenario is analyzed) and 1.7 (where the scaling issue and the importance of downscaling SIF imagery are discussed).

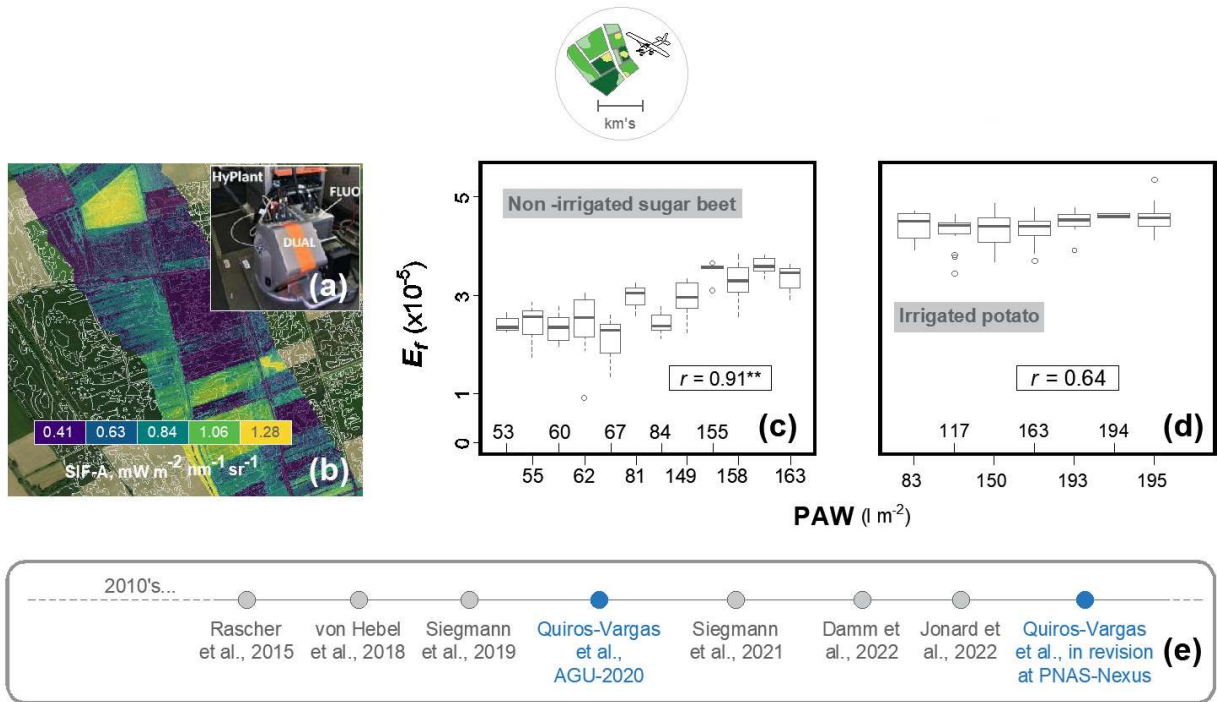


**Figure 7:** The high-performance airborne imaging spectrometer HyPlant used Quiros-Vargas et al. (in revision at PNAS-Nexus) airborne scale study (a), and an example of the solar-induced chlorophyll fluorescence (SIF) imagery used (b). The main results of the relation between the SIF emission efficiency ( $E_f$ ) and the estimated plant available water ( $PAW_{est}$ ) in the non-irrigated sugar beet and irrigated potato fields are presented in (c) and (d), respectively. Panel (e) shows where the Quiros-Vargas et al. (in revision at PNAS-Nexus) publication is located within research field of the assessment of SIF from the airborne scale. <sup>5</sup>

<sup>5</sup> Other conference posters (Quiros-Vargas et al., LPS-2022a and EMS-2022) are not considered as main (airborne-scale) contributions since most of their content was already presented in Quiros-Vargas et al. (2022a) under review in the PNAS-Nexus journal. The goal of those posters was to communicate the results to a broader audience (in the case of the LPS) and different communities (in the case of the EMS).

Future studies assessing the effect of water shortage on plants should use actual soil water content. Moreover, alongside emission based SIF information, reflectance-based vegetation indices (e.g. PRI, MTCI and NDVI) can provide complementary qualitatively data about vegetation traits and the effects of a water deficit (Damm et al., 2018). Indeed, the integration of multiple-sensor data (especially SIF- and thermal-based) has been reported as the most effective way to understand the effects of stressors in vegetation (Zarco Tejada et al., 2018).<sup>6</sup>

## 1.6 SIF assessments at satellite scale

Satellite-based SIF retrievals are based on data from missions that were originally planned for atmospheric chemistry applications. Such spaceborne-based SIF data provides key information for vegetation functioning studies from regional to global scale. The story about satellite-based SIF retrievals using data from missions that were originally planned for atmospheric chemistry applications. The Medium resolution imaging spectrometer (MERIS, from the European space agency -ESA-) and the moderate resolution imaging spectroradiometer (MODIS; from the national aeronautics and space administration –NASA-) were the firsts sensors allowing space born SIF retrieval based on the so called ‘fluorescence line height algorithm’ (Gower et al., 1999; Gower et al., 2004). Nevertheless, those studies were focused on the analysis of phytoplankton fluorescence and thus had low impact for the remote sensing of vegetation community. Further, those early studies were strongly affected by atmospheric conditions like the aerosol optical thickness (Bandopadhyay et al., 2020). The first spaceborne-SIF retrieval from vegetation was done based on the FLD principle by Guanter et al. (2007), who validated the satellite estimations with ground and airborne measurements. The subsequent launch of the greenhouse gases observing satellite (GOSAT) by the Japan aerospace exploration agency (JAXA) motivated further research on the retrieval of the seasonal SIF dynamics at global scale (Joiner et al., 2011). The low spatiotemporal resolution and poor signal to noise ratio (SNR) of GOSAT’s data were partly overcome with the launch of the global ozone monitoring experiment 2 (GOME-2; Joiner et al., 2013) satellite by the European organization for the exploitation of meteorological satellites (EUMETSAT) and ESA. SIF derived from

---

<sup>6</sup> This research subject (spatial relation between SIF and the soil water content) represents a transition between the two research projects. First promising results on the spatial relation between SIF and the soil water content were gathered in the frame of the Training on Remote Sensing for Ecosystem Modelling (TRuStEE) network (Quiros-Vargas et al., AGU-2020), and further investigated within the Photoproxy project, which yielded in the publication of Quiros-Vargas et al. (in revision at PNAS-Nexus).

GOME-2 data was used as an indicator of crop photosynthetic capacity (Zhang et al., 2014).

Besides the impact of the abovementioned platforms, satellite-based SIF retrieval was greatly improved afterwards with the launch of the orbiting carbon observatory 2 (OCO-2; Sun et al., 2017) satellite. Among other applications, OCO-2 data was used to analyze the relation of SIF and GPP in numerous studies (Bandopadhyay et al., 2020). Later, the launch of the tropospheric monitoring instrument (TROPOMI) onboard the Sentinel-5 Precursor (satellite) raised expectations to retrieve SIF with a quality similar to the OCO-2, but with higher spatiotemporal resolution (Guanter et al., 2015). This was confirmed by Köhler et al. (2018) who published a time series of global SIF dataset (TROPOMI-SIF) with a spatial resolution of  $7 \times 3.5 \text{ km pixel}^{-1}$  providing daily information over several years. A similar SIF product was recently also released by ESA in the frame of the TROPOSIF project (Guanter et al. 2021). A timeline showing the mentioned satellites is shown in Fig. 8a, whilst the carrying satellite and a global SIF map example from TROPOMI (data source used in Quiros-Vargas et al., EARSeL-2022) are shown in Fig. 8b and c. In addition, based on NASA's public information, Fig. 8d shows the SIF data availability from some of the North American missions since 1995 to the present. The unprecedented high spatiotemporal resolution of the TROPOMI-based SIF products encouraged novel studies addressing, e.g., in more detail the SIF-GPP relation (Li and Xiao, 2022), as well as variations of SIF in the dry season of tropical forests (Doughty et al., 2019).

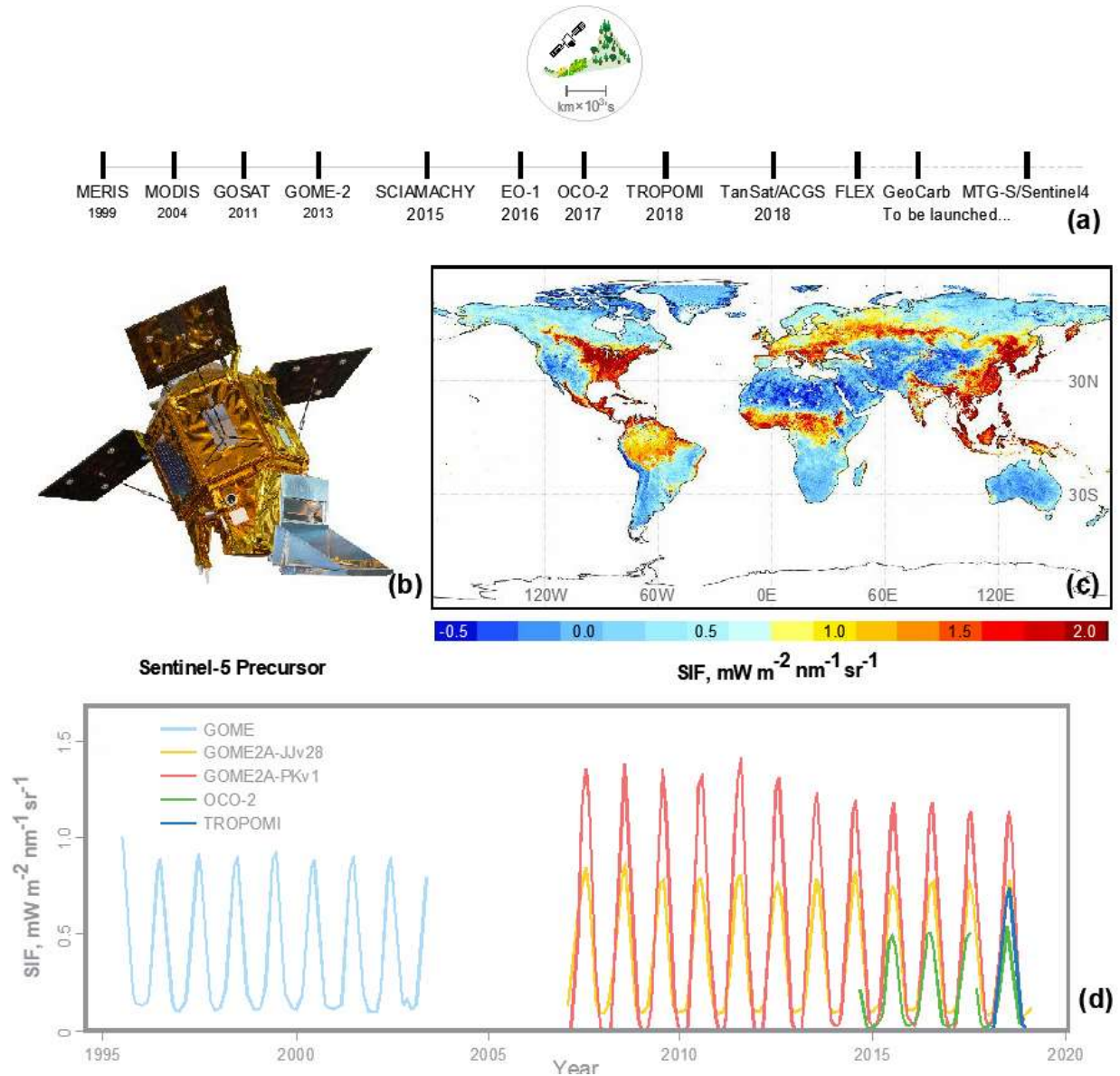


**Figure 8:** Satellite platforms that have been used to estimate SIF since 1999 (a; Bandopadhyay et al., 2020); in grey are those commented in the main text, and in red are other less relevant. The Sentinel-5 precursor satellite (b) holding the TROPospheric Monitoring Instrument (TROPOMI) sensor from which worldwide solar-induced chlorophyll fluorescence (SIF) data can be retrieved. An example of a global SIF map, recorded in July 2018, is presented in panel (c). Global SIF data since 1992 from GOME, OCO-2 and TROPOMI platforms (d; adapted from [HTPPS://climatesciences.jpl.nasa.gov/sif/download-data/level-2/](https://climatesciences.jpl.nasa.gov/sif/download-data/level-2/)).

The assessment of SIF from spaceborne sensors is to date in a ‘prove of specific research concepts’ stage. Investigations on the satellite scale address regional to continental and global scale vegetation functioning assessment. For instance, the use of satellite SIF data to analyze the effect of water limitations (the topic of particular interest in this thesis) was recently addressed by Jonard et al., (2022). The authors reported non-linear relations of photosynthesis with light and water at global scale. Another topic of utmost interest within the SIF research community is about the SIF-GPP relation during water scarcity periods. This has been addressed in some studies with ground data at (Martini et al., 2021), yet, it is still unknown how it may behave in a regional to continental and global scale.

The contribution of the present doctoral work in this (satellite-scale) context was a case study using European scale TROPOMI-SIF information integrated with satellite based soil moisture, information from NASA’s soil moisture active/passive (SMAP) mission, and the GPP data from ESA’s TerrA-P project (Quiros-Vargas et al., EARSeL-2022; Fig. 9a)<sup>7</sup>. The study was conducted with the overall goal of having an upscaled perspective of the spatial relation between SIF and soil water content (previously addressed only at airborne scale in Quiros-Vargas et al., in revision at PNAS-Nexus). The aim in Quiros-Vargas et al. (EARSeL-2022) was to elucidate how the SIF-GPP relation is influenced by soil moisture on European scale during a heatwave in summer 2018, in order to understand the continental scale response of vegetation to abnormal high temperatures. We found a strong positive SIF-soil moisture relation ( $r = 0.91$ ,  $p < 0.01$ ; Fig. 9b) and a lower SIF but more heat sensitive SIF pattern across time in the lower soil moisture classes (Fig. 9c). Moreover, our results suggest that the positive SIF-GPP relation observed under normal conditions becomes negative under abnormal high temperature conditions during a heat wave (as recently reported by Martini et al., 2021) in regions with soil moisture below  $15 \text{ l m}^{-2}$ , but remains positive in areas with higher soil water content (Fig. 9d).

---

<sup>7</sup> The Quiros-Vargas et al. (EARSeL-2022) study was presented as a conference abstract, and not addressed in more detail, since it was done in the last stage of the PhD program. The major goal of this study was to have an initial notion about how the spatial relation of SIF with soil water content would behave when up-scaled to continental scale.

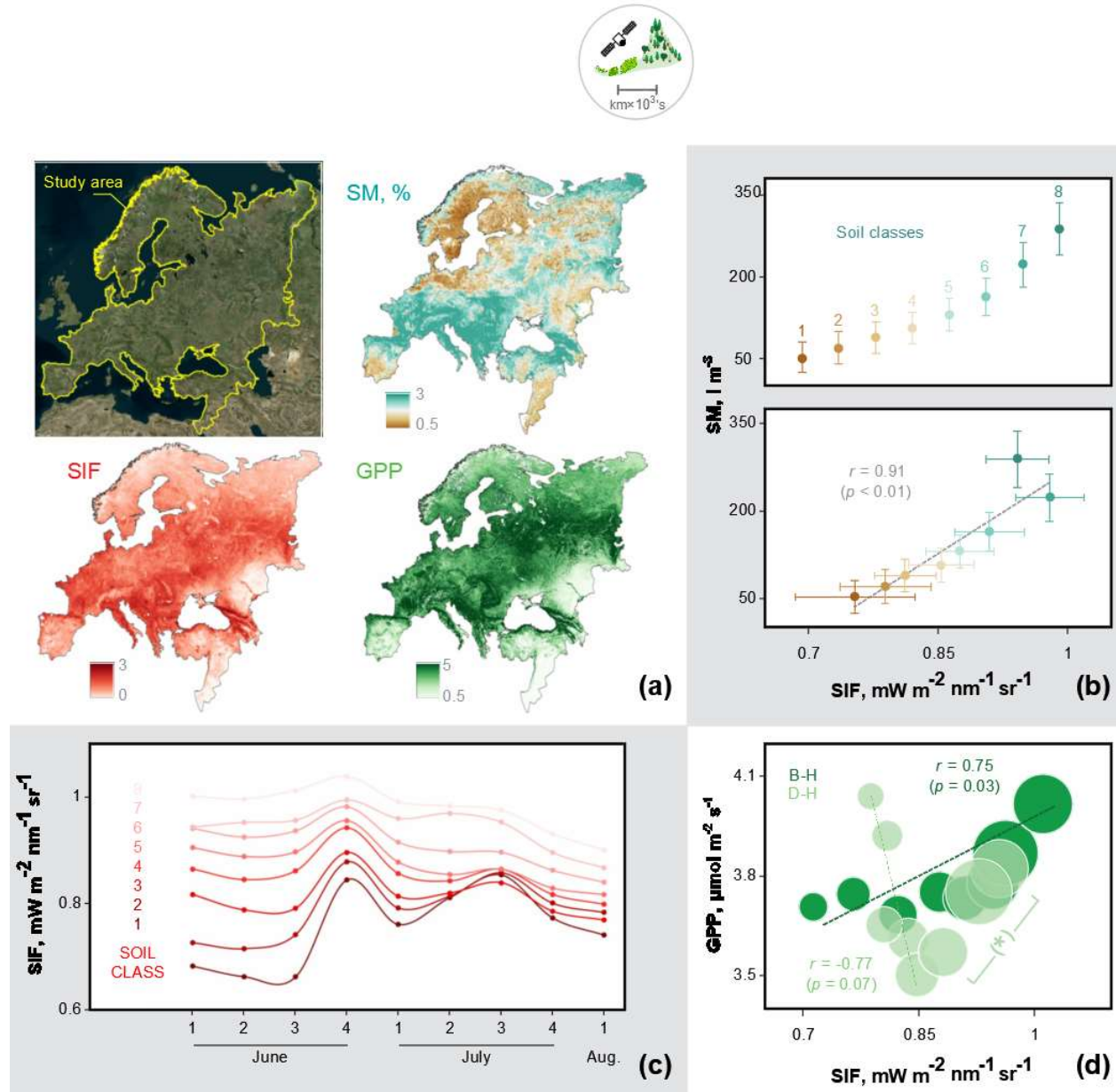


**Figure 9:** Average soil moisture (SM), solar-induced chlorophyll fluorescence (SIF) and gross primary productivity (GPP) maps computed over the study area (yellow boundary) across the nine time points analyzed (a). Values of the soil moisture classes and their correlation with SIF (b). Temporal variation of SIF for each soil moisture class before (B-H, June) and during (D-H, July) the peak of the heatwave (c). B-H (dark green) and D-H (light green) relation of GPP, SIF and soil moisture (circles size; d). (\*) Positive GPP-SIF relation kept D-H in regions with higher SM.

## 1.7 The SIF-scaling issue: importance of downscaling

The spatiotemporal resolution of remote sensing data determines the amount and quality of information that can further be used to assess vegetation functioning. While the spatial resolution is mainly determined by the sensor characteristics and the SSD, the temporal resolution is driven by the amount of data collected across time. In general, proximal-, aerial- and satellite-based information are more suitable to detect changes in the regulatory processes, canopy reflectance and structure and plant morphology, respectively (Fig. 10, based on Gamon et al., 2019). I.e., fine scale remote sensing information (in centimeters and minutes-hours) can capture a wide range of plant responses to stress, from regulatory processes which can potentially be useful for the early (asymptomatic) stress detection, to changes in the pigments composition and leaf angles; whereas lower spatiotemporal resolution information (in m's and days) might not be able to sense subtle changes in physiological process, but still can track changes in the canopy structure and color (reflectance) useful for the assessment of vegetation productivity. Coarser remote sensing information (in the order of kilometers and months to years) can only capture strong alterations on vegetation morphology over regional to global scales, which is generally used to quantify the impact of severe stress, or to study energy exchanges between the surface and atmosphere on the biome level.

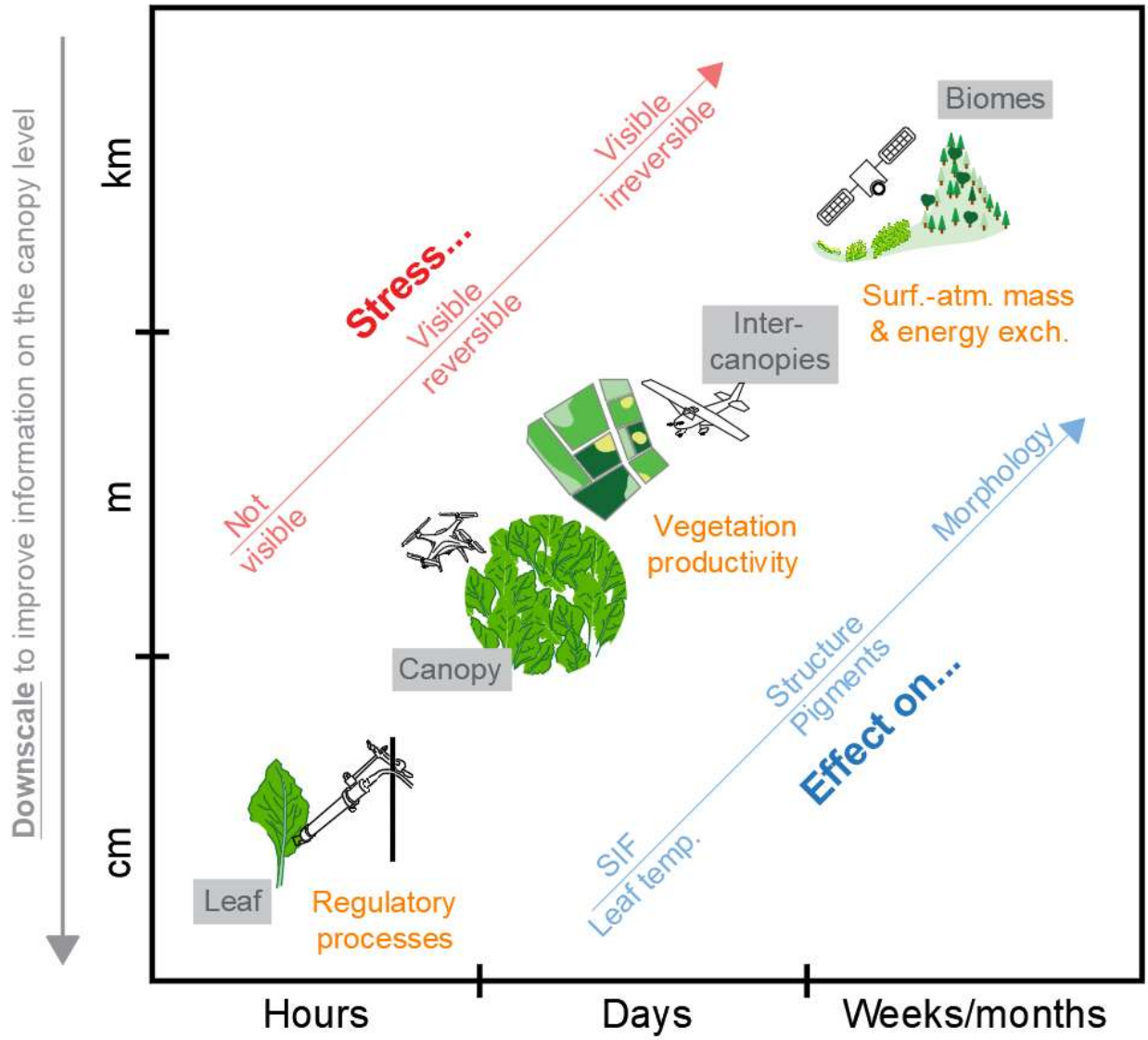


**Figure 10:** Spatial (y-axis, cm to km) and temporal (x-axis, hours to months) scales of ground-, unmanned aerial vehicles (UAV)-, airborne-, and satellite-based information, and the vegetation processes (in orange) for which each scale is particularly more suitable. The importance of downscaling, as well as the types of stress and their effect are presented in grey, red and blue, respectively. The figure is based on Gamon et al. (2019).

SIF information, compared with reflectance- and thermal-based data, is more affected by the scaling issue in the spatial domain. The spatial resolution of SIF products is particularly hindered by technical limitations; e.g., the low intensity of the SIF signal makes it necessary to sense larger areas in order to integrate a signal with high SNR. Consequently the SIF downscaling, herewith understood

as the increase in the spatial resolution, is nowadays of utmost importance within the SIF research community targeting the improvement of the amount and quality of information of SIF imagery. Currently, the SIF downscaling research is generally focused on the use of linear relations between SIF and explanatory variables like the light use efficiency (LUE; Duveiller et al. 2020), land surface temperature (LST) and VIs (Zhang et al. 2020) which were derived from remote sensing at higher spatial resolution. Yet, besides the abovementioned efforts, more flexible SIF-downscaling approaches have to be investigated trying to meet the dynamism of SIF in diverse ecosystems.

In Quiros-Vargas et al. (2022) we propose to consider the use of the fractal theory for SIF-downscaling, whose developer said: *“the success of fractals depend on people being familiar with the basic ideas and pushing them in different directions with more specialized topics”* (Mandelbrot 2012). The theory states that natural phenomena can be described as repetition of patterns (fractal geometry) across spatiotemporal scales. The presence of fractal geometry can be recognized through different mathematical approaches, e.g., based on power laws (PL's; Nagajothi et al., 2021) as addressed in Quiros-Vargas et al. (2022), where we found that the total SIF ( $SIF_{TOT}$ ) of vegetation objects within a 60 ha soybean field followed a PL distribution across spatial scales (1.5, 5, 10 and 15 m pixel<sup>-1</sup>; Fig. 11a). According to the fractal theory this indicates the presence of a fractal geometry composed by patterns where few incidences of high  $SIF_{TOT}$  values contrast with abundant occurrences of small values. We furthermore observed a linear increase and a nearly steady behavior of the dimension and scaling factors of the PLs across scales (Fig. 11b), which can be interpreted as evidence of the scale invariant property of fractals.

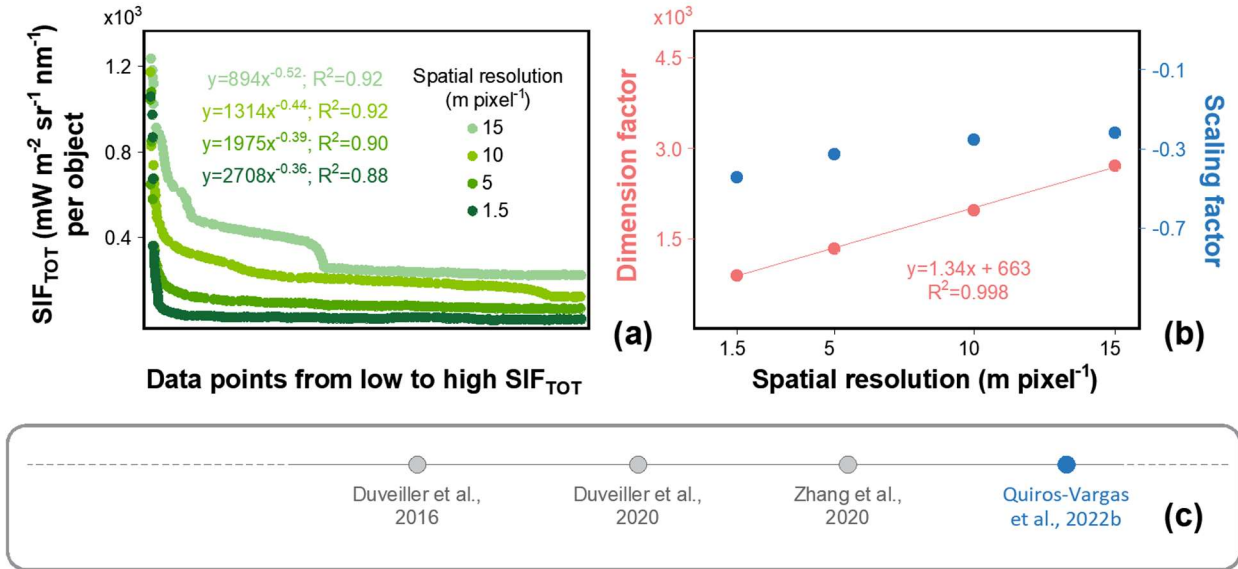


**Figure 11:** Total solar-induced chlorophyll fluorescence ( $SIF_{TOT}$ ) power law (PL) distributions observed at 1.5, 5, 10 and 15  $m\ pixel^{-1}$  spatial scales (a), and the respective dimension and scaling factors (b). Panel (c) shows where the abovementioned study is located among other studies addressing the spatial downscaling of SIF.

Future SIF downscaling efforts in this direction might aim to find explanatory variable(s) that can describe the  $SIF_{TOT}$  distribution through bi-variate SIF PL's. A potential variable could be related to the object geometry properties (like area and perimeter). Special interest has to be paid to the use of the object size as it was found to strongly determine the spatial dependency of near infrared reflectance of vegetation (NIRv; Badgley et al., 2017) data in another contribution of this thesis (Quiros-Vargas et al., EGU-2022). In preliminary analyses we observed that the direct linear relation between  $SIF_{TOT}$  and the average object size becomes a nearly perfect PL if the second variable is inverted (Quiros-Vargas et al., LPS-2022b). This will further be addressed in future studies and is not part of the presented doctoral work.

## 2 Knowledge gain and outlook

In the past two years three review-type publications have summarized the current status of the use of SIF for vegetation monitoring applications from the phenotyping (Mangalraj and Cho, 2022), multiple scale (Bandopadhyay et al., 2020) and historic perspectives (Mohammed et al., 2019). Further, Porcar-Castell et al. (2021) stressed the SIF-photosynthesis link emphasizing the research challenges that yet have to be overcome, i.e. leaf and canopy scattering, atmospheric reabsorption, integration of SIF information from different scales, etc. In this thesis, besides the short review of multiple scale SIF applications provided in the present introduction, new knowledge is provided through individual studies on ground, UAV, airborne and satellite scales. The Figure 11 presents a diagram where this thesis's publications are placed in the general SIF R&D context. This was done in order to represent the contribution of this thesis for the SIF research community.

At ground scale, the knowledge gained about Chlorophyll fluorescence emission of bean at  $e[CO_2]$  helps to improve our understanding about the potential physiological response of key food-security crops to the expected increase in the atmospheric  $[CO_2]$ . In particular, the impact of an augmented concentration of atmospheric  $CO_2$  on the bean plants biomass partitioning was missing in the literature. This knowledge provided in Quiros-Vargas et al. (2021) can help to better understand how specific genotypes of such staple food production could behave in the next decades when the  $[CO_2]$  is expected to constantly increase. Additionally, the genetic variation observed in the bean yield response to  $e[CO_2]$  can support further studies about productivity breeding (Ainsworth and Long, 2021). For instance, genotypes like the one reported in our investigation as the most positively responsive to increments in  $[CO_2]$  can be of interest for bean breeders in the future.

The review published about UAV-based systems for SIF retrieval (Quiros-Vargas et al., 2020a) was cited in multiple studies within the last two years, including investigations addressing the development of further aerial platforms for the assessment of SIF, e.g., the one published by Chang et al., 2020. This can suggest the relevance of this publication for the SIF research community, for which the UAV-based SIF retrieval has great potential as a cal/val instrument for future satellite missions providing information about SIF (e.g. the fluorescence explorer, FLEX, mission from ESA). Besides the remote sensing research area, our study was also cited in studies touching a variety of topics like chlorophyll fluorescence

physiology, plant disease monitoring, horticulture and field phenotyping. It is worth noting that most of the challenges and limitations of retrieving SIF from UAV platforms mentioned in our study are still valid.

The main contribution on the airborne scale (Quiros-Vargas et al., in revision at PNAS-Nexus) is among the first three studies analyzing in high resolution the effect of soil properties and water content on SIF (also see Hebel et al., 2018 and Damm et al., 2022). The spatial correlations reported between SIF and PAW with a multiple year and crop dataset were formerly unknown. Such knowledge provided in Quiros-Vargas et al. (in revision at PNAS-Nexus) can encourage further investigations addressing SIF as a potential real-time indicator for crop water demands, due to its direct link with the first physiological processes activated in response to water shortage. This makes SIF superior to thermal- and reflectance-based remote sensing information, since they will react hours or days later when the plant has already suffered more severe water stress symptoms, e.g., pigments degradation and morphology alterations. Such advantage of SIF can be used as the base for the development of precision water management, aiming scheduled irrigation events only in specific sites where it is required. Moreover, the numerical characterization of the spatial SIF-PAW relation provided in Quiros-Vargas et al. (in revision at PNAS-Nexus) helps to improve our understanding on how ground- and in the future UAV-based SIF information can be translated into crop water status; this is relevant since airborne data acquisition is expensive and not likely to be used for crop water management on a daily basis at farm level.

The analysis reported on the satellite-scale (Quiros-Vargas et al., EARSeL-2022) provides complementary information to recent studies in which the SIF-GPP relation was investigated on spatial higher resolution data (e.g. as Martini et al., 2021, did on the ground level). With our study we added knowledge to Martini et al.'s (2021) conclusions by contextualizing where the SIF-GPP relation breakdown may occur or not at continental scale during heat stress periods. In Quiros-Vargas et al., EARSeL-2022 we highlight the need of including soil moisture information to better understand the relation between SIF and GPP, a relevant aspect for global scale estimations of photosynthesis.

The information provided in the airborne- and satellite-scale studies can be relevant for the climate and land surface modeling research community, due to the key role of vegetation in the water and carbon cycles. In particular, SIF data has a great potential to support the estimation of GPP in land surface models that consider plant growth. Moreover, SIF can be used to recalibrate and parametrize functions and sub-components in the algorithms, e.g., those related to soil moisture stress. Another potential application of SIF in climate modeling is to constrain the evapotranspiration (ET) component, since both processes (SIF and ET) have the stomata closure as a common factor. However, to achieve such an advanced point it is necessary to first analyze remote sensing and ground (e.g., eddy covariance) measurements integrated in radiative transfer models (Jonard et al., 2020). In order to learn more about how SIF research advances can help the climate- and land surface-modeling communities, the results of the investigations addressing the relation between SIF and soil water content at airborne and satellite scales were presented at the European Meteorology Society conference this year (Quiros-Vargas et al., EMS-2022), being this a topic of high interest for the climate modeling community.

SIF downscaling studies have normally been focused on linear approaches using direct relations of SIF with explanatory variables. Therefore, there is a knowledge gap in using non-linear methods to address the SIF scaling issue. With the intention contributing to start filling this knowledge gap, we proposed a new direction based on a non-linear principle, which can be considered in the development of future SIF downscaling approaches. What we proposed was the potential application of the fractal theory to fragment the coarse SIF pixel into the  $SIF_{TOT}$  of smaller objects within its area of influence. We proposed it based on the statement that (unlike reflectance based information) the SIF signal is aggregated across scales, and therefore the  $SIF_{TOT}$  of one single coarse pixel is equal to the sum of the SIF emitted by all objects within the same pixel. Thus, we aimed to open a new perspective to increase the spatial resolution of aerial to satellite SIF products based on the distribution of geometric characteristics that are easily computed from imagery of any vegetation type.

MAIN CONTRIBUTIONS	TOPIC
[1] = Quiros-Vargas et al., 2020a	UAV-based SIF retrieval: state of the art
[2] = Quiros-Vargas et al., 2021	Ground ChlF information for field phenotyping
[3] = Quiros-Vargas et al., in revision at PNAS-Nexus	SIF-PAW spatial relation
[4] = Quiros-Vargas et al., 2022	Fractal geometry fro SIF-downscaling
[5] = Quiros-Vargas et al., AGU-2020	SIF-soil_characteristics spatial relation
[6] = Quiros-Vargas et al., EGU-2022	Spatial dependency of SIF-emitting objects (of interest for downscaling studies)
[7] = Quiros-Vargas et al., LPS-2022a	SIF-PAW spatial relation + upscaled (satellite) initial analysis
[8] = Quiros-Vargas et al., LPS-2022b	Quiros-Vargas et al., LPS-2022b
[9] = Quiros-Vargas et al., EARSeL-2022	SIF-PAW spatial relation + upscaled (satellite) initial analysis + GPP analysis
[10] = Quiros-Vargas et al., EMS-2022	Disseminating SIF-PAW relation findings to the climate modeling community

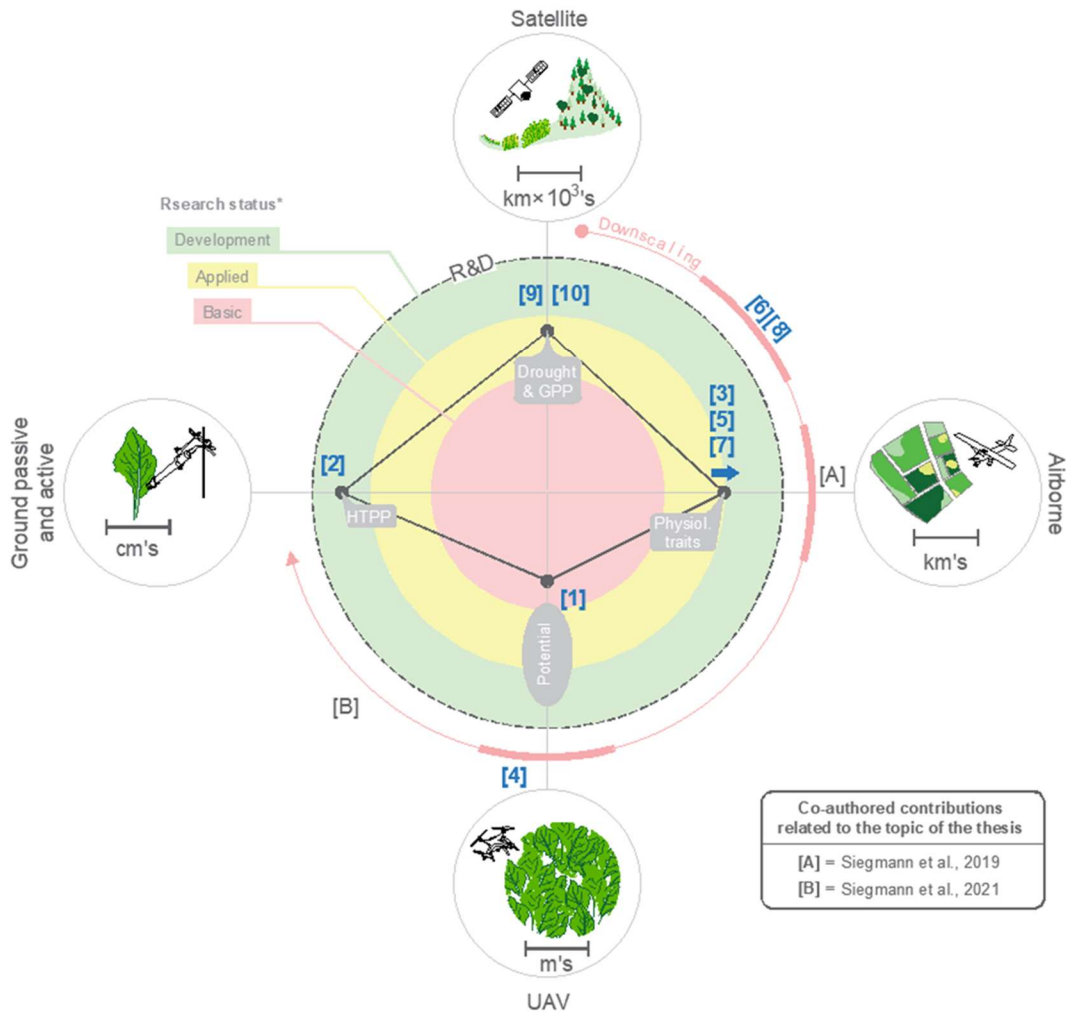


**Figure 12:** Location of this thesis’s studies within the general context of solar-induced chlorophyll fluorescence (SIF) research at ground-, unmanned aerial vehicles (UAV)-, airborne- and satellite-scales. The distinction between ‘development’ (green ring), ‘applied’ (yellow ring) and ‘basic’ (red circle) R&D stages is based on the Organization for Economic Co-operation and Development (OECD) classification. The role of downscaling is highlighted in the concentric red line. The main first-author contributions of this thesis are presented in blue numbers in brackets, whereas two co-authored contributions (related to the topic of the thesis) are presented in grey letters in brackets.

### 3 References <sup>8</sup>

- [1] H. Aasen, A. Burkart, A. Bolten, G. Bareth, Generating 3D hyperspectral information with lightweight UAV snapshot cameras for vegetation monitoring: From camera calibration to quality assurance. *I SPRS J. Photogramm. Remote Sens.* 108, 245-259 (2015).
- [2] T. Adão, J. Hruška, L. Pádua, J. Bessa, E. Peres, R. Morais, J.J. Sousa, Hyperspectral Imaging: A Review on UAV-Based Sensors, Data Processing and Applications for Agriculture and Forestry. *Remote Sens.* 9(11), 1110 (2017).
- [3] R. Akkerman, P. Farahani, M. Grunow, Quality, safety and sustainability in food distribution: a review of quantitative operations management approaches and challenges. *OR Spectrum* 32, 863-904 (2010).
- [4] P. Andrade-Sanchez, M.A. Gore, J.T. Heun, K.R. Thorp, A.E. Carmo-Silva, A.N. French, M.E. Salvucci, J.W. White, Development and evaluation of a field-based high-throughput phenotyping platform. *Funct. Plant Biol.* 41(1), 68-79 (2014).
- [5] G. Badgley, C.B. Field, J.A. Berry, Canopy near-infrared reflectance and terrestrial photosynthesis. *Sci. Adv.* 3, e1602244 (2017).
- [6] S. Bandopadhyay, A. Rastogi, R. Juszczak, Review of Top-of-Canopy Sun-Induced Fluorescence (SIF) Studies from Ground, UAV, Airborne to Spaceborne Observations. *Sensors* 20(4), 1144 (2020).
- [7] J. Bendig, C. Y. Chang, N. Wang, J. Atherton, Z. Malenovský and U. Rascher, “Measuring Solar-Induced Fluorescence from Unmanned Aircraft Systems for Operational Use in Plant Phenotyping and Precision Farming” in *Proceedings of the 38th IEEE International Geoscience and Remote Sensing Symposium (IGARSS, Brussels, Belgium, 2021)*, pp. 1921-1924.
- [8] K. Berger, M. Kycko, M. Celesti, J. Verrelst, M. Machwitz, U. Rascher, I. Herrmann, V.S. Paz, S. Fahrner, R. Pieruschka, E.T. Gormus, M. Gerhards, A. Halabuk, C. Atzberger, C. van der Tol, M. Rossini, M. Foerster, B. Siegmann, G. Tagliabue, T. Hank, H. Aasen, I. Pocas, M. Garcia, S.C. Kefauver, S. Bandopadhyay, A. Damm, E. Tomelleri, O. Rozenstein, L. Filchev, G. Stancile, M. Schlerf, Stress detection in agriculture with focus on the synergistic use of different optical domains: a review. *Remote Sens. Environ.* 280, 113198 (2022).
- [9] B. Biswal, J.K. Pandey, “Development of Chloroplast: Biogenesis, Senescence, and Regulations” in *Handbook of Photosynthesis*, M. Pessarakli, Ed. (CRC Press, 2016), pp. 75-92.
- [10] G. Camps-Valls, “Machine learning in remote sensing data processing” in *Proceedings of the 38th IEEE International Workshop on Machine Learning for Signal Processing (MLSP, Grenoble, France, 2009)*, pp. 1-6.
- [11] E. Chakhvashvili, B. Siegmann, O. Muller, J. Verrelst, J. Bendig, T. Kraska, U. Rascher, Retrieval of Crop Variables from Proximal Multispectral UAV Image Data Using PROSAIL in Maize Canopy. *Remote Sens.* 14, 1247 (2022).

---

<sup>8</sup> The citations of the first author publications associated to this doctoral thesis are highlighted in brackets and bold characters (at the beginning of each respective reference).

- [12] C.Y. Chang, R. Zhou, O. Kira, S. Marri, J. Skovira, L. Gu, Y. Sun, An Unmanned Aerial System (UAS) for concurrent measurements of solar-induced chlorophyll fluorescence and hyperspectral reflectance toward improving crop monitoring. *Agric. For. Meteorol.* 294, 108145 (2020).
- [13] T. Chu, M.J. Starek, M.J. Brewer, S.C. Murray, L.S. Pruter, Assessing Lodging Severity over an Experimental Maize (*Zea mays* L.) Field Using UAS Images. *Remote Sens.* 9(9), 923 (2017).
- [14] T.H. Chung, M.R. Clement, M.A. Day, K.D. Jones, D. Davis, M. Jones, Live-fly, large-scale field experimentation for large numbers of fixed-wing UAVs” in *Proceedings of the IEEE International Conference on Robotics and Automation (ICRA, Sweden, 2016)*, pp. 1255-1262.
- [15] S. Cogliati, M. Celesti, I. Cesana, F. Miglietta, L. Genesio, T. Julitta, D. Schuettemeyer, M. Drusch, U. Rascher, P. Jurado, R. Colombo. A Spectral Fitting Algorithm to Retrieve the Fluorescence Spectrum from Canopy Radiance. *Remote Sens.* 11, 1840 (2019).
- [16] S. Cogliati, W. Verhoef, S. Kraft, N. Sabater, L. Alonso, J. Vicent, J. Moreno, M. Drusch, R. Colombo, Retrieval of sun-induced fluorescence using advanced spectral fitting methods. *Remote Sens. Environ.* 169, 344–357 (2015).
- [17] A. Damm, E. Paul-Limoges, E. Haghghi, C. Simmer, F. Morsdorf, F.D. Schneider, C. van der Tol, M. Migliavacca, U. Rascher, Remote sensing of plant-water relations: An overview and future perspectives. *J. Plant Physiol.* 277, 3-19 (2018).
- [18] A. Damm, S. Cogliati, R. Colombo, L. Fritsche, A. Genangeli, L. Genesio, J. Hanus, A. Peressotti, P. Rademske, U. Rascher, D. Schuettemeyer, B. Siegmann, J. Sturm, F. Miglietta, Response times of remote sensing measured sun-induced chlorophyll fluorescence, surface temperature and vegetation indices to evolving soil water limitation in a crop canopy. *Remote Sens. Environ.* 273, 112957 (2022).
- [19] J. Dash, P.J. Curran, The MERIS terrestrial chlorophyll index. *Int. J. Remote Sens.* 25(23), 5403-5413 (2004).
- [20] S. De Cannière, H. Vereecken, P. Defourny, F. Jonard, Remote Sensing of Instantaneous Drought Stress at Canopy Level Using Sun-Induced Chlorophyll fluorescence and Canopy Reflectance. *Remote Sens.* 14, 2642 (2022).
- [21] L. Deng, Z. Mao, X. Li, Z. Hu, F. Duan, Y. Yan, UAV-based multispectral remote sensing for precision agriculture: A comparison between different cameras. *ISPRS J. Photogramm. Remote Sens.* 146, 124-136 (2018).
- [22] S.F. Di Gennaro, E. Battiston, S. Di Marco, O. Facini, A. Matese, M. Nocentini, A. Palliotti, L. Mugnai, Unmanned Aerial Vehicle (UAS)-based remote sensing to monitor grapevine leaf stripe disease within a vineyard affected by esca complex. *Phytopathol. Mediterr.* 55(2), 262-275 (2016).
- [23] R. Doughty, P. Köhler, C. Frankenberg, T.S. Magney, X. Xiao, Y. Qin, X. Wu, B. Moore, TROPOMI reveals dry-season increase of solar-induced chlorophyll fluorescence in the Amazon forest. *Proc Natl Acad Sci USA (PNAS)* 116(44), 22393-22398 (2019).

- [24] G. Duveiller, F. Filippini, S. Walther, P. Köhler, C. Frankenberg, L. Guanter, A. Cescatti, A spatially downscaled sun-induced fluorescence global product for enhanced monitoring of vegetation productivity. *Earth Syst Sci Data* 12, 1101–1116 (2020).
- [25] European Space Agency (2022a) “Photosynthesis Report” ESA. Photosynthetic-Proxy (Photoproxy, report No. 3).
- [26] European Space Agency (2022c) “Flexsense Campaign 2018” ESA. Flexsense (final report).
- [27] European Space Agency (2022d) “Flexsense Campaign 2019” ESA. Flexsense (final report).
- [28] Food and Agricultural Organization of the United Nations (FAO) (2018) The future of food and agriculture: alternative pathways to 2050. Available at fao.org. Accessed July 26, 2022. *Remote Sens.* 14, 2642 (2022).
- [29] J. Flexas, J.M. Escalona, S. Evain, J. Gulías, I. Moya, C.B. Osmond, H. Medrano, Steady-state chlorophyll fluorescence (Fs) measurements as a tool to follow variations of net CO<sub>2</sub> assimilation and stomatal conductance during water-stress in C<sub>3</sub> plants. *Physiol. Plant.* 114, (2002).
- [30] C. Frankenberg, P. Köhler, T.S. Magney, S. Geier, P. Lawson, M. Schwochert, J. McDuffie, D.T. Drewry, R. Pavlick, A. Kuhnert, The Chlorophyll fluorescence Imaging Spectrometer (CFIS), mapping far red fluorescence from aircraft. *Remote Sens. Environ.* 217, 523-536 (2018).
- [31] J. Gamon, G. Hmimina, G. Miao, K. Guan, K. Springer, R. Wang, R. Yu, H. Gholizadeh, R. Moore, E. Walter-Shea, T. Arkebauer, A. Suyker, T. Franz, B. Wardlow, D. Wedin. “Imaging Spectrometry and Fluorometry in Support of Flex: What Can We Learn from Multi-Scale Experiments?” in *Proceedings of the 38th IEEE International Geoscience and Remote Sensing Symposium* (IGARSS, Valencia, Spain, 2018), pp. 3931-3934.
- [32] J.A. Gamon, B. Somers, Z. Malenovský, E.M. Middleton, U. Rascher, M.E. Schaepman, “Assessing Vegetation Function with Imaging Spectroscopy” in *Surveys in Geophysics*, M. Rycroft, Ed. (Springer, 2019), pp. 489-513.
- [33] J.A. Gamon, J. Penuelas, C.B. Field, A narrow-waveband spectral index that tracks diurnal changes in photosynthetic efficiency. *Remote Sens. Environ.* 41, 35-44 (1992).
- [34] D. Gautam, A. Lucieer, J. Bendig and Z. Malenovský, Footprint Determination of a Spectroradiometer Mounted on an Unmanned Aircraft System. *IEEE Trans. Geosci. Remote Sens.* 58(5), 3085-3096 (2020).
- [35] M. Gerhards, M. Schlerf, K. Mallick, T. Udelhoven, Challenges and Future Perspectives of Multi-/Hyperspectral Thermal Infrared Remote Sensing for Crop Water-Stress Detection: A Review. *Remote Sens.* 11(10), 1240 (2019).
- [36] A.A. Gitelson, Wide Dynamic Range Vegetation Index for Remote Quantification of Biophysical Characteristics of Vegetation. *J. Plant Physiol.* 161(2), 165-173 (2004).
- [37] J.F.R. Gower, L. Brown, G.A. Borstad, Observation of chlorophyll fluorescence in west coast waters of Canada using the MODIS satellite sensor. *Can. J. Remote Sens.* 30, 17–25 (2004).

- [38] J.F.R. Gower, R. Doerer, G.A. Borstad, Interpretation of the 685 nm peak in water-leaving radiance spectra in terms of fluorescence, absorption and scattering, and its observation by MERIS. *Int. J. Remote Sens.* 20, 1771–1786 (1999).
- [39] L. Guanter, C. Bacour, A. Schneider, I. Aben, T.A. van Kempen, F. Maignan, C. Retscher, P. Köhler, C. Frankenberg, J. Joiner, Y. Zhang, The TROPOSIF global sun-induced fluorescence dataset from the Sentinel-5P TROPOMI mission. *Earth Syst. Sci. Data* 13, 5423–5440 (2021).
- [40] L. Guanter, I. Aben, P. Tol, J.M. Krijger, A. Hollstein, P. Köhler, A. Damm, J. Joiner, C. Frankenberg, J. Landgraf, Potential of the TROPOspheric Monitoring Instrument (TROPOMI) onboard the Sentinel-5 Precursor for the monitoring of terrestrial chlorophyll fluorescence. *Atmos. Meas. Tech.* 8, 1337–1352 (2015).
- [41] L. Guanter “New Algorithms for Atmospheric Correction and Retrieval of Biophysical Parameters in Earth Observation”. Ph.D. Thesis, Universitat de València, Valencia, Spain, 2007.
- [42] InfoRow “Automatic detection of sugar cane planting lines.” Available at [HTTps://inforow.com.b](https://inforow.com.b) (accessed January 14, 2022).
- [43] JB Hyperspectral Devices. Available at [HTTps://www.jb-hyperspectral.com/](https://www.jb-hyperspectral.com/) (accessed January 18, 2022).
- [44] A. Jablonski, E.L. Kruger, P.A. Townsend, “Comparative responses of solar-induced fluorescence (SIF) and leaf photosynthetic parameters to short term atmospheric CO<sub>2</sub> enrichment” in *Proceedings of the American Geophysical Union Fall Meeting (AGU, New Orleans, USA, 2017)*.
- [45] J. Joiner, L. Guanter, R. Lindstrot, M. Voigt, A.P. Vasilkov, E.M. Middleton, K.F. Huemmrich, Y. Yoshida, C. Frankenberg, Global monitoring of terrestrial chlorophyll fluorescence from moderate-spectral-resolution near-infrared satellite measurements: Methodology, simulations, and application to GOME-2. *Atmos. Meas. Tech.* 6, 2803–2823 (2013).
- [46] J. Joiner, Y. Yoshida, A.P. Vasilkov, Y. Yoshida, L.A. Corp, E.M. Middleton, First observations of global and seasonal terrestrial chlorophyll fluorescence from space. *Biogeosciences* 8, 637–651 (2011).
- [47] F. Jonard, A.F. Feldman, D.J.S. Gianotti, D. Entekhabi, Observed Water- and Light-Limitation Across Global Ecosystems. *European Geophysical Union (EGU) [Preprint]* (2022). <https://doi.org/10.5194/bg-2022-25> (accessed 28 July 2022).
- [48] F. Jonard, S. De Cannière, N. Brüggemann, P. Gentine, D.J.S. Gianotti, G. Lobet, D.G. Miralles, C. Montzka, B.R. Pagán, U. Rascher, H. Vereecken, Value of sun-induced chlorophyll fluorescence for quantifying hydrological states and fluxes: Current status and challenges. *Agric. For. Meteorol.* 291, 108088 (2020).
- [49] B. Keller, I. Vass, S. Matsubara, K. Paul, C. Jedmowski, R. Pieruschka, L. Nedbal, U. Rascher, O. Muller, Maximum fluorescence and electron transport kinetics determined by light-induced fluorescence transients (LIFT) for photosynthesis phenotyping. *Photosynth. Res.* 140, 221–233 (2019).

- [50] B.K. Kenduiywo, M.R. Carter, A. Ghosh, R.J. Hijmans, Evaluating the quality of remote sensing products for agricultural index insurance. *PLoS One* 6(10), e0258215 (2021).
- [51] N. Kirchgessner, F. Liebisch, K. Yu, J. Pfeifer, M. Friedfli, A. Hund, A. Walter, The ETH field phenotyping platform FIP: a cable-suspended multi-sensor system. *Funct. Plant Biol.* 44, 154-168 (2016).
- [52] S. Khorram, F.H. Koch, C.F. van der Wiele, S.A.C. Nelson, "Introduction" in *Remote Sensing*, S. Khorram, F.H. Koch, C.F. van der Wiele, S.A.C. Nelson, Eds. (Springer Cham, 2012), 1-15 pp.
- [53] O. Knopf, A. Castro, J. Quiros-Vargas, L. Zinken, D. Lenzen, S. Markwitz, M. Quarten, A. Steier, E. Kleist, H. Poorter, R. Pude, U. Rascher, O. Muller, Effects of free-air CO<sub>2</sub> enrichment (FACE) on photosynthesis and growth of winter wheat. In progress.
- [54] F. Kogan, "Remote Sensing for Food Security" (Springer Cham, 2019), 255 pp.
- [55] P. Köhler, C. Frankenberg, T.S. Magney, L. Guanter, J. Joiner, J. Landgraf, Global Retrievals of Solar-Induced Chlorophyll fluorescence With TROPOMI: First Results and Intersensor Comparison to OCO-2. *Geophys. Res. Lett.* 45, 10–456 (2018).
- [56] Z.S. Kolber, O. Prasil, P.G. Falkowski, Measurements of variable chlorophyll fluorescence using fast repetition rate techniques: defining methodology and experimental protocols. *BBA* 1367, 88–106 (1998).
- [57] F.J. Krieglner, W.A. Malila, R.F. Nalepka, W. Richardson, "Preprocessing transformations and their effects on multispectral recognition" in *Proceedings of the Sixth International Symposium on Remote Sensing of Environment* (Ann Arbor, Michigan, USA, 1969).
- [58] C. Lum, M. Mackenzie, C. Shaw-Feather, E. Luker, M. Dunbabin, "Multispectral Imaging and Elevation Mapping from an Unmanned Aerial System for Precision Agriculture Applications", in *Proceedings of the 13th International Conference on Precision Agriculture* (ICPA, St. Louis, Missouri, USA, 2016).
- [59] Lemnatec. "Field Scanalyzer: automated outdoor phenotyping." Available at [HTPPS://www.lemnatec.com/](https://www.lemnatec.com/) (accessed November 20, 2019).
- [60] X. Li, J. Xiao, TROPOMI observations allow for robust exploration of the relationship between solar-induced chlorophyll fluorescence and terrestrial gross primary production, *Remote Sens. Environ.* 268, 112748 (2022).
- [61] H.Q. Liu, A.R. Huete, "A feedback based modification of the NDVI to minimize canopy background and atmospheric noise. *IEEE Trans. Geosci. Remote Sens.* 33(2), 481-486 (1995).
- [62] K. Maxwell, G.N. Johnson, Chlorophyll fluorescence—a practical guide. *J. Exp. Bot.* 51(345), 659-668 (2000).
- [63] J. Mäkynen, H. Saari, C. Holmlund, R. Mannila, T. Antila, "Multi- and hyperspectral UAV imaging system for forest and agriculture applications" in *Proceedings of the Society of Photographic Instrumentation Engineers* (SPIE, 837409, Baltimore, Maryland, USA, 2012).
- [64] B. Mandelbrot, "A word and a book: 'fractal' and the fractal geometry of nature" in *The fractalist: memoir of a maverick scientist*, (Knopf Doubleday Publishing Group, 2012), pp. 264-278.

- [65] S. Manfreda, M.F. McCabe, P.E. Miller, R. Lucas, V. Pajuelo Madrigal, et al., On the Use of Unmanned Aerial Systems for Environmental Monitoring. *Remote Sens.* 10, 641 (2018).
- [66] P. Mangalraj, B.K. Cho, Recent trends and advances in hyperspectral imaging techniques to estimate solar induced fluorescence for plant phenotyping. *Ecol. Indic.* 137, 108721 (2022).
- [67] D. Martini, K. Sakowska, G. Wohlfahrt, J. Pacheco-Labrador, C. van der Tol, A. Porcar-Castell, T.S. Magney, A. Carrara, R. Colombo, T.S. El-Madany, R. Gonzalez-Cascon, M. Pilar Martín, T. Julitta, G. Moreno, U. Rascher, M. Reichstein, M. Rossini, M. Migliavacca, Heatwave breaks down the linearity between sun-induced fluorescence and gross primary production. *New Phytol.* 233, 2415-2428 (2021).
- [68] A. Matese, , P. Toscano, , S.F. Di Gennaro, , L. Genesio, , F.P. Vaccari, , J. Primicerio, , C. Belli, , A. Zaldei, , R. Bianconi, , B. Gioli, Intercomparison of UAV, Aircraft and Satellite Remote Sensing Platforms for Precision Viticulture. *Remote Sens.* 7, 2971-2990 (2015).
- [69] A.E. Maxwell, T.A. Warner, F. Fang, Implementation of machine-learning classification in remote sensing: an applied review. *Int. J. Remote Sens.* 39(9), 2784-2817 (2017).
- [70] A.G. Mengistu, G.M. Tsidu, G. Koren, M.L. Kooreman, K.F. Boersma, T. Tagesson, J. Ardö, Y. Nouvellon, W. Peters, Sun-induced fluorescence and near-infrared reflectance of vegetation track the seasonal dynamics of gross primary production over Africa. *Biogeosciences* 18, 2843-2857 (2021).
- [71] M. Meroni, L. Busetto, R. Colombo, L. Guanter, J. Moreno, W. Verhoef. Performance of Spectral Fitting Methods for vegetation fluorescence quantification. *Remote Sens. Environ.* 114 (2), 363-374 (2010).
- [72] M. Meroni, M. Rossini, L. Guanter, L. Alonso, U. Rascher, R. Colombo, J. Moreno, Remote sensing of solar-induced chlorophyll fluorescence: Review of methods and applications. *Remote Sens. Environ.* 113, 2037–2051 (2009).
- [73] G.H. Mohammed, R. Colombo, E.M. Middleton, U. Rascher, C. van der Tol, L. Nedbal, Y. Goulas, O. Pérez-Priego, A. Damm, M. Meroni, J. Joiner, S. Cogliati, W. Verhoef, Z. Malenovský, J-P. Gastellu-Etchegorry, J.R. Miller, L. Guanter, J. Moreno, I. Moya, J.A. Berry, C. Frankenberg, P.J. Zarco-Tejada, Remote sensing of solar-induced chlorophyll fluorescence (SIF) in vegetation: 50 years of progress. *Remote Sens. Environ.* 231, 111177 (2019).
- [74] O. Muller, B. Keller, L. Zimmermann, C. Jedmowski, E. Kleits, V. Pingle, K. Acerbon, N. Zendonadi dos Santos, A. Steier, L. Freiwald, I. Munoz-Fernandez, N. Wilke, T. Kraska, R. Pieruschka, U. Schurr, U. Rascher. "Field phenotyping and an example of proximal sensing of photosynthesis under elevated CO<sub>2</sub>" in *Proceedings of the 38th IEEE International Geoscience and Remote Sensing Symposium (IGARSS, Valencia, Spain, 2018)*, pp. 8252-8254.
- [75] R. Näsi, E. Honkavaara, P. Lyytikäinen-Saarenmaa, M. Blomqvist, P. Litkey, T. Hakala, N. Viljanen, T. Kantola, T. Tanhuanpää, M. Holopainen, Using UAV-Based Photogrammetry and Hyperspectral Imaging for Mapping Bark Beetle Damage at Tree-Level. *Remote Sens.* 7, 15467-15493 (2015).

- [76] O. Nevalainen, E. Honkavaara, S. Tuominen, N. Viljanen, T. Hakala, X. Yu, J. Hyyppä, H. Saari, I. Pölönen, N.N. Imai, A.M.G. Tommaselli, Individual Tree Detection and Classification with UAV-Based Photogrammetric Point Clouds and Hyperspectral Imaging. *Remote Sens.* 9(3), 185 (2017).
- [77] C.Y.N. Norasma, M.A. Fadzilah, N.A. Rolsin, Z.W.N. Zanariah, Z. Tarmidi, F.S. Candra, “Unmanned Aerial Vehicle Applications in Agriculture” in *Proceedings of the 1<sup>st</sup> South Aceh International Conference on Engineering and Technology* (SAICOET, Kabupaten Aceh Selatan, Indonesia, 2019), 012063.
- [78] B. Osmond, W.S. Chow, R. Wyber, A. Zavafer, B. Keller, B.J. Pogson, S.A. Robinson, Relative functional and optical absorption cross-sections of PSII and other photosynthetic parameters monitored in situ, at a distance with a time resolution of a few seconds, using a prototype light-induced fluorescence transient (LIFT) device. *Funct. Plant Biol.* 44, 985-1006 (2017).
- [79] C. Panigada, et al., Fluorescence, PRI and canopy temperature for water stress detection in cereal crops. *Int. J. Appl. Earth Obs. Geoinf.* 30, 167-178 (2014).
- [80] Phenospex. “FieldScan High-Throughput Field Phenotyping.” Available at [HTPPs://phenospex.com/](https://phenospex.com/) (accessed November 20, 2019).
- [81] J.A. Plascyk, The MK II Fraunhofer line discriminator (FLD-II) for airborne and orbital remote sensing of solar-stimulated luminescence. *Opt. Eng.* 14, 339-346 (1975).
- [82] A. Porcar-Castell, et al., Chlorophyll a fluorescence illuminates a path connecting plant molecular biology to Earth-system science. *Nat. Plants* 7, 998-1009 (2021).
- [83] A. Porcar-Castell, et al., E. Tyystjärvi, J. Atherton, C. van der Tol, J. Flexas, E.E. Pfündel, J. Moreno, C. Frankenberg, J.A. Berry, Linking chlorophyll a fluorescence to photosynthesis for remote sensing applications: mechanisms and challenges. *J. Exp. Bot.* 65(15), 4065-4095 (2014)
- [84] A.B. Potgieter, J. Watson, M. Eldridge, K. Laws, B. George-Jaeggli, C. Hunt, A. Borrell, E. Mace, S.C. Chapman, D.R. Jordan, and G.L. Hammer, “Determining crop growth dynamics in sorghum breeding trials through remote and proximal sensing technologies” in *Proceedings of the 38th IEEE International Geoscience and Remote Sensing Symposium* (IGARSS, Valencia, Spain, 2018), pp. 8244-8247.
- [85] P. Psirofonis, V. Samaritakis, P. Eliopoulos, Use of Unmanned Aerial Vehicles for Agricultural Applications with Emphasis on Crop Protection: Three Novel Case-Studies. *J. Agric. Sci. Technol.* 5(1), 30-39 (2017).
- [86] **[Quiros-Vargas et al., 2022]** J. Quiros-Vargas, B. Siegmann, A. Damm, R. Wang, J. Gamon, V. Krieger, B.S.D. Sagar, O. Muller, U. Rascher, “Fractal Geometry and the Downscaling of Sun-induced Chlorophyll fluorescence Imagery” in *Encyclopedia of Mathematical Geosciences*, B.S. Daya Sagar, Q. Cheng, J. McKinley, F. Agterberg, Eds. (Springer Nature, 2022).
- [87] **[Quiros-Vargas et al., in revision at PNAS-Nexus]** J. Quiros-Vargas, C. Brogi, A. Damm, B. Siegmann, P. Rademske, V. Burchard, V. Krieger, M. Schmidt, J. Hanuš, L. Weihermueller, O. Mueller, U. Rascher, Spatial relation between the Solar-Induced chlorophyll

- fluorescence (SIF) and the Plant Available Water (PAW) in the root zone: an insight in high resolution. *Proc. Natl. Acad. Sci. U.S.A. (PNAS)-NEXUS*, in revision.
- [88] **[Quiros-Vargas et al., EARSeL-2022]** J. Quiros-Vargas, B. Siegmann, A. Damm, C. Brogi, P. Köhler, R. Van Hoolst, D. Martini, O. Muller, U. Rascher, “Solar-induced chlorophyll fluorescence (SIF) relation with soil moisture (SM) and gross primary productivity (GPP) at European scale in a heat wave” in *Proceedings of the European Association of Remote Sensing Laboratories (EARSeL, Potsdam, Germany, 2022)*.
- [89] **[Quiros-Vargas et al., EGU-2022]** J. Quiros-Vargas, B. Siegmann, A. Damm, V. Krieger, O. Muller, U. Rascher, “Spatial dependency of Solar-induced Chlorophyll fluorescence (SIF)-emitting objects in the footprint of a Fluorescence EXplorer (FLEX) pixel: a SIF-downscaling perspective” in *Proceedings of the European Geophysical Union (EGU, Vienna, Austria, 2022)*.
- [90] **[Quiros-Vargas et al., LPS-2022a]** J. Quiros-Vargas, C. Brogi, A. Damm-Reiser, B. Siegmann, P. Redemske, V. Burchard-Levine, V. Krieger, L. Weihermueller, O. Mueller, U. Rascher, “Spatial relation between Sun-induced Chlorophyll fluorescence (SIF) and the Plant Available Water (PAW)” in *Proceedings of the Living Planet Symposium (LPS, Bonn, Germany, 2022a)*.
- [91] **[Quiros-Vargas et al., LPS-2022b]** J. Quiros-Vargas, B. Siegmann, A. Damm, R. Wang, J. Gamon, V. Krieger, B.S. Daya Sagar, O. Muller, U. Rascher, “Sun-induced Chlorophyll fluorescence (SIF)-downscaling from the fractal geometry perspective” in *Proceedings of the Living Planet Symposium (LPS, Bonn, Germany, 2022b)*.
- [92] **[Quiros-Vargas et al., EMS-2022]** J. Quiros-Vargas, Bastian Siegmann, Alexander Damm, Uwe Rascher, “Vegetation and climate: initial concepts about the relation between the sun-induced chlorophyll fluorescence (SIF) and the soil water content (SWC)” in *Proceedings of the European Meteorological Society (EMS, Bonn, Germany, 2022)*.
- [93] **[Quiros-Vargas et al., IGARSS-2021]** J. Quiros-Vargas, R.D. Caldeira, N. Zendonadi dos Santos, L. Zimmermann, B. Siegmann, T. Kraska, M.W. Vasconcelos, U. Rascher, O. Muller, “Response of Bean (*Phaseolus vulgaris* L.) to Elevated CO<sub>2</sub> in Yield, Biomass and Chlorophyll fluorescence” in *Proceedings of the IEEE International Geoscience and Remote Sensing Symposium (IGARSS, Brussels, Belgium, 2021)*, pp. 5861-5864.
- [94] **[Quiros-Vargas et al., 2020a]** J. Quiros-Vargas, J. Bendig, A. Mac Arthur, A. Burkart, T. Julitta, K. Maseyk, R. Thomas, B. Siegmann, M. Rossini, M. Celesti, D. Schüttemeyer, T. Kraska, O. Muller, U. Rascher, Unmanned Aerial Systems (UAS)-Based Methods for Solar Induced Chlorophyll fluorescence (SIF) Retrieval with Non-Imaging Spectrometers: State-of-the-art. *Remote Sens.* 12, 1624 (2020a).
- [95] **[Quiros-Vargas et al., AGU-2020]** J. Quiros-Vargas, C. Brogi, V. Krieger, B. Siegmann, M. Celesti, M. Rossini, S. Cogliati, L. Weihermüller, U. Rascher, “Solar Induced Chlorophyll fluorescence and Vegetation Indices for Heat Stress Assessment in Three Crops at Different Geophysics-Derived Soil Units” in *Proceedings of the American Geophysical Union (AGU, online, 2020)*.

- [96] J. Quiros-Vargas, L.R. Khot, R.T. Peters, A.K. Chandel, B. Molaei, Low Orbiting Satellite and Small UAS-Based High-Resolution Imagery Data to Quantify Crop Lodging: A Case Study in Irrigated Spearmint. *IEEE Geoscience and Remote Sensing Letters* 17(5), 755-759 (2020b).
- [97] J. Quiros-Vargas, C. Zhang, J.A. Smitchger, R.J. McGee, S. Sankaran, Phenotyping of Plant Biomass and Performance Traits Using Remote Sensing Techniques in Pea (*Pisum sativum*, L.). *Sensors* 19(9), 2031 (2019).
- [98] J. Quiros-Vargas, L.R. Khot, Potential of low altitude multispectral imaging for in-field apple tree nursery inventory mapping. *IFAC-PapersOnLine* 49(16), 421-425 (2016).
- [99] U. Rascher, L. Alonso, A. Burkart, C. Cilia, S. Cogliati, R. Colombo, A. Damm, M. Drusch, L. Guanter, J. Hanus, T. Hyvärinen, T. Julitta, J. Jussila, K. Kataja, P. Kokkalis, S. Kraft, T. Kraska, M. Matveeva, J. Moreno, O. Muller, C. Panigada, M. Píkl, F. Pinto, L. Prey, R. Pude, M. Rossini, A. Schickling, U. Schurr, D. Schüttemeyer, J. Verrelst, et al., Sun-induced fluorescence – a new probe of photosynthesis: First maps from the Imaging spectrometer HyPlant. *Glob. Change Biol.* 21(12), 4673–4684 (2015).
- [100] G.J. Rebetzke, J.A. Jimenez-Berni, W.D. Bovill, D.M. Deery, and R.A. James, High-throughput phenotyping technologies allow accurate selection of stay-green. *J. Exp. Bot.* 67, 4919-4924 (2016).
- [101] S. Sankaran, L.R. Khot, C.Z. Espinoza, S. Jarolmasjed, V.R. Sthuvalli, G.J. Vandemark, P.H. Miklas, A.H. Carter, M.O. Pumphrey, N.R. Knowels, M.J. Pavek, Low-altitude, high-resolution aerial imaging systems for row and field crop phenotyping: A review. *Eur. J. Agron.* 70, 112-123 (2015).
- [102] U. Schreiber, "Pulse-Amplitude-Modulation (PAM) Fluorometry and Saturation Pulse Method: An Overview" in *Chlorophyll a Fluorescence, Advances in Photosynthesis and Respiration*, G.C. Papageorgiou, Govindjee Eds. (Springer, Dordrecht, 2004) pp. 279-319.
- [103] B. Siegmann, M.-P. Cendrero-Mateo, S. Cogliati, A. Damm, J. Gamon, D. Herrera, C. Jedmowski, Laura Verena Junker-Frohn, T. Kraska, O. Muller, P. Rademske, C. van der Tol, J. Quiros-Vargas-Vargas, P. Yang, U. Rascher, Downscaling of far-red solar-induced chlorophyll fluorescence of different crops from canopy to leaf level using a diurnal data set acquired by the airborne imaging spectrometer HyPlant. *Remote Sens. Environ.* 264, 112609 (2021).
- [104] B. Siegmann, L. Alonso, M. Celesti, S. Cogliati, R. Colombo, A. Damm, S. Douglas, L. Guanter, J. Hanuš, K. Kataja, T. Kraska, M. Matveeva, J. Moreno, O. Muller, M. Píkl, F. Pinto, J. Quirós Vargas, P. Rademske, F. Rodriguez-Morene, N. Sabater, A. Schickling, D. Schüttemeyer, F. Zemek, U. Rascher, The High-Performance Airborne Imaging Spectrometer HyPlant—From Raw Images to Top-of-Canopy Reflectance and Fluorescence Products: Introduction of an Automatized Processing Chain. *Remote Sens.* 11, 2760 (2019).
- [105] J.C. Soares, L. Zimmermann, N. Zendonadi dos Santos, O. Muller, M. Pintado, M.W. Vasconcelos, Genotypic variation in the response of soybean to elevated CO<sub>2</sub>. Genotypic variation in the response of soybean to elevated CO<sub>2</sub>. *J. Plant Interact.* 2(6), 263-276 (2021).

- [106] I.C. Stangherlin, M.D. Barcellos, Drivers and barriers to food waste reduction. *BFG* 120(10), 2364-2387 (2018).
- [107] Y. Sun, C. Frankenberg, J.D. Wood, D.S. Schimel, M. Jung, L. Guanter, D.T. Drewry, M. Verma, A. Porcar-Castell, et al. OCO-2 advances photosynthesis observation from space via solar-induced chlorophyll fluorescence. *Science* 358, eaam5747 (2017).
- [108] G. Tagliabue, C. Panigada, M. Celesti, S. Cogliati, R. Colombo, M. Migliavacca, U. Rascher, D. Rocchini, D. Schüttemeyer, M. Rossini, Sun-induced fluorescence heterogeneity as a measure of functional diversity. *Remote Sens. Environ.* 247, 111934 (2020).
- [109] A.F. Theisen, "Detecting chlorophyll fluorescence from orbit: The Fraunhofer Line Depth model" in *From Laboratory Spectroscopy to Remotely Sensed Spectra of Terrestrial Ecosystems*, R.S. Mutiah, Ed. (Kluwer Academic Publishers, Dordrecht, 2002), pp. 203-232.
- [110] P.S. Thenkabail, J.G. Lyon, A. Huete, "Advances in Hyperspectral Remote Sensing of Vegetation and Agricultural Croplands" in *Hyperspectral Remote Sensing of Vegetation*, P.S. Thenkabail, J.G. Lyon, A. Huete, Eds. (Springer Cham, 2011), 4-31 pp.
- [111] C. Torresan, A. Berton, F. Carotenuto, S.F. Di Gennaro, B. Gioli, A. Matese, F. Miglietta, C. Vagnoli, A. Zaldei, L. Wallace, Forestry applications of UAVs in Europe: a review. *Int. J. Remote Sens.* 38(8), 2427-2447 (2017).
- [112] B. Tubuxin, P. Rahimzadeh-Bajgiran, Y. Ginnan, F. Hosoi, K. Omasa, Estimating chlorophyll content and photochemical yield of photosystem II ( $\Phi$ PSII) using solar-induced chlorophyll fluorescence measurements at different growing stages of attached leaves. *J. Exp. Bot.* 66(18), 5595-5603 (2015).
- [113] J. Verrelst, G. Camps-Valls, J. Muñoz-Marí, J.P. Rivera, F. Veroustraete, J.G. Clevers, J. Moreno, Optical remote sensing and the retrieval of terrestrial vegetation biogeophysical properties – a review. *ISPRS Journal of Photogrammetry and Remote Sensing* 108, 273-290 (2015).
- [114] C. von Hebel, M. Matveeva, E. Verweij, P. Rademske, M.S. Kaufmann, C. Brogi, H. Vereecken, U. Rascher, J. Van der Kur, Understanding Soil and Plant Interaction by Combining Ground-Based Quantitative Electromagnetic Induction and Airborne Hyperspectral Data. *Geophys. Res. Lett.* 45, 3 (2018).
- [115] N. Wang, J. Suomalainen, H. Bartholomeus, L. Kooistra, D. Masiliūnas, J.G.P.W. Clevers, Diurnal variation of sun-induced chlorophyll fluorescence of agricultural crops observed from a point-based spectrometer on a UAV. *Int. J. Appl. Earth Obs. Geoinf.* 96, 102276 (2021).
- [116] J.C. White, N.C. Coops, M.A. Wulder, M. Vastaranta, T. Hilker, P. Tompalski, Remote Sensing Technologies for Enhancing Forest Inventories: A Review. *Can. J. Remote Sens.* 42, 619-641 (2016).
- [117] J.W. White, and M.M. Conley, A Flexible, Low-Cost Cart for Proximal Sensing. *Crop Science* 53, 1646-1649 (2013).
- [118] S. Wieneke, H. Ahrends, A. Damm, F. Pinto, A. Stadler, M. Rossini, U. Rascher, Airborne based spectroscopy of red and far-red sun-induced chlorophyll fluorescence: implications

- for improved estimates of gross primary productivity. *Remote Sens. Environ.* 184, 654-667 (2016).
- [119] N. Wilke, B. Siegmann, L. Klingbeil, A. Burkart, T. Kraska, O. Muller, A. van Doorn, S. Heinemann, U. Rascher, Quantifying Lodging Percentage and Lodging Severity Using a UAV-Based Canopy Height Model Combined with an Objective Threshold Approach. *Remote Sens.* 11, 515 (2019).
- [120] J. Xue, B. Su, Significant Remote Sensing Vegetation Indices: A Review of Developments and Applications. *J. Sens.* 2017, 1353691 (2017).
- [121] P. Yang, C. van der Tol, P.-K.-E. Campbell, E.-M. Middleton, Fluorescence Correction Vegetation Index (FCVI): A physically based reflectance index to separate physiological and non-physiological information in far-red sun-induced chlorophyll fluorescence. *Remote Sens. Environ.* 240, 111676 (2020).
- [122] P.J. Zarco-Tejada, V. González-Dugo, J.A.J. Berni, Fluorescence, temperature and narrow-band indices acquired from a UAV platform for water stress detection using a micro-hyperspectral imager and a thermal camera. *Remote Sens. Environ.* 117, 322-337 (2012).
- [123] P.J. Zarco-Tejada, M.L. Guillén-Climent, R. Hernández-Clemente, A. Catalina, M.R. González, P. Martín, Estimating leaf carotenoid content in vineyards using high resolution hyperspectral imagery acquired from an unmanned aerial vehicle (UAV). *Agric. For. Meteorol.* 171/172, 281-294 (2013).
- [124] P.J. Zarco-Tejada, C. Camino, P.S.A. Beck, R. Calderon, A. Hornero, et al., Previsual symptoms of *Xylella fastidiosa* infection revealed in spectral plant-trait alterations. *Nat. Plants.* 4, 432-439 (2018).
- [125] N. Zendonadi dos Santos, H.P. Piepho, G.E. Condorelli, E.L. Groli, M. Newcomb, R. Ward, R. Tuberosa, M. Maccaferri, F. Fiorani, U. Rascher, O. Muller, High-throughput field phenotyping reveals genetic variation in photosynthetic traits in durum wheat under drought. *Plant Cell Environ.* 44, 2858-2878 (2021).
- [126] Y. Zeng, M. Chen, D. Hao, A. Damm, G. Badgley, U. Rascher, J.E. Johnson, B. Dechant, B. Siegmann, Y. Ryu, H. Qiu, V. Krieger, C. Panigada, M. Celesti, F. Miglietta, X. Yang, J.A. Berry, Combining near-infrared radiance of vegetation and fluorescence spectroscopy to detect effects of abiotic changes and stresses. *Remote Sens. Environ.* 270, 112856 (2022).
- [127] Y. Zhang, L. Guanter, J.A. Berry, J. Joiner, C. Van der Tol, A. Huete, A. Gitelson, M. Voigt, P. Köhler, Estimation of vegetation photosynthetic capacity from space-based measurements of chlorophyll fluorescence for terrestrial biosphere models. *Glob. Chang. Biol.* 20, 3727-3742 (2014).
- [128] Z. Zhang, W. Xu, Q. Qin, Z. Long, Downscaling solar-induced chlorophyll fluorescence based on convolutional neural network method to monitor agricultural drought. *IEEE Trans Geosci Remote Sens* 59(2), 1012-1028 (2020).
- [129] M.G. Ziliani, S.D. Parkes, I. Hoteit, M.F. McCabe, Intra-Season Crop Height Variability at Commercial Farm Scales Using a Fixed-Wing UAV. *Remote Sens.* 10(12), 2007 (2018).

## 4 Publications related to this thesis

## 4.1 First author peer-reviewed articles and book chapter

4.1.1 First publication [Quiros-Vargas et al., 2020a]

“Unmanned Aerial Systems (UAS)-Based Methods for Solar Induced Chlorophyll fluorescence (SIF) Retrieval with Non-Imaging Spectrometers: State-of-the-art”

**Authors (country):**

J. Quiros-Vargas (GE)  
Juliane Bendig (AU)  
A. Mac Arthur (UK)  
Andreas Burkart (GE)  
Tommaso Julitta (GE)  
Kadmiel Maseyk (UK)  
Rick Thomas (UK)  
B. Siegmann (GE)  
Micol Rossini (IT)  
Marco Celesti (IT)  
D. Schüttemeyer (NL)  
Thorsten Kraska (GE)  
Onno Muller (GE)  
Uwe Rascher (GE)

**Journal:** Remote Sensing - MDPI

**Status:** Published

**Contribution of the doctorate candidate:**

- Conceptualization: 85%
- Data analysis: 0%
- Writing: 95%
- Field work: 0%

DOI: [10.3390/rs12101624](https://doi.org/10.3390/rs12101624)

Article

# Unmanned Aerial Systems (UAS)-Based Methods for Solar Induced Chlorophyll Fluorescence (SIF) Retrieval with Non-Imaging Spectrometers: State of the Art

Juan Quirós Vargas <sup>1,\*</sup>, Juliane Bendig <sup>2</sup>, Alasdair Mac Arthur <sup>3,4</sup>, Andreas Burkart <sup>5</sup>, Tommaso Julitta <sup>5</sup>, Kadmiel Maseyk <sup>6</sup>, Rick Thomas <sup>7,8</sup>, Bastian Siegmann <sup>1</sup>, Micol Rossini <sup>9</sup>, Marco Celesti <sup>9</sup>, Dirk Schüttemeyer <sup>10</sup>, Thorsten Kraska <sup>11</sup>, Onno Muller <sup>1</sup> and Uwe Rascher <sup>1</sup>

<sup>1</sup> Institute of Biogeosciences, IBG2: Plant Sciences, Forschungszentrum Jülich GmbH, 52425 Jülich, Germany; b.siegmann@fz-juelich.de (B.S.); o.muller@fz-juelich.de (O.M.); u.rascher@fz-juelich.de (U.R.)

<sup>2</sup> School of Technology, Environments and Design, University of Tasmania, Hobart, TAS 7001, Australia; juliane.bendig@utas.edu.au

<sup>3</sup> School of Geosciences, University of Edinburgh, Edinburgh EH9 3FF, UK; Alasdair.MacArthur@ed.ac.uk or alasdair.macarthur@uv.es

<sup>4</sup> Laboratory for Earth Observation, Image Processing Laboratory, University of Valencia, 46980 Valencia, Spain

<sup>5</sup> JB Hyperspectral Devices UG, Am Botanischen Garten 33, Düsseldorf 40225, Germany; andreas@jb-hyperspectral.com (A.B.); tommaso@jb-hyperspectral.com (T.J.)

<sup>6</sup> School of Environment, Earth & Ecosystem Sciences, The Open University, Milton Keynes MK7 6AA, UK; kadmiel.maseyk@open.ac.uk

<sup>7</sup> Birmingham Institute of Forest Research (BIFoR), University of Birmingham, Birmingham B15 2TT, UK; rick@bigskyscience.com

<sup>8</sup> Big Sky Science Ltd., Sutton Coldfield B72 1SY, UK

<sup>9</sup> Remote Sensing of Environmental Dynamics Laboratory, Department of Earth and Environmental Sciences (DISAT), University of Milano-Bicocca, Piazza della Scienza1, 20126 Milano, Italy; micol.rossini@unimib.it (M.R.); marco.celesti@unimib.it (M.C.)

<sup>10</sup> ESA-ESTEC, 2201 AZ Noordwijk, The Netherlands; dirk.schuettemeyer@esa.int

<sup>11</sup> Field Lab Campus Klein-Altendorf, University of Bonn, 53359 Rheinbach, Germany; kraska@uni-bonn.de

\* Correspondence: j.quirros@fz-juelich.de

Received: 14 April 2020; Accepted: 13 May 2020; Published: 19 May 2020



**Abstract:** Chlorophyll fluorescence (ChlF) information offers a deep insight into the plant physiological status by reason of the close relationship it has with the photosynthetic activity. The unmanned aerial systems (UAS)-based assessment of solar induced ChlF (SIF) using non-imaging spectrometers and radiance-based retrieval methods, has the potential to provide spatio-temporal photosynthetic performance information at field scale. The objective of this manuscript is to report the main advances in the development of UAS-based methods for SIF retrieval with non-imaging spectrometers through the latest scientific contributions, some of which are being developed within the frame of the Training on Remote Sensing for Ecosystem Modelling (TRuStEE) program. Investigations from the Universities of Edinburgh (School of Geosciences) and Tasmania (School of Technology, Environments and Design) are first presented, both sharing the principle of the spectroradiometer optical path bifurcation throughout, the so called ‘Piccolo-Doppio’ and ‘AirSIF’ systems, respectively. Furthermore, JB Hyperspectral Devices’ ongoing investigations towards the closest possible characterization of the atmospheric interference suffered by orbital platforms are outlined. The latest approach focuses on the observation of one single ground point across a multiple-kilometer atmosphere vertical column using the high altitude UAS named as AirFloX, mounted on a specifically designed and manufactured fixed wing platform: ‘FloXPlane’. We present technical details and preliminary results obtained

from each instrument, a summary of their main characteristics, and finally the remaining challenges and open research questions are addressed. On the basis of the presented findings, the consensus is that SIF can be retrieved from low altitude spectroscopy. However, the UAS-based methods for SIF retrieval still present uncertainties associated with the current sensor characteristics and the spatio-temporal mismatching between aerial and ground measurements, which complicate robust validations. Complementary studies regarding the standardization of calibration methods and the characterization of spectroradiometers and data processing workflows are also required. Moreover, other open research questions such as those related to the implementation of atmospheric correction, bidirectional reflectance distribution function (BRDF) correction, and accurate surface elevation models remain to be addressed.

**Keywords:** hyperspectral remote sensing; light weight spectroradiometer; telluric bands; ESA-FLEX; VNIR; SIF; UAS

---

## 1. Introduction

Chlorophyll fluorescence (ChlF) is defined as the light emitted by photosynthetic organisms with peaks at 687 (red ChlF) and 740 nm (far-red ChlF) [1]. The study of ChlF goes further than the estimation of basic structural plant traits like those usually analyzed from conventional multispectral remote sensing [2], e.g., throughout vegetation indices based on red-green-blue (RGB) and near infrared (NIR) reflectance. ChlF occurs in competition with heat to dissipate absorbed radiation not used in the light reactions of photosynthesis. Thus, the variation in the efficiency of one process affects the efficiencies of the others. This link forms the rationale for the use of ChlF to infer the plant physiological status, improving the understanding of the health ↔ stress status dynamics of plants in agricultural and environmental studies [3]. Recent studies successfully used ChlF as a proxy for water stress [4], leaf nitrogen [5], nutrient status [6], biomass determination [7], and gross primary production (GPP) [8]. The authors of [9] summarize the main physiological processes, such those related to photo-protection, that might be affected by specific ChlF drivers at ecological and temporal scales.

Several options are available for the assessment of ChlF, such as the light induced fluorescence transient (LIFT) active sensing method, which provides accurate ChlF field estimations especially useful in the context of high-throughput phenotyping field experiments [10]. However, this proximal technique is not viable for open field studies, as it is only suitable for close range observations. Large scale monitoring becomes feasible with the passive sensing of solar induced ChlF (SIF) [9] on the basis of hyperspectral techniques using spectroradiometers, e.g., on airborne and orbital platforms [11]. SIF can be quantitatively obtained throughout spectral measurements by the Oxygen-A (O<sub>2</sub>-A, 760 nm) and Oxygen-B (O<sub>2</sub>-B, 687 nm) absorption features of the atmosphere, where the ratio between the ChlF signal and the reflected radiance is higher [12] due to the absorption of the incoming irradiance (>90% in O<sub>2</sub>-A) [2,9]. SIF is considered the most direct remote sensing signal to infer the actual functional state of the photosynthetic apparatus and its dynamics at leaf, canopy, ecosystem, or even global scale. However, the SIF–photosynthesis relationship is influenced by several factors, including environmental conditions, structural traits, stress effects, and re-absorption processes by chlorophyll [9]. Hence, ancillary information is needed to interpret fluorescence changes and link them to variations in the photosynthetic efficiency. Moreover, an accurate retrieval of SIF is crucial to understand photosynthesis and its dynamics [13]. The three main SIF retrieval methods are: the Fraunhofer Lines Depth (FLD) [14], the spectral fitting methods (SFM) [15], and the singular vector decomposition (SVD) [16].

The relatively low intensity of the ChlF signal (<1%–5% of the reflected NIR radiation) [2] makes the retrieval of SIF challenging, and numerous studies tried to address this. Satellite missions, for example the Orbiting Carbon Observatory-2 (OCO-2), the Gases Observing Satellite (GOSAT), and the Global Ozone Monitoring Experiment-2 (GOME-2) were used to retrieve SIF for the assessment

of physiological parameters like carbon fixation [17,18]. Other missions such as the Scanning Imaging Absorption Spectrometer for Atmospheric Cartography (SCIMACHY), the Tropospheric Monitoring Instrument (TROPOMI), and the Exploratory Satellite for Atmospheric CO<sub>2</sub> (TanSat) have been used for similar purposes [19]. Airborne SIF estimations are also being explored by means of the HyPlant sensor: a system composed by two spectroradiometers covering the 400–2500 nm and 670–780 nm spectral ranges [20]. During the last years, HyPlant data has been the subject of a number of preliminary studies [21–23] related to the FLuorescence EXplorer (FLEX) mission of the European Space Agency (ESA) [24]. The first validated HyPlant maps were published in 2015, where contrasting SIF values among crops were found and attributed to differences in the photosynthetic apparatus activity [25]. Further studies reported the relation between HyPlant-derived SIF information and GPP [26]. Moreover, Tagliabue et al. [8] recently generated GPP maps over a forest area based on SIF retrieved from HyPlant imagery. They found significant correlations among SIF, GPP and absorbed photosynthetically active radiation in a range of  $R^2 = 0.43\text{--}0.46$  ( $p < 0.001$ ).

The interpretation and validation of space-borne and airborne SIF retrievals rely on the comparison with field measurements [27]. Yet, there is a scaling difference between these levels of observation that could possibly be addressed by unmanned aerial systems (UAS) [28] due to their intermediate sensor-surface distance. In a wide review of the existing remote sensing studies to retrieve top-of-canopy SIF, the authors of [29] commented about the lack of literature about UAS-based developments, and the lack of systematic protocols for data processing leading to uncertainties. Zarco-Tejada et al. [30] simulated the effect of aggregated reflectance on satellite imagery by decreasing the pixel size of low altitude hyperspectral data. These authors found that the correlation between key physiological traits, specifically stomatal conductance and ChlF, was reduced from  $R^2 = 0.69$  ( $p < 0.01$ ) to  $R^2 = 0.38$  ( $p < 0.05$ ) when using the original UAS imagery and the decreased spatial resolution image, respectively. In a similar approach, in the study of [31] they flew up to 500 m above ground level (AGL) to simulate satellite-like conditions for SIF retrieval, but only preliminary results were presented without a deeper insight in the high altitude results.

Contrary to UAS based imaging sensors, the technical feasibility for field measurements of non-imaging spectrometers [32], combined with their higher signal to noise ratio (SNR) and higher spectral and dynamic resolutions (allowing quantitative ChlF retrievals), as well as the reduced size and energy consumption encouraged employing these systems on UAS for SIF retrieval [33]. This concept has been in development for the past eight years, and notably in the last three to five years, it has been materialized in UAS models and prototypes leading to encouraging results. Nevertheless, further investigations are necessary until the point of a full operational UAS for SIF retrieval is reached. Thus, the aim of the present manuscript is to communicate the state of the art and future challenges in the development of UAS-based methods for SIF.

The manuscript is organized in four sections. Section 2 presents an overview of previous efforts using UAS-mounted spectroradiometers for reflectance measurements. In Section 3, the main three projects for UAS-based retrieval of SIF are presented: ‘Piccolo Doppio’ [34,35], ‘AirSIF’ [36], and ‘FloXPlane’ [37]. Section 4 is dedicated to a discussion about remaining challenges and open research questions.

## 2. Previous Efforts with UAS-Mounted Spectroradiometers for Reflectance Measurements

Ground based spectroradiometer measurements can be carried out relatively easily following standard protocols for setup, calibration, and data storage. When the instrument is mounted on an aerial platform, the accurate footprint (defined as the sampled Earth surface area from which radiance is received) geolocation on the ground, and the measurement of ambient light changes during the flight become the main challenges, which have been addressed in previous studies from different perspectives:

- (a) Burkart et al. [38] calculated reflectance based on synchronized measurements from two, one on-board and one on-ground, equally configured and cross calibrated STS micro-spectroradiometers (STS Series Spectrometers, Ocean Optics, Dunedin, Florida, USA) under the same environmental conditions. In this case, the radiometric calibration was performed indirectly from comparisons

between STS and an Analytical Spectral Device (ASD) FieldSpec 4 (Analytical Spectral Devices, Inc., Boulder, Colorado, USA) calibrated spectroradiometer. Results proved the high precision of the reasonably priced STS measurements, notwithstanding a second order effect was detected influencing NIR readings. The 338–412 nm stray light interfered with bands within 676–823 nm, especially in the O<sub>2</sub>-A band. Consequently, the authors suggested additional studies for STS-based SIF retrieval. Current investigations are focused on the use of STS micro-spectroradiometers, not for SIF measurements, but for the assessment of reflectance factors as a complementary (canopy scale) data source to leaf level spectral information acquired with an ASD spectroradiometer. The system, from the Environmental Remote Sensing and Spectroscopy Laboratory (SpecLab), included a real time optimization of the integration time, seeking to maximize signal independently of target brightness or changes in illumination. This feature was relevant considering the low signal-to-noise ratio of the STS spectrometers, and the variability of surface reflectance factors in heterogeneous Mediterranean tree-grass ecosystems, where bright dry grass is mixed with dark tree canopies during summer [39].

- (b) Garzonio et al. [40] realized downwelling irradiance measurements with a USB4000 spectroradiometer (Ocean Optics, Dunedin, Florida, USA) through linear interpolation of two measurements of the radiance reflected by a reference tarp, and the use of a second on-ground hand held ASD FieldSpec measuring a Lambertian surface (Spectralon<sup>®</sup>) as reference (both spectroradiometers were synchronized). The robust radiometric and spectral calibration of the instruments, despite not being temperature stabilized (e.g., the STS and the USB4000), permitted accurate radiance measurements especially at O<sub>2</sub>-A. Both approaches present a relative root mean square error lower than 10% compared with ground information.

### 3. Currently Operational UAS Systems for SIF Retrieval

#### 3.1. “Piccolo-Doppio”—A Dual-Field of View (FOV) Dual Spectrometer System

Remote sensing protocols for accurate SIF retrieval, based on high spectral resolution data at the oxygen absorption features, require the sunlight irradiance (downwelling) and surface energy emissions (upwelling) being simultaneously measured. These measurements generally mismatch in time in a range of multiple seconds, thus causing uncertainties in the SIF estimation. To overcome this, Mac Arthur et al. [34] split the fore optic path into a QEPro spectroradiometer (Ocean Optics, Dunedin, Florida, USA) aiming at a dual FOV system as proposed by [41]. The sensor measures in the 650–800 nm spectral range at a resolution of 0.15 nm, with a full width at half maximum (FWHM) between 0.31 and 0.35 nm. The SNR, dynamic range, and integration times are: 1000:1,  $8.5 \times 10^4$ :1, and up to 60 min, respectively. The detector has  $1048 \times 64$  pixels (two-dimensional) with columns summed to give increased dynamic range (Table 1). The system, named Piccolo-Doppio, is capable to perform upwelling and downwelling (cosine error <2%) measurements almost simultaneously ( $\approx 50$  ms difference between each measurement), diminishing reported uncertainties in field readings [42]. Moreover, the capability to work with two spectroradiometers (with a double bifurcated fiber optic assembly) differentiates the Piccolo-Doppio from some other UAS-based methods, since it allows synchronized Visible and NIR (VNIR; 400–950 nm) and the SIF (640–800 nm) measurements using the same fore optic for upwelling and the same fore optic for downwelling readings. Thus, any VNIR index, e.g., the photochemical reflectance index (PRI), can be derived together with SIF. As a drawback, light transmittance is reduced in one channel (either upwelling or downwelling) as fibers of two different diameters have been used which increases integration times and reduces SNR of the channel with the smaller diameter fiber. The use of one spectrometer, rather than two with independent optical paths, is necessary (i) to avoid the interpolation of one wavelength scale to the other (which might lead to loose detail in particular across the O<sub>2</sub> absorption features); and (ii) to ensure the radiometric calibration is constant for both up and downwelling measurements.

**Table 1.** Summary of the main characteristics of the spectroradiometer and UAS utilized for each project.

Platform	Spectroradiometer		Additional Components	Unmanned Aerial System (UAS)		Highlights	
Piccolo-Doppio	QEPro (Ocean Optics, Inc., USA)	Dimensions	182 × 110 × 47 mm	Radio control for data transferring	Custom hexacopter	Tarot T910 frame KDE 4213 motors pixhawk autopilot	Can be used with two spectroradiometers
		Spectral range (nm)	650–800	Battery Lithium Polymer 14.7 V, 1 A			Two independent channels
		Approximate spectral interval (nm)	0.15	Originally a raspberry Pi Model A. Currently updated to Pi3	Custom quadcopter	T-motor U8 100 kv motors Pixhawk autopilot Based on a Gryphon dynamics frame	Dual FOV for NIR reflectance and SIF (O <sub>2</sub> -A/O <sub>2</sub> -B)
		FWHM (nm)	0.31 (5 μm optical slit)–0.35 (10 μm optical slit)	RTK or PPK correction		Dimensions: 1.67 × 1.52 × 0.75 m	Upwelling and downwelling measurements near simultaneously
		Digital range (analogue to digital converter; bit)	18		DJI Matrice 600 A3 Pro	Payload 6 kg (16 min hovering)	Etaloning effect correction.
		SNR	1000:1			take-off weight 15 kg	Feasible installation on aerial and ground based platforms
		Dynamic range	8.5 × 10 <sup>4</sup> :1			Vertical and horizontal hovering accuracy 0.5 m and 1.5 m	
		Integration time	up to 60 min			Vertical take-off and landing	DJI GNS- RTK system (3 GPS antenna)
Has been tested with:	NIRQuest, QEPro, Flame, HR4000 and Maya				3 GNSS antennas and IMU's		
AirSIF	QEPro (Ocean Optics, Inc., USA)	Dimensions	182 × 110 × 47 mm	Dual GNSS antenna		Dimensions: 1.67 × 1.52 0.75 m	Adaption of the two independent channels system
		Spectral range (nm)	500–870	IMU		Payload 7 kg	Characterization of cosine corrector homogeneity and linearity
		Approximate spectral interval (nm)	0.37	Grasshopper 3 machine vision camera	DJI Matrice 600	take-off weight 15 kg	Upwelling and downwelling measurements near simultaneously
		FWHM (nm)	0.80	RTK correction		Vertical and horizontal hovering accuracy 0.5 m and 1.5 m	NIR reflectance and SIF (O <sub>2</sub> -A/O <sub>2</sub> -B)
		Digital range (bit)	18			Average flight speed: 2 m/s	Etaloning effect correction
		SNR	1000:1			Vertical take-off and landing	Dual GNSS antennae for accurate georeferencing in post processing
		Dynamic range	8.5 × 10 <sup>4</sup> :1				

Table 1. Cont.

Platform		Spectroradiometer		Additional Components	Unmanned Aerial System (UAS)	Highlights	
<b>AirFloX/ FloXPlane</b>	QEPro (Ocean Optics, Inc., USA)	Dimensions	182 × 110 × 47 mm	Data acquisition module	Wingspan 4.40 m	The QEPro is integrated with a large but light UAS capable to elevate several kilometers with one spectrometer coupled	
		Spectral range (nm)	650–800		Length 3.32 m		
		Approximate spectral interval (nm)	0.17	Independent battery management	take-off weight 24 kg		
		FWHM (nm)	0.30	Stabilizing gimbal	Payload 2.5 kg		
		Digital range (bit)		GPS times stamps for synchronizing	Battery weight 9 kg		
		SNR	1000:1		Average cruise speed: 10 m/s		Single spot constant monitoring
		Dynamic range	8.5 × 10 <sup>4</sup> :1		- Endurance: 1.5 h normal cruise flight. High altitude 40 min. Runway length of about 10 m for start and landing.		Characterize SIF retrieved at very high altitude for a closer understanding of satellite-based estimations

Figure 1 summarizes the main steps to process Piccolo-Doppio data, from the extraction of JavaScript Object Notation (JSON) files into MATLAB® (Mathworks, Field Spectroscopy Facility Post Processing Toolbox) [43] to the multiplication of the radiance (or irradiance) by the non-linearity corrected, the normalized, and the dark current corrected values per pixel for each spectroradiometer and optical direction. Currently, the data processing workflow and codes are updated to Python3.

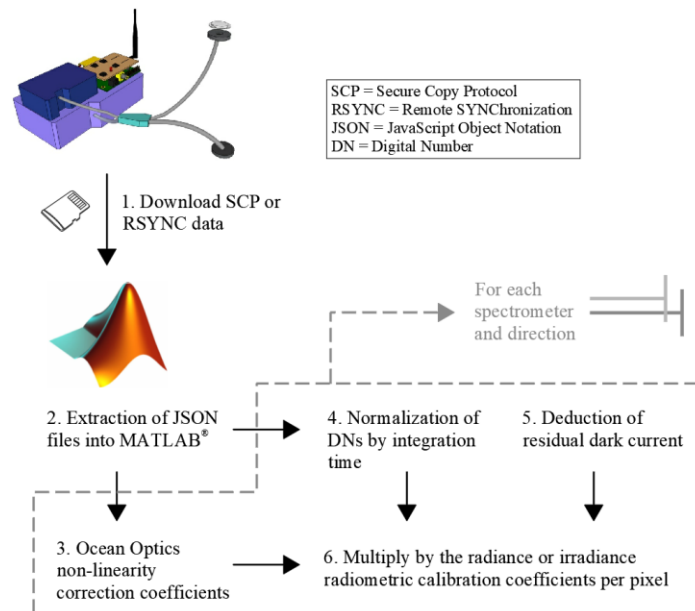


**Figure 1.** Piccolo-Doppio data processing workflow to obtain radiance. In step 2, an analogue data processing flow was developed in Python3.

Alongside the software solutions, the authors worked on hardware developments, e.g., the design of the fore optic and fiber optic assembly in order to maximize the light transmission, thus achieving integration times of 50–75 ms at VNIR, and 500–1500 ms at SIF wavelengths under clear-sky conditions in northern Europe (when the spectroradiometer’s maximum dynamic range is utilized). Nonetheless, the QEPro is prone to the etaloning effect caused by the interference of the light reflected in the boundaries of its thinned back-illuminated charge coupled device [42] detector, consequently producing wavy-aspect outputs. Founded on the statements of the instrument’s near-linear response to light intensity (when the generic non-linearity correction of the instrument is applied to the data in post processing) plus the etaloning stationarity in respect to the wavelength, [34] carried out laboratory experiments and presented two post-processing techniques for the etaloning correction for any system using QEPro spectrometers:

- (i) ‘By reference’: employing etaloning correction factors obtained from the division between the measured spectra of a calibrated light source and the known outputs per wavelength. The factors were applied to tungsten halogen readings at 20 levels of intensity (Figure 2a). The instrument response was then convolved with the respective spectral measurements to obtain the spectrum with the etaloning effect corrected. A variance of  $\pm 0.7\%$  was detected (Figure 2b) and linked to the instrument non-perfect linear response.
- (ii) ‘By curve-fitting and residual interpolation’: using correction coefficients obtained from the rounded residuals between actual and spline-smoothed reflectance at 17 levels of intensity of a tungsten halogen light source. A validation test performed with three additional levels of intensity demonstrated the efficiency of the method by reproducing a smooth spectrum (Figure 2c). Furthermore, the residuals of measured wavelengths were interpolated to enable the etaloning correction at unassessed ranges. The results obtained, differed by no more than 10 raw digital

counts (DN) from the etaloning corrected spectra (Figure 2d), hence demonstrating higher performance in the correction of the effect compared with the ‘referencing’ method.

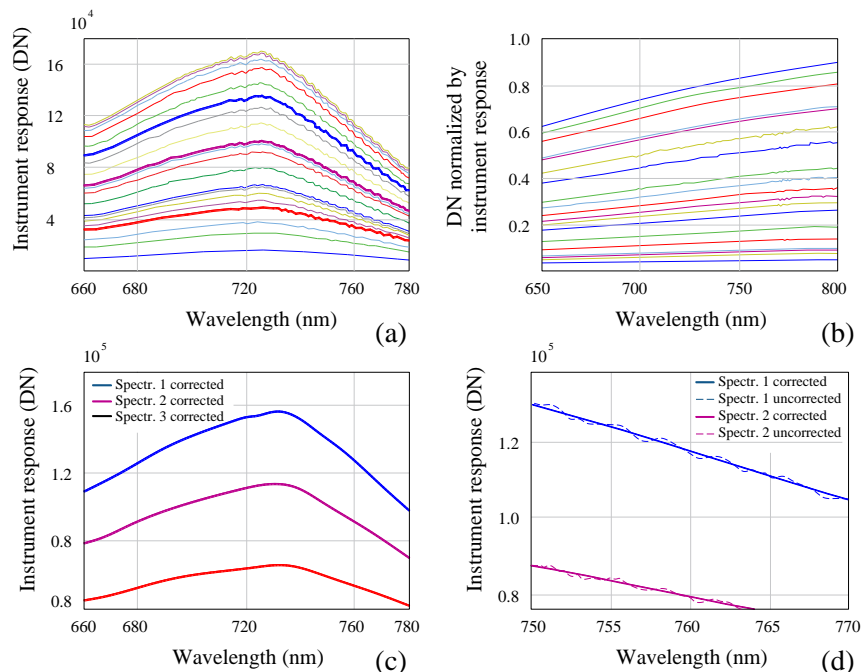


**Figure 2.** (a) Uncorrected spectral measurements of 20 light intensity levels of the tungsten halogen calibrated light and (b) their respective ‘by-reference’ corrected wavelengths. (c) Presents the ‘by curve-fitting and residual interpolation’ corrected spectra of the three curves highlighted in (a) with the same colors, and the detailed example of corrected vs. uncorrected instrument response is shown in (d) [34].

Mac Arthur et al. [34] demonstrated a feasible route to solve the discrepancies in time between surface radiance and solar irradiance wavelengths collected from individual spectroradiometers. The authors clarified that the application of both methods for etaloning correction under field conditions is challenging and will necessitate to push the spectroradiometer dynamic range to the maximum. Later, the authors of [33] reported the feasibility to mount the Piccolo-Doppio onto the UAS DJI Matrice 600 with an interchangeable gimbal where the spectroradiometer could be installed together with an RGB or thermal camera (Figure 3a). The Piccolo-Doppio design was further used by [31] who recorded information at several altitudes (up to 500 m) and time points confirming the viability of the Piccolo-Doppio system to be mounted on aerial platforms. However, at the time of the present manuscript publication the authors had not completed the data processing.

Additionally, a Piccolo-Doppio was also installed on a DJI Matrice 600 Pro [44] to monitor SIF in a mature oak woodland (UK) over a 30 m diameter free air CO<sub>2</sub> enrichment experiment [45]. A significant correlation of  $R^2 = 0.8821$  ( $p < 0.01$ ; Figure 3b) was found between UAS-based SIF and the incoming radiation, suggesting reliable variations of the SIF data retrieved with this system especially in a context where other approaches (e.g., eddy covariance) are not appropriate due to the scale of the treatments. Additionally, SIF information was useful to identify treatment effects and its relationship with environmental drivers.

Furthermore, the spectral calibration and characterization of three spectroradiometers using a Piccolo-Doppio-like system design could be analyzed [46] by the implementation of two methodologies, using Ar and Ne lamps or a double monochromator respectively. The versatility of Piccolo-Doppio makes it practical to be used even on a ground platform mounted on a tractor, as demonstrated by [47] who estimated soy bean populations on early vegetative states under changing atmospheric conditions.

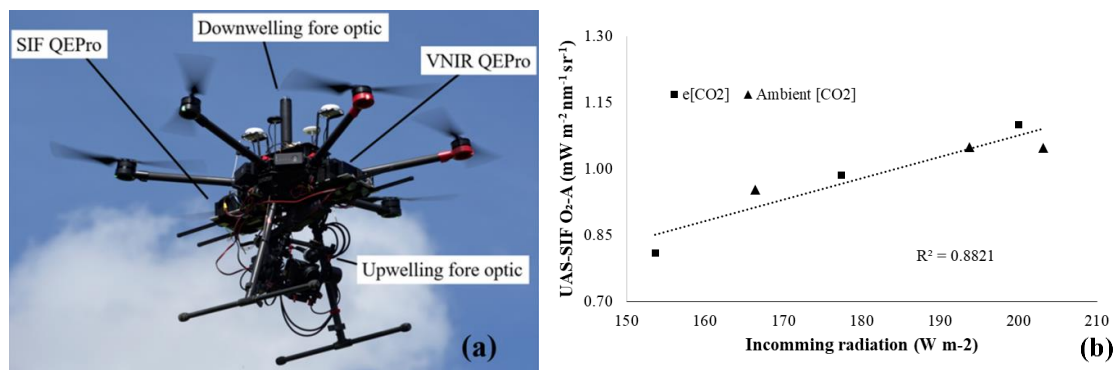


**Figure 3.** (a) Instrument presented by [33] and used by [31,44], highlighting the position of the solar induced ChlF (SIF) QEPro, downwelling and upwelling fore optics and VNIR QEPro (source: Dr. Andrew Reville, BBSRC/NERC ATEC project at University of Edinburgh-GeoSciences); and (b) the relationship between incoming radiation and SIF under ambient and elevated [CO<sub>2</sub>] in a mature oak forest, measured at the BIFoR FACE site in the UK.

### 3.2. “AirSIF”—A UAS-Based Spectroradiometer

The AirSIF platform (Figure 4a) shares the Piccolo-Doppio concept of splitting the optical path but using a single spectroradiometer (500–870 nm spectral range at an interval of 0.37 nm, with a FWHM of 0.8 nm), for collecting real time downwelling and upwelling radiance. AirSIF includes a dual global navigation satellite system (GNSS) antenna. Furthermore, in [36] the authors implemented the etaloning effect correction suggested by [34]. Additionally, they retrieved the corrected zenith angle between sun and cosine corrector (Ocean Optics CC-3), and the fore optic measuring downwelling radiance, depending on sun position and inclination of the cosine corrector during the UAS flight [28]. This information was computed from the platform pitch, roll and yaw obtained from an inertial measurement unit (IMU) mounted next to the cosine corrector. Cosine corrector measurements were not influenced by the azimuth angle, but sun zenith angles of  $>10^\circ$  resulted in a significant deviation from the expected cosine response of the cosine corrector. Common flight conditions led to platform tilt angles of  $6^\circ$  maximum. In order to correct the uncertainty caused by the irradiance underestimation of the cosine corrector, the authors of [28] proposed to estimate a corrected zenith angle based on the dot product principle accounting for the two vectors involved: the vectors between cosine sensor and sun and the cosine corrector pointing direction. With the implementation of this function mean and maximum differences of 1.7% and 3.2% from the original radiance measurements were obtained.

The latest results presented in March 2019 by [48] at the International Network on Remote Sensing of Terrestrial and Aquatic Fluorescence conference, reported the results of a comparison between AirSIF-derived spectra measured at 8 m AGL over barley experiment plots versus ground-based SIF retrieved with a high-resolution references system, the Fluorescence Box (Flox, JB Hyperspectral Devices, Düsseldorf, Germany) [37] mounted on a field-bike (Figure 4b). The results are visualized in a map of spatially explicit and geolocated AirSIF footprints with their respective O<sub>2</sub>-A SIF ranges at edge and middle sampled plots overlaid over an orthophoto derived from UAS imagery (Figure 4c). Flox footprints were estimated as round shapes, where the size was estimated from sensor height above canopy according the  $25^\circ$  FOV of the Flox instrument. The study had four main shortcomings: (i) the spatial misalignment of the footprints between repeated UAS flights, (ii) the lack of accurate geolocation of Flox ground measurements, (iii) the difference in footprint size between AirSIF and Flox (0.5–2.5 m<sup>2</sup>), and (iv) the resulting significant difference between UAS- and Flox-based SIF measurements. The accuracy of the footprint determination of the AirSIF platform was analyzed in a recent study being  $\pm 15$  cm for 10 m AGL height [49].

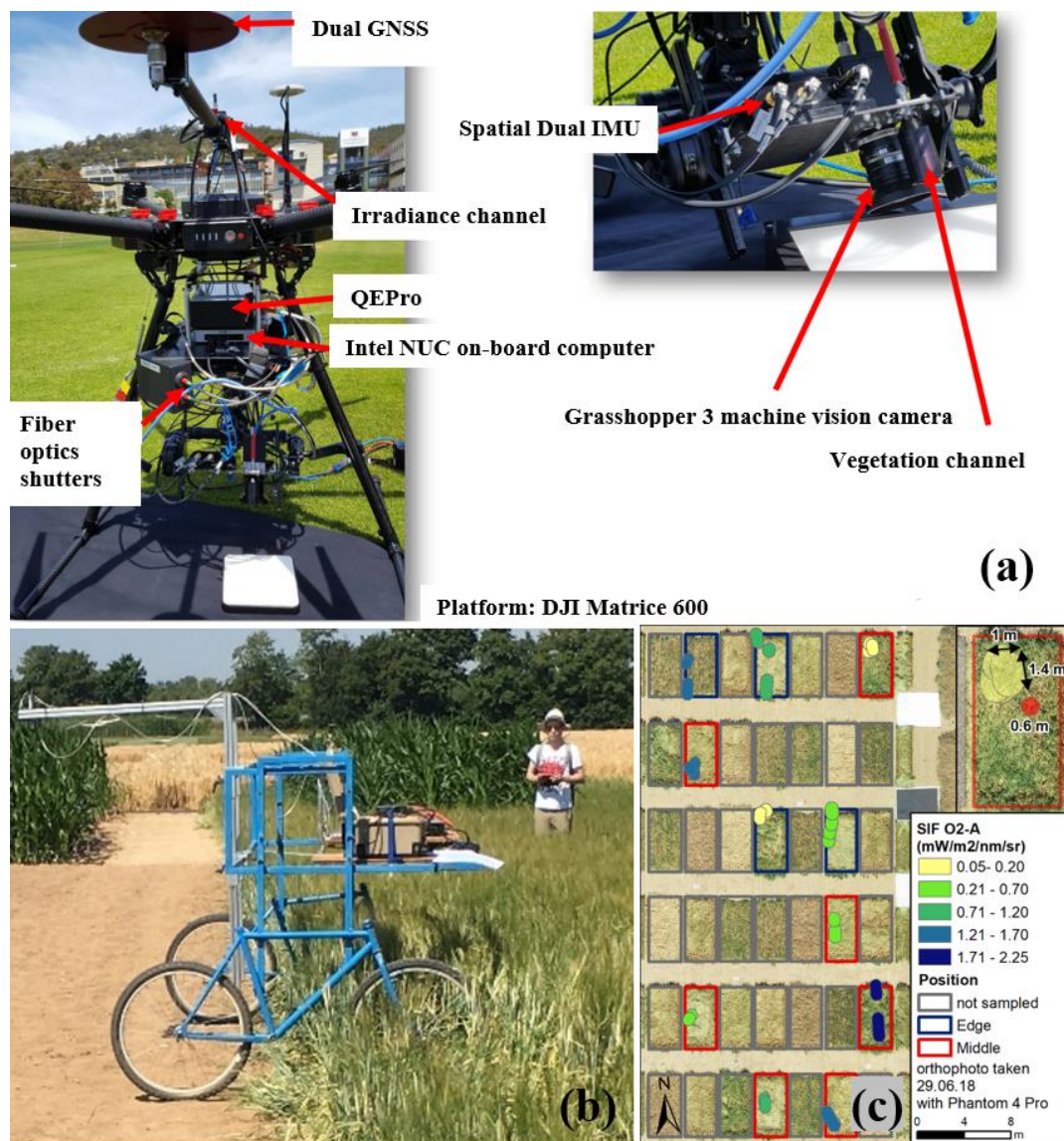


**Figure 4.** (a) AirSIF system components, (b) field bike used for ground Flox measurements, and (c) footprints of the flight at 12:00 local time with their respective O<sub>2</sub>-A SIF at edge (blue) and middle (red) sampled plots over the orthophoto derived from UAS photogrammetry [49].

An initial test was carried out by comparing a single AirSIF flight with Flox observations from the field bike. The measurements were collected at the Campus Klein-Altendorf, an agricultural research station affiliated to the Agricultural Faculty of the University of Bonn (Germany). In total, 55 observations over nine 3 × 5 m barley plots were collected, three per plot by the Flox instrument, and between one and four per plot by AirSIF at 10:45–12:00 (Flox) and 12:00–12:15 (AirSIF), respectively. The results showed a link between the SIF retrieved from both platforms, which was stronger but negative for UAS footprints located at the plot edge (Figure 5a). A paired *t*-test showed no significant differences between the mean SIF retrieved from UAS and Flox. Moreover, there seems to be an underestimation of ≈13% with UAS-based measurements (Figure 5b).

The implementation of a dual GNSS antenna system [50], the use of an IMU in the correct position, and the appropriate flight and sensor configurations [51] were found crucial to acquire the highest accuracy in the platform pose characterization and footprint localization for the improvement of SIF estimates, especially over small experimental plots like the ones presented here. Consequently,

the authors of [52] published the results of research concerning boresight (IMU-spectroradiometer-camera misalignment) and lever arm (GNSS antenna-spectroradiometer offset) correction methods.

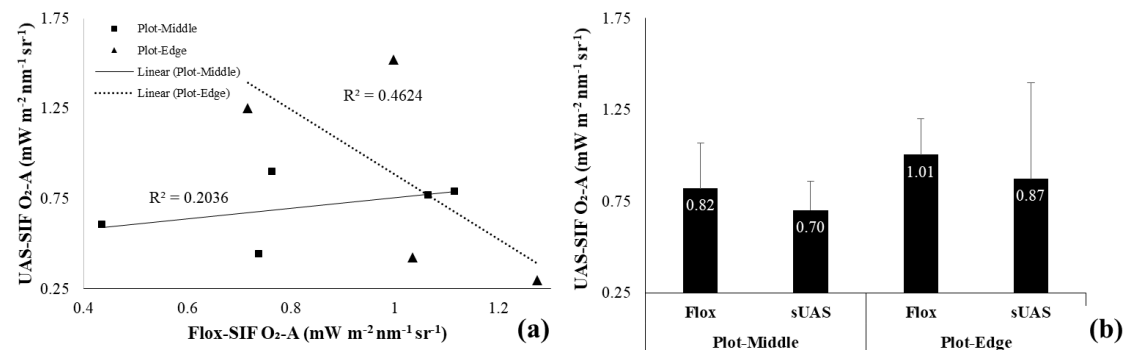


**Figure 5.** (a) Linear regression and (b) comparison between mean values of Flox instrument and UAS SIF measurements. Flox footprints were always located at the center of the plots, and UAS footprints were at the middle and edge of the plots.

### 3.3. “AirFloX” on Board of the “FloXPlane”—Atmospheric Interference on SIF Retrieval Across a Multiple Kilometer Air Column

The AirFloX is the lighter and simplified version of the Flox system manufactured by JB Hyperspectral Devices [53], and up to date the only existing commercially available instrument for the continuous long-term top of canopy SIF measurements. Whilst FloX design, reported in [54], relies on the use of two channels to collect nearly simultaneously upwelling and downwelling at sensor radiance, AirFloX is designed to only acquire data collected by one channel (downward looking fiber), making it more similar, in a conceptual approach, to an image sensor. Due to the distance from the canopy at which the sensor is expected to fly, up to 4 km, the upwelling at sensor radiance is expected to be biased by atmospheric absorption, thus not easily used for SIF retrieval. The fluorescence retrieval will be performed by applying a similar processing scheme as the one used in imaging sensors data processing, e.g., HyPlant [20].

The investigations described here, alongside airborne (HyPlant) studies for SIF retrieval, contribute to integrate into the bigger picture of the FLEX satellite mission expected to be launched in 2022 [55]. Within this context, one of the major challenges is to precisely understand the impact of large atmosphere columns on a kilometer scale and their impact on SIF retrieval. Background studies started elucidating this topic, as presented by [56], who showed that SIF is strongly influenced by the atmospheric scattering and absorption, which in turn are defined by factors such as the surface pressure and concentration of aerosols. In practice, the higher the sensor-surface distance, the larger the air column above the targets [19], the stronger the scattering and the extinction of the signal in the atmosphere due to the absorption by aerosols and oxygen molecules, respectively. Hence, at this multiple km vertical scale, retrieving SIF becomes more challenging due to the need of increasing the accuracy of the atmospheric correction.

Recently, researchers from JB Hyperspectral Devices developed a high altitude and light fixed wing UAS, called ‘FloXPlane’ (Figure 6a), equipped with the AirFloX system (Figure 6b,c). The FloXPlane was manufactured with two purposes: (i) sampling large areas suitable for satellite calibration/validation (cal/val), and (ii) characterizing the surface radiance of one fixed spot at ground level across a multiple kilometer (up to 4000 m) air column. Their goal is to measure the atmospheric absorption of the upwelling SIF emission, considering that the majority of oxygen and aerosols are present in the innermost atmosphere layers. This is achieved by a steep screw-like flight pattern, incorporating a stabilizing gimbal, which ensures accurate pointing of the sensor to the target. A co-aligned camera provides proof of the gimbal pointing accuracy and allows structure from motion processing for highly accurate positioning of the sensor in 3D space. Using a fixed wing aircraft turned out to be mandatory

for this mission, since it can provide enough range to reach 4 km and will sail down to ground level. This concept ensures the necessary safety and fallback scenarios to achieve legal clearance into public airspace.

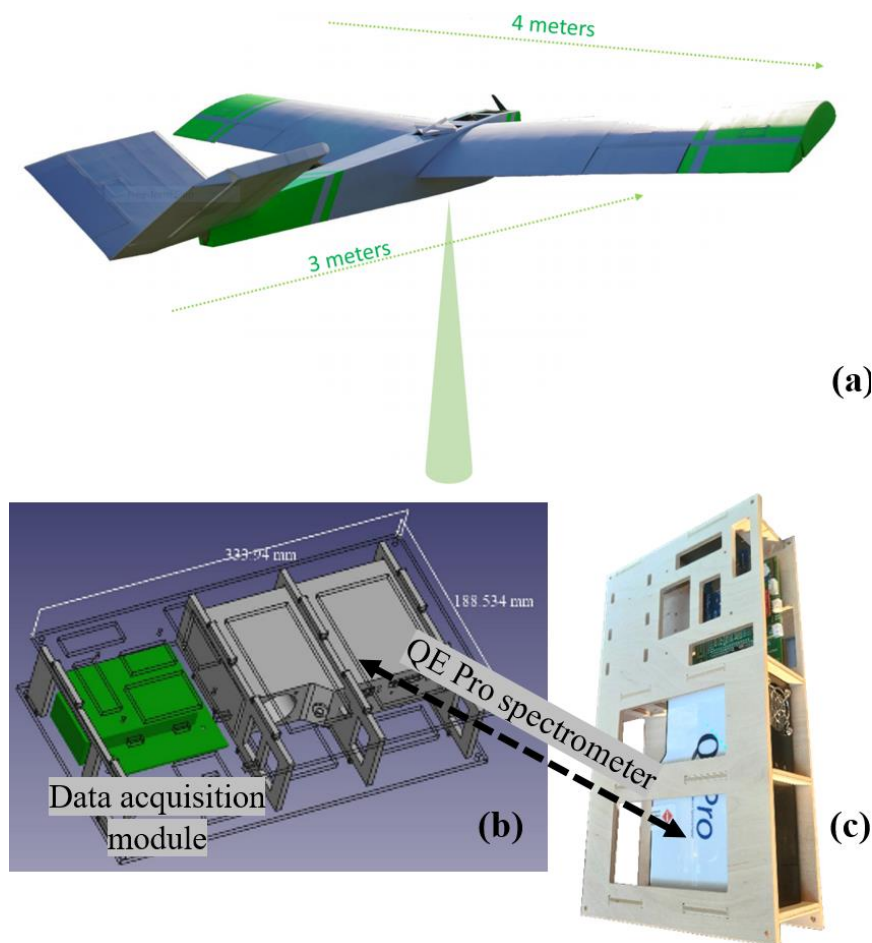


**Figure 6.** The FloXPlane fixed wing UAS (a), equipped with AirFloX system (b,c).

At the time of writing, the complex legislation process allowing the experimental UAS flights in the controlled airspace has been successful. However, in this manuscript the results of previous tests flying to a maximum altitude of 600 m AGL are shown. Further experiments with the AirFloX system onboard a manned aircraft, a manned gas balloon, and a rotary wing DJI Matrice 600 have been performed in 2018 and 2019. A focus of the medium-altitude vertical flights is the determination of the change in the O<sub>2</sub>-A and O<sub>2</sub>-B absorption versus the distance from the target (i.e., flight altitude). In fact, the change of absorption in these two bands is directly affecting the SIF estimates, therefore, an accurate parametrization is a key factor for accurate SIF retrieval using flying platforms. Due to the changing light conditions during flights, the absolute oxygen band depth value could lead to erroneous results. Therefore, the relative band depth was calculated as reported in the following formula:

$$\text{Band depth} = \frac{L_{\lambda out} - L_{\lambda in}}{L_{\lambda out}} \quad (1)$$

where  $L_{\lambda out}$  and  $L_{\lambda in}$  are the wavelength of the shoulder and the deepest point of the oxygen absorption band, respectively. Preliminary results reported in Figure 7 are promising. The O<sub>2</sub>-B and O<sub>2</sub>-A at sensor radiance spectra (Figure 7a,b) show a stable spectral and radiometric behavior i.e., no spectral shift caused by grating distortion due to air pressure is found.

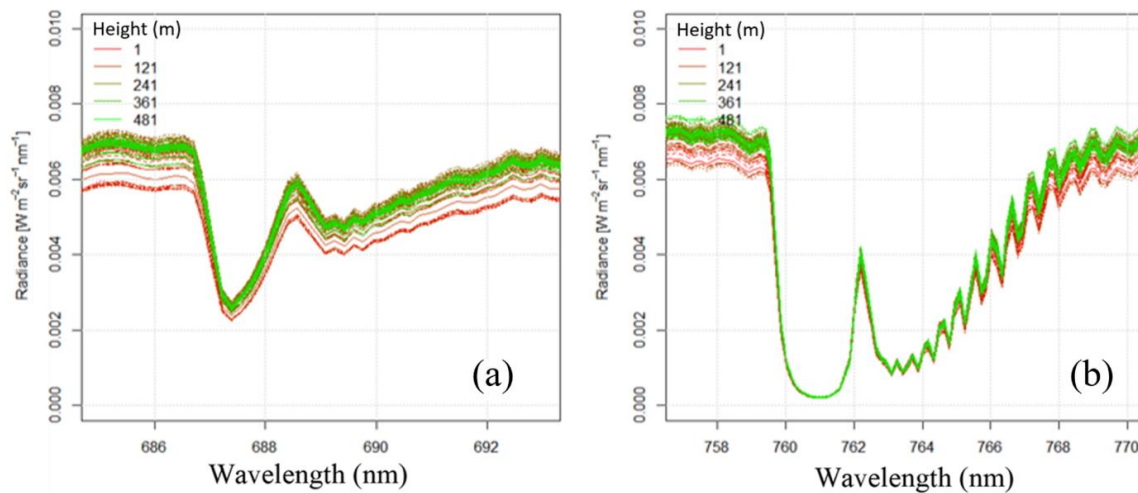


**Figure 7.** Zoom to the (a) O<sub>2</sub>-B and (b) O<sub>2</sub>-A at sensor radiance spectra of the first flight of the FloX-Plane UAS [36].

As shown in Figure 8, the two flights performed were made on a 600 m vertical column. A pseudo normalized difference vegetation index (NDVI; at sensor radiance based) was calculated showing that the target was remaining the same during the whole ascending flight duration (bare soil). The invariant target selection is a key point, since no confounding SIF emission is expected to alter the oxygen band depth. Looking at the relative band depth change, an increase of 1% was found in the O<sub>2</sub>-B band, whilst for O<sub>2</sub>-A results are less clear. Although the preliminary results are aligned with theory, a stronger absorption takes place under a larger air column leading to SIF underestimations [57]. Thus, the encouraging results obtained hitherto support the needs of more and repeated flights, covering a wider range of atmospheric conditions (e.g., different solar zenith angle ranges, aerosol concentrations, and air pressure conditions).

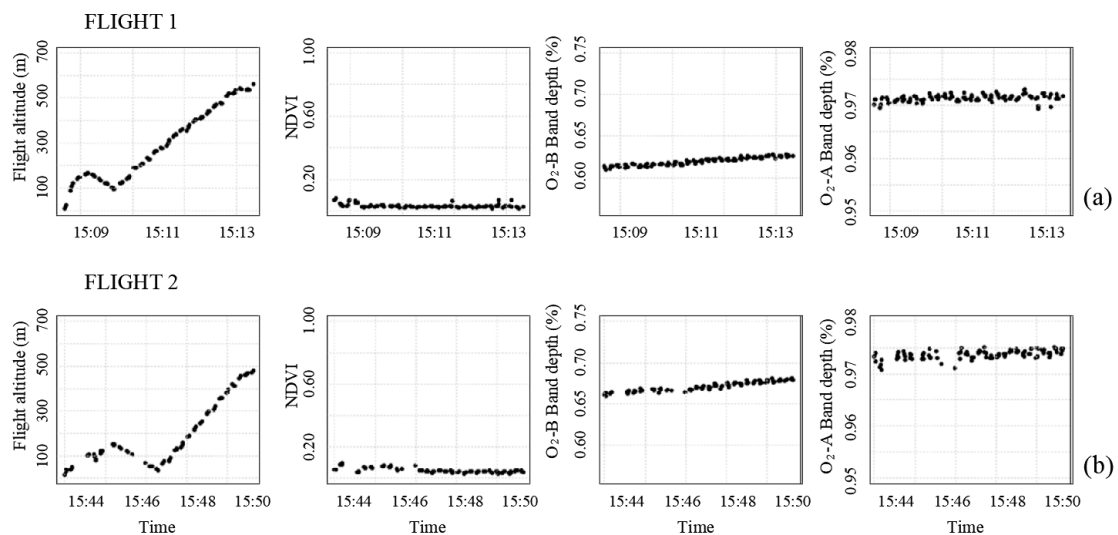


**Figure 8.** Flight altitude, pseudo-NDVI, and O<sub>2</sub>-A and O<sub>2</sub>-B relative bands depth for the (a) first and (b) second preliminary flights up to 600 m AGL. The first plots on each panel show the relation between the time and the flight altitude.

### 3.4. Summary of the UAS-Based Methods Presented

The presented projects are summarized in Figure 9, where the main components of the Piccolo-Doppio, AirSIF, and FloXPlane are displayed. The figure tracks the progress in development

of UAS-based platforms for quantitative retrieval of SIF in physical units starting with the fiber optic bifurcation of [34], who also conducted a valuable characterization of the etaloning effect, and afterwards adapted by [35,36] who installed a similar-principle system on-board a UAS including the implementation of an IMU and a dual GNSS antenna for a better pose characterization and cosine corrector performance analysis. Researchers from [37] added the investigation of the atmospheric influence on SIF retrieval under a 600 m air column.

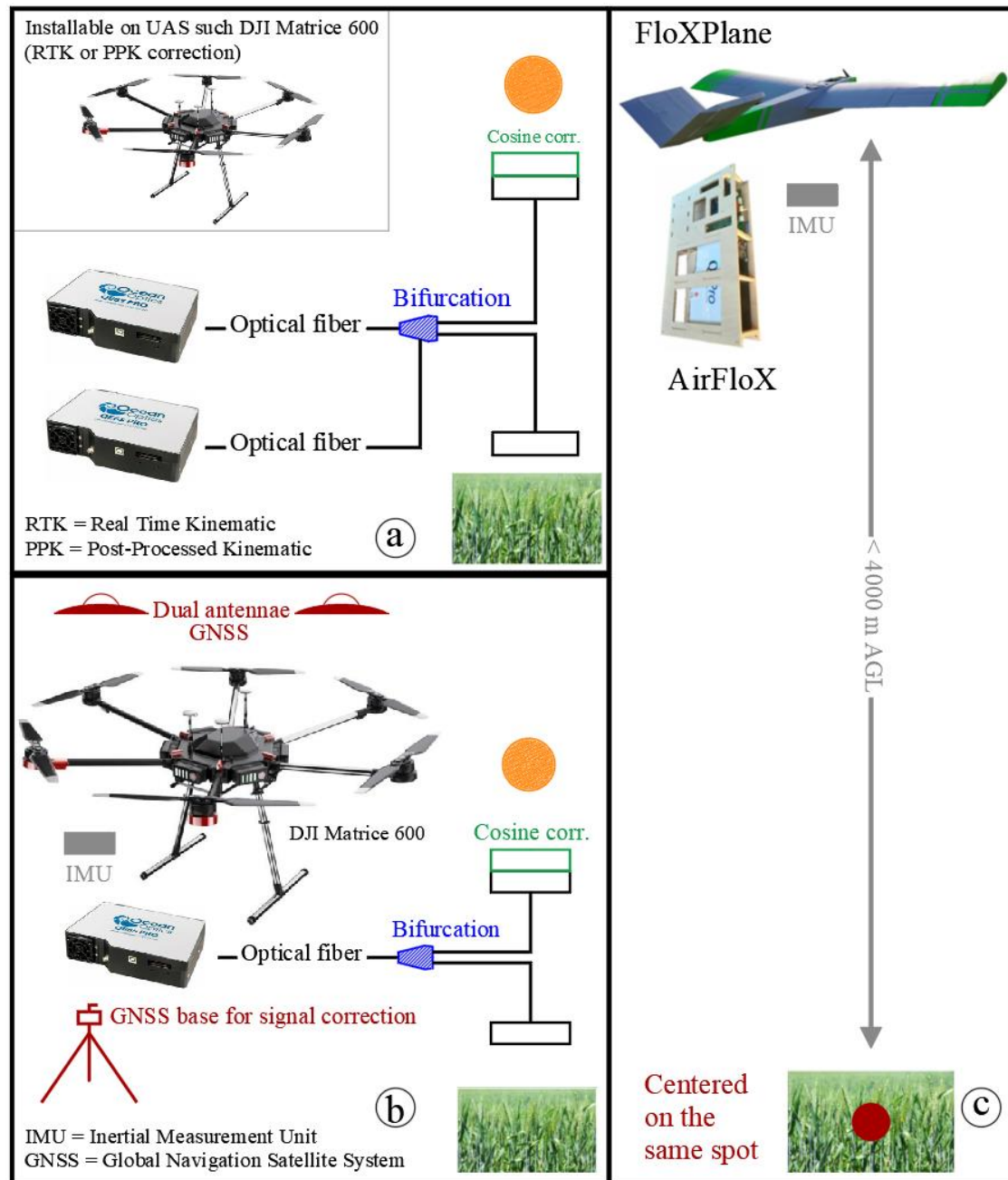


**Figure 9.** Schemes summarizing the main characteristics of (a) Piccolo-Doppio, (b) AirSIF, and (c) FloXPlane.

More systems may be under development, e.g., a platform called FluorSpec, not discussed here, is currently being developed by researchers of the Geo-information Science and Remote Sensing laboratory, at Wageningen University and Research [58]. The core components of the system are the QEPro spectrometer, an RGB camera, a GNSS, and a Laser rangefinder sensor, all boarded on a DJI

S1000 octocopter. The spectrometer is configured with a split fiber, one channel for downwelling and one for upwelling measurements, covering a spectral range from 630 to 800 nm, with an FWHM of 0.14 nm and a spectral sampling interval of 0.31 nm. The irradiance, radiance, and reflectance factors at the top of UAS and canopy level can be derived after radiometric calibration and atmospheric correction processing.

#### 4. Remaining Challenges and Open Research Questions

Beyond the valuable advances achieved so far, several challenges are yet to be overcome and several issues related to the UAS-based methods for SIF retrieval remain open. First, the sensitivity of the cosine corrector to varying sun zenith angles, and the etaloning effect caused by the interfering of the light reflected in the borders of the back-illuminated thinned charge coupled device add uncertainty to SIF estimations. In addition, sensor calibration methods, data collection, and data processing protocols need to be standardized and spectroradiometers need to be characterized [46] in order to enable measurements from different instruments at diverse geographical locations and temporal periods to be directly compared. The main features to be characterized are the FWHM as proposed by [42], and the SNR, spectral sampling interval, and spectral shift, which were identified by [59] as the most impacting characteristics on SIF retrieved with FLD methods. Besides, inherent issues of the SIF retrieval must be considered, such as the higher variation and lower SNR generally obtained in the O<sub>2</sub>-B, and the lack of required information to run an accurate correction to diminish the effect of atmospheric interference.

Besides the sensor-associated issues, complementary studies should be conducted suggesting ways to improve the FOV geolocation accuracy, and the spatio-temporal match between on-board and proximal measurements of same targets. Indeed, robust validations of UAS-based SIF estimations are up to now hindered by these spatio-temporal discrepancies of the two levels of information, since their comparison is not fully convincing with differences of few meters and/or minutes. Some ideas have been proposed to improve the spatio-temporal match between UAS-based and ground SIF retrievals aiming at conclusive validations; for instance, in [40] the authors suggest to overlay the spectrometer data with RGB imagery derived maps, while the authors of [51] recommend the use of real time kinematic (RTK) correction for the geolocation of footprints, plus the implementation of lever arm and boresight corrections [52].

Moreover, the precise characterization of the spectroradiometer footprint might also be achieved with the support of automated ground platforms for SIF assessment, particularly those developed and used in plant phenotyping. These instruments can be programmed to collect SIF data at specific points with an accuracy of few seconds and centimeters, which consequently can be precisely aligned with the moment and place of the UAS-based data points. Some ground platforms for SIF phenotyping can be configured to collect information at specific sensor angles and AGL elevation, therefore they might also be used for optimal UAS flight simulations with a precise pose characterization and footprint spatio-temporal location, targeting to (i) elucidate the real maximum scope of UAS-based methods for SIF retrieval, which is so far unclear, (ii) facilitate the robust validation of aerial retrievals, thus (iii) allowing deeper analyses and understanding of the SIF estimated from low altitude hyperspectral data, e.g., throughout the comparison of retrieval methods, and a thorough comprehension of the sensor multi-angularity effect.

Furthermore, according to [60], the effect of the atmospheric conditions should be incorporated into the retrieval throughout model-based approaches notwithstanding if the data is acquired at proximal, airborne, or orbital level, which opens another query: would the accuracy of UAS-based SIF retrievals be significantly increased by implementing new dedicated atmospheric correction methods where current models are not easily adapted? In addition, the authors of [61] reported the impact of the bidirectional reflectance distribution function (BRDF) on the canopy chlorophyll content estimation from UAS hyperspectral imagery. The authors recommend the correction of the BRDF for reliable and consistent estimations, as it accounts for the surface reflectance anisotropy and varying solar and instrument-view angles. Although the authors of [61] used an imaging sensor, the same principle

applies to the UAS-mounted point spectrometers [62] since the BRDF effect is inherent to remote sensing information [63].

Pinto et al. [63] studied the SIF directionality according to the surface, inclination, and orientation of leaves, as well as the sensor and sun angles. Nonetheless, the authors worked with single and static measurements, therefore a full characterization of the BRDF was not possible due to the limited range of illumination and viewing angles. In this respect, hypothetically, the implementation of a detailed canopy slopes map computed from a UAS-derived crop surface model might contribute to upscale and improve the results found by [63]. Moreover, considering that surface elevation differences of 0.50–1.50 m AGL (common crop canopy height range) represent 5%–15% of the sensor-surface distance in low altitude (e.g., 10 m AGL) UAS flights, we can also hypothesize that the incorporation of a crop surface model into the UAS-based methods for SIF assessment might help to better account for the ChlF re-absorption effect. Accordingly, more scientific questions arise: does the implementation of accurate surface elevation models significantly improve the quality of SIF estimations? Could a slope map derived from a crop surface model represent the canopy architecture complexity? Might this be useful for a full canopy BRDF characterization thus precise SIF retrievals from UAS-based methods?

## 5. Conclusions

The UAS-based retrieval of SIF with non-imaging spectroradiometers is possible and has been demonstrated by a number of groups. Recent advances in the platform and instrument design contributed:

- (i) The optical path bifurcation presented in the Piccolo-Doppio system for nearly simultaneous upwelling and downwelling measurements with two spectroradiometers, allowing synchronized VNIR and SIF measurements.
- (ii) The implementation of a dual GNSS antenna system and IMU placed in the correct position, alongside the appropriate flight and sensor configurations reported in the AirSIF project, for the accurate pose characterization and footprint geolocation accuracies.
- (iii) The development of the FloXPlane as a fixed wing UAS for very high altitude measurements, which will provide crucial information to understand the impact of large atmosphere columns on the retrieval of SIF.

Despite many important advances achieved by [34,36,37], UAS-based SIF observations from non-imaging spectroradiometers still present uncertainties associated to the current sensor characteristics and the spatio-temporal mismatching between aerial and ground measurements, mostly caused by the footprint spatial extent and form and location dependency on the flying height and pose geometry. The latest complicated the proper robust validation of aerial UAS-SIF measurements. Consequently, more investigations are required addressing the accurate FOV size and location, along with the spatio-temporal matching of UAS-based and ground SIF measurements of the same targets. Complementary studies regarding the standardization of calibration methods and the characterization of spectroradiometers and data processing workflows are required. Open research questions like those related to the implementation of atmospheric correction, BRDF correction, and accurate surface elevation models should be addressed in the future.

**Author Contributions:** Conceptualization, J.Q.V., U.R., M.R., M.C.; investigation, J.B., A.M.A., A.B., K.M., R.T.; writing—original draft preparation, J.Q.V.; writing—review and editing, J.Q.V., J.B., A.M.A., T.J., B.S., M.R., M.C., T.K.; supervision, U.R., O.M., B.S., M.R., M.C.; project administration, M.R., M.C., D.S., T.K.; funding acquisition, M.R., M.C., U.R., O.M., D.S. All authors have read and agreed to the published version of the manuscript.

**Funding:** The research has received funding from the European Union’s Horizon 2020 research and innovation program under the Marie Skłodowska-Curie grant agreement no. 721995. This document was prepared within the Training on Remote Sensing for Ecosystem Modelling (TRuStEE) consortium. The “AirFloX” on board of the “FloXPlane” system (Section 3.3) is funded by the European Space Agency (ESA) project number 4000120771: Technical Assistance for the Development of Ground-based Systems for Long term measurements of Red and Far-red Sun Induced chlorophyll Fluorescence (DEFLOX).

**Acknowledgments:** The authors acknowledge the contribution of Kai Wittneben as collaborator in the development of the FloXPlane at JB Hyperspectral Devices; Zbyněk Malenovský, Deepak Gautam, and Arko Lucieer at the

University of Tasmania for the development of AirSIF; Magnus Hagdorn and Richard Taylor at University of Edinburgh, Scotland, Iain Robinson at RAL, UK and Luis Alonso at University of Valencia, Spain, for their contribution to the Piccolo-Doppio project. We thank to Maria Pilar Martin, Na Wang, and Lammert Kooistra, the first from the Environmental Remote Sensing and Spectroscopy Laboratory (SpecLab), Spanish National Research Council (CSIC), and the latest two from the Geo-information Science and Remote Sensing laboratory, at Wageningen University and Research (WUR), for their support sharing information about the SpecLab and FluorSpec ongoing investigations, respectively. We also acknowledge the contribution of the Field Lab Campus Klein-Altendorf (CKA), University of Bonn, for their support enabling field experiments for the data collection of the AirSIF study case.

**Conflicts of Interest:** The authors declare no conflict of interest.

## Abbreviations

The following abbreviations are used in this manuscript:

AGL	Above ground level
ASD	Analytical spectral device
BRDF	Bidirectional reflectance distribution function
ChlF	Chlorophyll fluorescence
DN	Raw digital counts
ESA	European Space Agency
FLD	Fraunhofer Lines Depth
FLEX	FLuorescence EXplorer
Flox	Fluorescence box
FOV	Field of view
FWHM	Full Width at Half Maximum
GNSS	Global navigation satellite system
GOME-2	Global Ozone Monitoring Experiment-2
GOSAT	Gases Observing Satellite
GPP	Gross primary production
IMU	Inertial measurement unit
JSON	JavaScript Object Notation
LIFT	Light induced fluorescence
NDVI	Normalized difference vegetation index
NIR	Near infrared
O <sub>2</sub> -A	Oxygen-A band
O <sub>2</sub> -B	Oxygen-B band
OCO-2	Orbiting Carbon Observatory-2
PRI	Photochemical reflectance index
RGB	red-green-blue
SCIMACHY	Scanning Imaging Absorption Spectrometer for Atmospheric Cartography
SFM	Spectral fitting method
SIF	Solar induced chlorophyll fluorescence
SNR	Signal to noise ratio
SpecLab	Environmental Remote Sensing and Spectroscopy Laboratory
SVD	Singular vector decomposition
TanSat	Tropospheric Monitoring Instrument (TROPOMI) and the Exploratory Satellite for Atmospheric CO <sub>2</sub>
TRuStEE	Training on Remote Sensing for Ecosystem Modelling
UAS	Unmanned aerial systems
VNIR	Visible and near-infrared

## References

1. Kalaji, H.M.; Schansker, G.; Brestic, M.; Bussotti, F.; Calatayud, A.; Ferroni, L.; Goltsev, V.; Guidi, L.; Jajoo, A.; Li, P.; et al. Frequently asked questions about chlorophyll fluorescence, the sequel. *Photosynth. Res.* **2017**, *132*, 13–66. [[CrossRef](#)] [[PubMed](#)]

2. Meroni, M.; Rossini, M.; Guanter, L.; Alonso, L.; Rascher, U.; Colombo, R.; Moreno, J. Remote sensing of solar-induced chlorophyll fluorescence: Review of methods and applications. *Remote Sens. Environ.* **2009**, *113*, 2037–2051. [[CrossRef](#)]
3. Murchie, E.; Kefauver, S.; Araus-Ortega, J.L.; Muller, O.; Rascher, U.; Flood, P.; Lawson, T. Measuring the dynamic photosynthetic. *Ann. Bot.* **2018**, *122*, 207–220. [[CrossRef](#)] [[PubMed](#)]
4. Camino, C.; Zarco-Tejada, P.J.; Gonzalez-Dug, V. Effects of Heterogeneity within tree crowns on airborne-quantified SIF and the CWSI as indicators of water stress in the context of precision agriculture. *Remote Sens.* **2018**, *10*, 604. [[CrossRef](#)]
5. Jia, M.; Zhu, J.; Ma, C.; Alonso, L.; Li, D.; Cheng, T.; Tian, Y.; Zhu, Y.; Yao, X.; Cao, W. Difference and potential of the upward and downward sun-induced chlorophyll fluorescence on detecting leaf nitrogen concentration in wheat. *Remote Sens.* **2018**, *10*, 1315. [[CrossRef](#)]
6. Kalaji, H.M.; Bąba, M.; Gediga, K.; Goltsev, V.; Samborska, I.A.; Cetner, M.D.; Dimitrova, S.; Piszcz, U.; Bielecki, K.; Karmowska, K.; et al. Chlorophyll fluorescence as a tool for nutrient status identification in rapeseed plants. *Photosynth. Res.* **2018**, *136*, 329–343. [[CrossRef](#)]
7. Thoren, D.; Schmidhalter, W. Nitrogen status and biomass determination of oilseed rape by laser-induced chlorophyll fluorescence. *Eur. J. Agron.* **2009**, *30*, 238–242. [[CrossRef](#)]
8. Tagliabue, G.; Panigada, C.; Dechant, B.; Baret, F.; Cogliati, S.; Colombo, R.; Migliavacca, M.; Rademske, P.; Schickling, A.; Schüttemeyer, D.; et al. Exploring the spatial relationship between airborne-derived red and far-red sun-induced fluorescence and process-based GPP estimates in a forest ecosystem. *Remote Sens. Environ.* **2019**, *231*, 1–19. [[CrossRef](#)]
9. Mohammed, G.H.; Colombo, R.; Middleton, E.M.; Rascher, U.; vanderTol, C.; Nedbal, L.; Goulas, Y.; Pérez-Priego, O.; Damm, A.; Meroni, M.; et al. Remote sensing of solar-induced chlorophyll fluorescence (SIF) in vegetation: 50 years of progress. *Remote Sens. Environ.* **2019**, *231*, 1–39. [[CrossRef](#)]
10. Muller, O.; Keller, B.; Zimmerman, L.; Jedmowski, C.; Kleits, E.; Pingle, V.; Acebron, K.; dos Santos, N.Z.; Steier, A.; Freiwald, L.; et al. Field phenotyping and an example of proximal sensing of photosynthesis under elevated CO<sub>2</sub>. *IEEE IGARSS 2018*, 8252–8254. [[CrossRef](#)]
11. Matese, A.; Toscano, P.; Di Gennaro, S.F.; Genesio, L.; Vaccari, F.P.; Primicerio, J.; Belli, C.; Zaldei, A.; Bianconi, R.; Gioli, B. Intercomparison of UAV, aircraft and satellite remote sensing platforms for precision viticulture. *Remote Sens.* **2015**, *7*, 2971–2990. [[CrossRef](#)]
12. Liu, L.; Zhang, Y.; Wang, J.; Zhao, C. Detecting solar-induced chlorophyll fluorescence from field radiance spectra based on the fraunhofer line principle. *IEEE Trans. Geosci. Remote Sens.* **2005**, *43*, 827–832. [[CrossRef](#)]
13. Porcar-Castell, A.; Tyystjärvi, E.; Atherton, J.; van der Tol, C.; Flexas, J.; Pfündel, E.E.; Moreno, J.; Frankenberg, C.; Berry, J.A. Linking chlorophyll a fluorescence to photosynthesis for remote sensing applications: Mechanisms and challenges. *J. Exp. Bot.* **2014**, *65*, 4065–4095. [[CrossRef](#)] [[PubMed](#)]
14. Thesien, A.F. Detecting chlorophyll fluorescence from orbit: The fraunhofer line depth model. In *From Laboratory Spectroscopy to Remotely Sensed Spectra of Terrestrial Ecosystems*, 1st ed.; Muttiah, R.S., Ed.; Springer: Dordrecht, The Netherlands, 2002; pp. 203–232. [[CrossRef](#)]
15. Cogliati, S.; Verhoef, W.; Kraft, S.; Sabater, N.; Alonso, L.; Vicent, J.; Moreno, J.; Drusch, M.; Colombo, R. Retrieval of sun-induced fluorescence using advanced spectral fitting methods. *Remote Sens. Environ.* **2015**, *169*, 344–357. [[CrossRef](#)]
16. Guanter, L.; Frankenberg, C.; Dudhia, A.; Lewis, P.E.; Gómez-Dans, J.; Kuze, A.; Suto, H.; Grainger, R.G. Retrieval and global assessment of terrestrial chlorophyll fluorescence from GOSAT space measurements. *Remote Sens. Environ.* **2012**, *121*, 236–251. [[CrossRef](#)]
17. Sun, Y.; Frankenberg, C.; Jung, M.; Joiner, J.; Guanter, L.; Köhler, P.; Magney, T. Overview of Solar-Induced chlorophyll Fluorescence (SIF) from the Orbiting Carbon Observatory-2: Retrieval, cross-mission comparison, and global monitoring for GPP. *Remote Sens. Environ.* **2018**, *209*, 808–823. [[CrossRef](#)]
18. Zhang, Y.; Xiao, X.; Zhang, Y.; Wolf, S.; Zhou, S.; Joiner, J.; Guanter, L.; Verma, M.; Sun, Y.; Yang, I.; et al. On the relationship between sub-daily instantaneous and daily total gross primary production: Implications for interpreting satellite-based SIF retrievals. *Remote Sens. Environ.* **2018**, *205*, 276–289. [[CrossRef](#)]
19. Ni, Z.; Lu, Q.; Huo, H.; Zhang, H. Estimation of chlorophyll fluorescence at different scales: A review. *Sensors* **2019**, *19*, 3000. [[CrossRef](#)]

20. Siegmann, B.; Alonso, L.; Celesti, M.; Cogliati, S.; Colombo, R.; Damm, A.; Douglas, S.; Guanter, L.; Hanuš, J.; Kataja, K.; et al. The high-performance airborne imaging spectrometer HyPlant—From raw images to top-of-canopy reflectance and fluorescence products: Introduction of an automatized processing chain. *Remote Sens.* **2019**, *11*, 2760. [CrossRef]
21. Cogliati, S.; Colombo, R.; Celesti, M.; Tagliabue, G.; Rascher, U.; Schickling, A.; Rademske, P.; Alonso, L.; Sabater, N.; Schuettemeyer, D.; et al. Red and far-red fluorescence emission retrieval from airborne high resolution spectra collected by the hyplant-fluo sensor. *IEEE IGARSS* **2018**, 3935–3938. [CrossRef]
22. Bhandopadhyay, S.; Rastogi, A.; Juszczak, R.; Rademske, P.; Schickling, A.; Cogliati, S.; Julitta, T.; Mac Arthur, A.; Hueni, A.; Tomelleri, E.; et al. Examination of Sun-induced Fluorescence (SIF) signal on heterogeneous ecosystem platforms using 'HyPlant'. In Proceedings of the European Geosciences Union General Assembly (EGU), Vienna, Austria, 8–13 April 2018.
23. Tagliabue, G.; Panigada, C.; Dechant, B.; Baret, F.; Cogliati, S.; Colombo, R.; Migliavacca, M.; Rademske, P.; Schickling, A.; Schuettemeyer, D.; et al. Sun-Induced Fluorescence and photosynthesis estimation in a mixed forest ecosystem using high resolution airborne imagery. In Proceedings of the American Geophysical Union, Fall Meeting, Washington, DC, USA, 12–14 December 2018.
24. European Space Agency (ESA). Available online: <https://earth.esa.int/web/guest/missions/esa-future-missions/flex> (accessed on 9 April 2020).
25. Rascher, U.; Alonso, L.; Burkart, A.; Cilia, C.; Cogliati, S.; Colombo, R.; Damm, A.; Drusch, M.; Guanter, L.; Hanus, J.; et al. Sun-induced fluorescence—A new probe of photosynthesis: First maps from the imaging spectrometer HyPlant. *Glob. Change Biol.* **2015**, *21*, 4673–4684. [CrossRef] [PubMed]
26. Wieneke, S.; Ahrends, H.; Damm, A.; Pinto, F.; Stadler, A.; Rossini, M.; Rascher, U. Airborne based spectroscopy of red and far-red sun-induced chlorophyll fluorescence: Implications for improved estimates of gross primary productivity. *Remote Sens. Environ.* **2016**, *184*, 654–667. [CrossRef]
27. Ni, Z.; Liu, Z.; Li, Z.L.; Nerry, F.; Huo, H.; Sun, R.; Yang, P.; Zhang, W. Investigation of atmospheric effects on retrieval of Sun-Induced Fluorescence using hyperspectral imager. *Sensors* **2016**, *16*, 480. [CrossRef] [PubMed]
28. Bendig, J.; Gautam, D.; Malenovský, Z.; Lucieer, A. Influence of cosine corrector and uas platform dynamics on airborne spectral irradiance measurements. *IEEE IGARSS* **2018**, 8822–8825. [CrossRef]
29. Bhandopadhyay, S.; Rastogi, A.; Juszczak, R. Review of Top-of-Canopy Sun-Induced Fluorescence (SIF) studies from ground, UAV, airborne to spaceborne observations. *Sensors* **2020**, *20*, 1144. [CrossRef]
30. Zarco-Tejada, J.P.; Catalina, A.; González, M.R.; Martín, P. Relationships between net photosynthesis and steady-state chlorophyll fluorescence retrieved from airborne hyperspectral imagery. *Remote Sens. Environ.* **2013**, *136*, 247–258. [CrossRef]
31. Atherton, J.; Mac Arthur, A.; Hakala, T.; Maseyk, K.; Robinson, I.; Liu, W.; Honkavaara, E.; Porcar-Castell, A. Drone measurements of solar-induced chlorophyll fluorescence acquired with a low-weight DFOV spectrometer system. *IEEE IGARSS* **2018**, 8834–8836. [CrossRef]
32. Milton, E.J.; Schaepman, M.E.; Anderson, K.; Kneubühler, M.; Fox, N. Progress in field spectroscopy. *Remote Sens. Environ.* **2009**, *113*, 92–109. [CrossRef]
33. Mac Arthur, A.; Robinson, I. A critique of field spectroscopy and the challenges and opportunities it presents for remote sensing for agriculture, ecosystems, and hydrology. In Proceedings of the SPIE 9637 Remote Sensing for Agriculture, Ecosystems, and Hydrology XVII, Toulouse, France, 14 October 2015. [CrossRef]
34. Mac Arthur, A.; Robinson, I.; Rossini, M.; Davis, N.; MacDonald, K. A dual-field-of-view spectrometer system for reflectance and fluorescence measurements (Piccolo Doppio) and correction of etaloning. In Proceedings of the 5th International Workshop on Remote Sensing of Vegetation Fluorescence, Paris, France, 22–24 April 2014; Available online: [https://www.research.ed.ac.uk/portal/files/17385047/A\\_DFOV\\_spectrometer\\_system\\_for\\_reflectance\\_and\\_fluorescence\\_Piccolo.pdf](https://www.research.ed.ac.uk/portal/files/17385047/A_DFOV_spectrometer_system_for_reflectance_and_fluorescence_Piccolo.pdf) (accessed on 9 April 2020).
35. Mac Arthur, A.; Robinson, I.; Hagdorn, M.; Wood, J.; Kershaw, R.; Taylor, R. Piccolo spectrometer system for reflectance and fluorescence measurement from mobile and fixed platforms. In Proceedings of the Innovative Optical Tools for Proximal Sensing of Ecophysiological Processes (OPTIMISE), Vienna, Austria, 23–28 April 2017.
36. Bendig, J.; Malenovský, Z.; Gautam, D.; Lucieer, A. Solar-induced chlorophyll fluorescence measured from an unmanned aircraft system—Sensor etaloning and platform motion correction. *IEEE Trans. Geosci. Remote Sens.* **2019**. [CrossRef]

37. JB Hyperspectral Devices. Available online: <https://www.jb-hyperspectral.com/> (accessed on 7 July 2019).
38. Burkart, A.; Cogliati, S.; Schickling, A.; Rascher, U. A novel UAV-based ultra-light weight spectrometer for field spectroscopy. *IEEE Sens. J.* **2014**, *14*, 62–67. [[CrossRef](#)]
39. Becerra, J.; Martin, M.P.; Pacheco-Labrador, J.; Gonzalez-Cascon, R.; Melendo-Vega, J.R.; Angás, J. Chlorophyll Estimation in Mediterranean Quercus *ilex* tree canopies with hyperspectral vegetation indices at leaf and crown scales. In Proceedings of the IEEE YP Remote Sensing Conference, Aachen, Germany, 7–8 June 2018.
40. Garzonio, R.; Di Mauro, B.; Colombo, R.; Cogliati, S. Surface reflectance and sun-induced fluorescence spectroscopy measurements using a small hyperspectral UAS. *Remote Sens.* **2017**, *9*, 472. [[CrossRef](#)]
41. Cogliati, S.; Rossini, M.; Meroni, M.; Barducci, A.; Julitta, T.; Colombo, R. Unattended instruments for ground-based hyperspectral measurements: Development and application for plant photosynthesis monitoring. In Proceedings of the American Geophysical Union, Fall Meeting, San Francisco CA, USA, 5–9 December 2011.
42. Anderson, K.; Rossini, M.; Pacheco-Labrador, J.; Balzarolo, M.; Mac Arthur, A.; Fava, F.; Julitta, T.; Vescovo, L. Inter-comparison of hemispherical conical reflectance factors (HCRF) measured with four fibre-based spectrometers. *Opt. Express* **2013**, *21*, 605–617. [[CrossRef](#)] [[PubMed](#)]
43. Mathworks. Field Spectroscopy Facility Post Processing Toolbox—File Exchange—MATLAB Central. Available online: <https://uk.mathworks.com/matlabcentral/fileexchange/31547-field-spectroscopy-facility-post-processing-toolbox> (accessed on 9 April 2020).
44. Maseyk, K.; Atherton, J.; Thomas, R.; Wood, K.; Tausz-Posch, S.; Mac Arthur, A.; Porcar-Castell, A.; Tausz, M. Investigating forest photosynthetic response to elevated CO<sub>2</sub> using UAV-based measurements of Solar Induced Fluorescence. *IEEE IGARSS* **2018**, 8830–8833. [[CrossRef](#)]
45. Hart, K.M.; Curioni, G.; Blaen, P.; Harper, N.J.; Miles, P.; Lewin, K.F.; Nagy, J.; Bannister, E.J.; Cai, X.M.; Thomas, R.M.; et al. Characteristics of free air carbon dioxide enrichment of a northern temperate mature forest. *Glob. Change Biol.* **2019**, *26*, 1023–1037. [[CrossRef](#)] [[PubMed](#)]
46. Mihai, L.; Mac Arthur, A.; Hueni, A.; Robinson, I.; Sporea, D. Optimized spectrometers characterization procedure for near ground Support of ESA FLEX Observations: Part 1 Spectral Calibration and Characterization. *Remote Sens.* **2018**, *10*, 289. [[CrossRef](#)]
47. Herrmann, I.; Vosberg, S.K.; Townsend, P.A.; Conley, S.P. Spectral data collection by dual Field-of-View System under Changing Atmospheric Conditions—A case study of estimating early season soybean populations. *Sensors* **2019**, *19*, 457. [[CrossRef](#)]
48. Bendig, J.; Malenovský, Z.; Siegmann, B.; Rademske, P.; Krause, A.; Gruenhagen, L.; Koeing, S.; Prum, M.; Gautam, D.; Rascher, U.; et al. UAS-based chlorophyll fluorescence measurements of barley canopies—Results from FLEXsense 2019. In Proceedings of the International Network on Remote Sensing of Terrestrial and Aquatic Fluorescence, Davos, Switzerland, 5–8 March 2019.
49. Gautam, D.; Lucieer, A.; Bendig, J.; Malenovský, Z. Footprint determination of a spectroradiometer mounted on an unmanned aircraft system. *IEEE Trans. Geosci. Remote Sens.* **2019**. [[CrossRef](#)]
50. Gautam, D.; Lucieer, A.; Malenovsz, Z.; Watson, C. Comparison of MEMS-Based and FOG-Based IMUs TO Determine Sensor Pose on an Unmanned Aircraft System. *J. Surv. Eng.* **2017**, *143*. [[CrossRef](#)]
51. Gautam, D.; Watson, C.; Lucieer, A.; Malenovský, Z. Error Budget for Geolocation of Spectroradiometer Point Observations from an Unmanned Aircraft System. *Sensors* **2018**, *18*, 3465. [[CrossRef](#)]
52. Gautam, D.; Lucieer, A.; Watson, C.; McCoull. Lever-arm and boresight correction, and field of view determination of a spectroradiometer mounted on an unmanned aircraft system. *ISPRS J. Photogramm. Remote Sens.* **2019**, *155*, 25–36. [[CrossRef](#)]
53. Julitta, T.; Burkart, A.; Colombo, R.; Rossini, M.; Schickling, A.; Migliavacca, M.; Cogliati, S.; Wutzler, T.; Rascher, U. Accurate measurements of fluorescence in the O2A and O2B band using the FloX spectroscopy system—Results and prospects. In Proceedings of the Potsdam GHG Flux Workshop: From Photosystems to Ecosystems, Potsdam, Germany, 24–26 October 2017.
54. Cogliati, S.; Celesti, M.; Cesana, I.; Miglietta, F.; Genesio, L.; Julitta, T.; Schuettemeyer, D.; Drusch, M.; Rascher, U.; Jurado, P.; et al. A spectral fitting algorithm to retrieve the fluorescence spectrum from canopy radiance. *Remote Sens.* **2019**, *11*, 1840. [[CrossRef](#)]
55. Drusch, M.; Moreno, J.; Del Bello, U.; Franco, R.; Goulas, Y.; Huth, A.; Kraft, S.; Middleton, E.; Miglietta, F.; Mohammed, G.; et al. The FLuorescence EXplorer mission concept—ESA’s Earth Explorer 8. *IEEE Trans. Geosci. Remote Sens.* **2018**, *55*, 1273–1284. [[CrossRef](#)]

56. Damm, A.; Guanter, L.; Laurent, C.E.; Schaepman, M.E.; Schickling, A.; Rascher, U. FLD-based retrieval of sun-induced chlorophyll fluorescence from medium spectral resolution airborne spectroscopy data. *Remote Sens. Environ.* **2014**, *256*–266. [[CrossRef](#)]
57. Sabater, N.; Vicent, J.; Alonso, L.; Verrelst, J.; Middleton, E.M.; Porcar-Castell, A.; Moreno, J. Compensation of Oxygen transmittance effects for proximal sensing retrieval of canopy-leaving sun-induced chlorophyll fluorescence. *Remote Sens.* **2018**, *10*, 1551. [[CrossRef](#)]
58. Wang, N.; Bartholomeus, H.; Kooistra, L.; Suomalainen, J.; Brede, B.; Novani, M.; Masiliunas, D.; Clevers, J. Measuring temporal patterns of crop sun-induced chlorophyll fluorescence at canopy and plot scale. In Proceedings of the 11th EARSeL SIG IS Workshop, Brno, Czech Republic, 6–8 February 2019.
59. Damm, A.; Erler, A.; Hillen, W.; Meroni, M.; Schaepman, M.E.; Verhoef, W.; Rascher, U. Modeling the impact of spectral sensor configurations on the FLD retrieval accuracy of sun-induced chlorophyll fluorescence. *Remote Sens. Environ.* **2011**, *115*, 1882–1892. [[CrossRef](#)]
60. Alonso, L.; Sabater, N.; Vicent, J.; Mihai, N.; Moreno, J. Atmospheric and instrumental effects on the fluorescence remote sensing retrieval. *IEEE IGARSS* **2018**. [[CrossRef](#)]
61. Li, D.; Zheng, H.; Xu, X.; Lu, N.; Yao, X.; Jiang, J.; Wang, X.; Tian, Z.; Zhu, Z.; Cao, W.; et al. BRDF effect on the estimation of canopy chlorophyll content in paddy rice from UAV-based hyperspectral imagery. *IEEE IGARSS* **2018**, 6464–6467. [[CrossRef](#)]
62. Burkart, A.; Aasen, H.; Alonso, L.; Menz, G.; Bareth, G.; Rascher, U. Angular dependency of hyperspectral measurements over wheat characterized by a novel UAV based goniometer. *Remote Sens.* **2015**, *7*, 725–746. [[CrossRef](#)]
63. Pinto, F.; Müller-Linow, M.; Schickling, A.; Cendrero-Mateo, M.P.; Ballvora, A.; Rascher, U. Multiangular observation of canopy sun-induced chlorophyll fluorescence by combining imaging spectroscopy and stereoscopy. *Remote Sens.* **2017**, *9*, 415. [[CrossRef](#)]



© 2020 by the authors. Licensee MDPI, Basel, Switzerland. This article is an open access article distributed under the terms and conditions of the Creative Commons Attribution (CC BY) license (<http://creativecommons.org/licenses/by/4.0/>).

1.1.1 *Second publication [Quiros-Vargas et al., in preparation]*

“Spatial relation between solar-induced chlorophyll fluorescence and plant available water in the root zone”

**Authors (country):**

J. Quiros-Vargas (GE)  
Cosimo Brogi (GE)  
A. Damm (CH)  
B. Siegmann (GE)  
P. Redemske (GE)  
V. Burchard (ES)  
Vera Krieger (GE)  
Marius Schmidt (GE)  
Jan Hanuš (CZ)  
L. Weihermueller (GE)  
Onno Mueller (GE)  
Uwe Rascher (GE)

**Aimed journal:** Remote Sensing of Environment

**Status:** In preparation

**Contribution of the doctorate candidate:**

- Conceptualization: 80%
- Data analysis: 80%
- Writing: 90%
- Field work: 10%

**CLARIFICATION NOTE:** in the original (first) version of the thesis (delivered to the University of Bonn in October 2022) this paper was reported as “in revision at PNAS-Nexus”, however, the manuscript was rejected by the journal on December 2022.

In the present thesis’s re-print I kept the same former version of the study. Nevertheless, it is worth mentioning that during 2023 the study was fundamentally revisited and updated, and the new version is aimed to be re-submitted, this time to Remote Sensing of Environment.

# **Spatial relation between solar-induced chlorophyll fluorescence and plant available water in the root zone**

Juan Quiros-Vargas<sup>1,\*</sup>, Cosimo Brogi<sup>2</sup>, Alexander Damm<sup>3,4</sup>, Bastian Siegmann<sup>1</sup>, Patrick Rademske<sup>1</sup>, Vicente Burchard-Levine<sup>5</sup>, Vera Krieger<sup>1</sup>, Marius Schmidt<sup>2</sup>, Jan Hanuš<sup>6,7</sup>, Lutz Weihermüller<sup>2</sup>, Onno Muller<sup>1</sup>, Uwe Rascher<sup>1</sup>

<sup>1</sup>Institute of Bio- and Geosciences, Plant Sciences (IBG-2), Forschungszentrum Jülich GmbH, Jülich, Germany, 52428; <sup>2</sup>Institute of Bio- and Geosciences, Agrosphere (IBG-3), Forschungszentrum Jülich GmbH, Jülich, Germany, 52428; <sup>3</sup>Department of Geography, University of Zurich, Zurich, Switzerland, CH-8057; <sup>4</sup>Eawag, Swiss Federal Institute of Aquatic Science & Technology, Surface Waters – Research and Management, Dübendorf, Switzerland, CH-8600; <sup>5</sup>Environmental Remote Sensing and Spectroscopy Laboratory (SpecLab), Spanish National Research Council (CSIC), Madrid, Spain; <sup>6</sup>Global Change Research Institute of the Czech Academy of Sciences, Brno, Czech Republic, 603 00; <sup>7</sup>Czech Technical University, Faculty of Civil Engineering, Department of Geomatics, Czech Republic

\*Corresponding author

**Email:** [j.quiros@fz-juelich.de](mailto:j.quiros@fz-juelich.de)

**Author Contributions:** J.Q-V, C.B., A.D., B.S., V.K., O.M., L.W. and U.R. designed research; J.Q-V and C.B. performed research; J.Q-V, C.B., P.R., V.B-L, M.S. and J.H. analyzed data; and J.Q-V, A.D., B.S. and U.R. wrote the paper.

**Classification:** Biological sciences; agricultural sciences

**Keywords:** fluorescence emission efficiency, mild water stress assessment, water management

**This PDF file includes:** Main Text; Figures 1 to 3; Supplemental information figures S1 to S3

## **Abstract**

The use of water in agricultural activities is huge, and alarmingly inefficient. Recent advances on the remote sensing (RS) of solar-induced chlorophyll fluorescence (SIF) opens the possibility for the development of new approaches to assess the water status of crops, since SIF is directly related to photosynthesis and thus to plant physiological responses to limitations in the water supply. In principle, the understanding given by SIF information about the spatial and temporal dynamics of crop water needs can be used to improve irrigation practices and therefore water use in agriculture. Nevertheless, this is still a young research line and there are multiple questions to be answered before SIF-based irrigation practices can be implemented on the field. In this study we provide one further step in such direction by developing new knowledge concerning the effect of variable plant available water in the root zone (PAW) levels on the canopy SIF emission efficiency, or  $E_f$ . Based on data from three vegetation periods (2018, 2019 and 2020), we found a significant positive correlation between PAW and  $E_f$  in mildly water stressed fields, but no correlation in well-watered fields. Moreover, we found that SIF responded stronger and faster to low PAW compared to reflectance- and thermal-based information in the spatial and temporal domains, respectively. The spatial characterization of the  $E_f$ -PAW

relation herewith reported at high resolution (1 m pixel<sup>-1</sup>) lays the foundation for future SIF-based precision irrigation studies.

## **Significance Statement**

Agriculture is one of the most water-demanding and -wasting activities in times when global warming threaten to increase the risk of water scarcity. The early detection of water shortage in crops is currently of utmost importance to improve water use efficiency in agriculture. Developments in remote sensing (RS) of solar-induced chlorophyll fluorescence (SIF) opens the opportunity for new farm level approaches, due to the direct relation of SIF with plant physiological responses to early soil water shortage. In this context, we provide new insight on the spatial sensitivity of SIF to variations of plant available water in the root zone (PAW), serving as one step further towards the development of SIF-based precision irrigation techniques for a sustainable agricultural water use.

## **Introduction**

Climate change and water wasting customs at domestic and industrial scales threaten to limit the access to freshwater for a large part of the population. Agriculture is the most water consuming sector (FAO, 2021) and one of the most inefficient activities using such resource as well. Sensitive and harmonized information of actual crop-water status is essential to make agricultural water use more sustainable, while remote sensing (RS) is particularly suitable for providing such data continuously over large crop areas. Nevertheless, widely used RS approaches based on canopy reflectance and derived vegetation indices (VIs) tend to represent interwoven sensitivities for evolving crop water stress caused by physiological, biochemical, and canopy structural responses that are difficult to disentangle (Damm et al., 2018). Moreover, results of thermal-based approaches are difficult to interpret, since canopy temperature can also vary due to external factors not related to limitations in the water supply, e.g., wind speed, air temperature, and humidity (Gerhards et al., 2019).

Solar-induced chlorophyll fluorescence (SIF) is a low intensity light released from the photosynthetic apparatus between 600 to 800 nm with emission peaks in the red (SIF<sub>Red</sub>, 687 nm) and far-red light (SIF<sub>Far-red</sub>, 760 nm, used for all the calculations in this study and hereafter referred just as SIF; Mohammed et al., 2019; Meroni et al., 2009). Due to its direct link with photosynthesis (Guanter et al., 2014), and thus with plant physiological responses to limitations in the water supply (Jonard et al., 2020), SIF information has been reported as a suitable complement of reflectance- and temperature-based RS approaches for crop water stress assessment. In particular, the sensitivity of SIF for subtle plant physiological reactions (Zeng et al., 2022) happening before changes in leaf temperature (Damm et al., 2022), orientation (Damm et al., 2018) or pigments content (Xu et al., 2018), suggest its potential use for the detection of initial effects of mild water stress at fine spatial (cm-m's) and temporal (min-h's) resolutions.

The use of SIF information for operational crop water stress assessment is nevertheless not established yet, and it requires further investigations involving efforts from several research areas like remote sensing, plant physiology and soil science. The first fundamental questions to be answered are those related to the spatio-temporal variations of SIF emission in the course of gradually reducing water supply in natural field conditions. In this sense, Shen et al. (2021) found SIF information to be more sensitive

than the normalized difference vegetation index (NDVI) to changes in the surface soil moisture at satellite ( $> 1\text{ km pixel}^{-1}$ ) scale. Besides, using higher spatial resolution ( $\sim 1\text{ m pixel}^{-1}$ ) data of one agricultural field, von Hebel et al. (2018) reported the significant relation between subsoil apparent electrical conductivity (related to soil physical properties) and airborne-based SIF. At a similar scale, Quiros et al. (2020) found a significant spatial match between varying SIF and qualitative soil units in an area where the NDVI data was homogeneous. More recently, Damm et al. (2022) assessed the temporal domain and could for the first time observe a short-term rise and a subsequent decline of SIF (theoretically known as 'double response') to evolving water stress with airborne data. Despite these meaningful advances, further studies at high spatiotemporal resolution are necessary to fill the knowledge gap concerning the SIF response of crops to varying water supply levels.

In this study our goal was to (i) elucidate for the first time the spatial relation between SIF and PAW with high resolution ( $1\text{ m pixel}^{-1}$ ) datasets of sugar beet, potato, and winter wheat fields observed over three growing seasons (2018, 2019 and 2020), and characterized by different water supply conditions: mild water stress (non-irrigated fields without precipitation within two weeks before SIF data acquisition) and no water stress (e.g., artificial irrigation, precipitation). The analysis of mild water stress scenarios is of utmost importance, since it can help to improve our understanding of the dynamic relation between SIF and PAW, which can be the basis to further develop precision irrigation techniques. This could help farmers to detect water shortage effects early enough and initialize irrigation to avoid crop losses. Additionally, we also aimed to (ii) compare the response of SIF to varying PAW levels with the response observed from reflectance- and temperature-based data in one specific field.

For a more detailed analysis, SIF data was further processed to represent the SIF emission efficiency ( $E_f$ ), which accounts for the scattering of emitted SIF within the canopy and absorbed photosynthetically active radiation. Thus, we use  $E_f$  as the fraction of SIF actually linked to physiological processes, since it is expected to be more sensitive to changes in soil water supply.  $E_f$  was calculated using the fluorescence correction vegetation index (FCVI) as proposed by Yang et al. (2020).  $E_f$  data was then compared with PAW information, which represents the fraction of the gross soil water content that is actually available to be consumed by plants (Wong and Assen, 2006). High resolution PAW maps were derived from soil mapping techniques that combine hydrogeophysical measurements (i.e., electromagnetic induction (EMI) for the measurement of apparent electrical conductivity (ECa)) and direct soil sampling (Brogi et al., 2019) proved by Brogi et al. (2021) to be effective for this study area.

This research was done within the frame of preparatory studies for the forthcoming fluorescence explorer (FLEX) mission of the European Space Agency (ESA; Drusch et al., 2017) planned to be launched in 2025.

## **Results**

The  $E_f$ -PAW spatial relation for different crops (i.e., sugar beet, potato, and winter wheat), growing seasons (i.e., 2018-2020) and water supply conditions (i.e., mild water stress and no water stress) is presented graphically and numerically in Figs. 1 and 2, respectively. A distinction is made between fields located in the upper (UT) or lower (LT) terraces that shape the landscape of the study area, characterized by lower and higher PAW values, respectively. Absolute  $E_f$  values show great differences, with the lowest ( $\sim 1 \times 10^{-5}\text{ nm}^{-1}$ ) and highest ( $> 6 \times 10^{-5}\text{ nm}^{-1}$ ) values in a mild water stressed winter wheat and irrigated potato

fields, respectively. Higher  $E_f$  is observed in the zones with higher PAW as frequently present in the LT, which is more pronounced in winter wheat in 2018 and 2020 but not visible in 2019 probably due to an earlier planting date in that year (Fig. 2a-c). Remarkably,  $E_f$  of mild water stressed sugar beet fields significantly increases with higher levels of PAW in 2018 (Fig. 2d) and 2019 (Fig. 2e). Particularly,  $E_f$  values in (irrigated) potato fields remained nearly constant regardless of the spatial heterogeneity in PAW (Fig. 2g-i). Similarly,  $E_f$  remains mostly constant in all 2020 fields (Fig. 2c, f and i), which are considered as non-stressed due to the accumulation of  $25 \text{ l m}^{-2}$  of precipitation a few days before the airborne campaign.

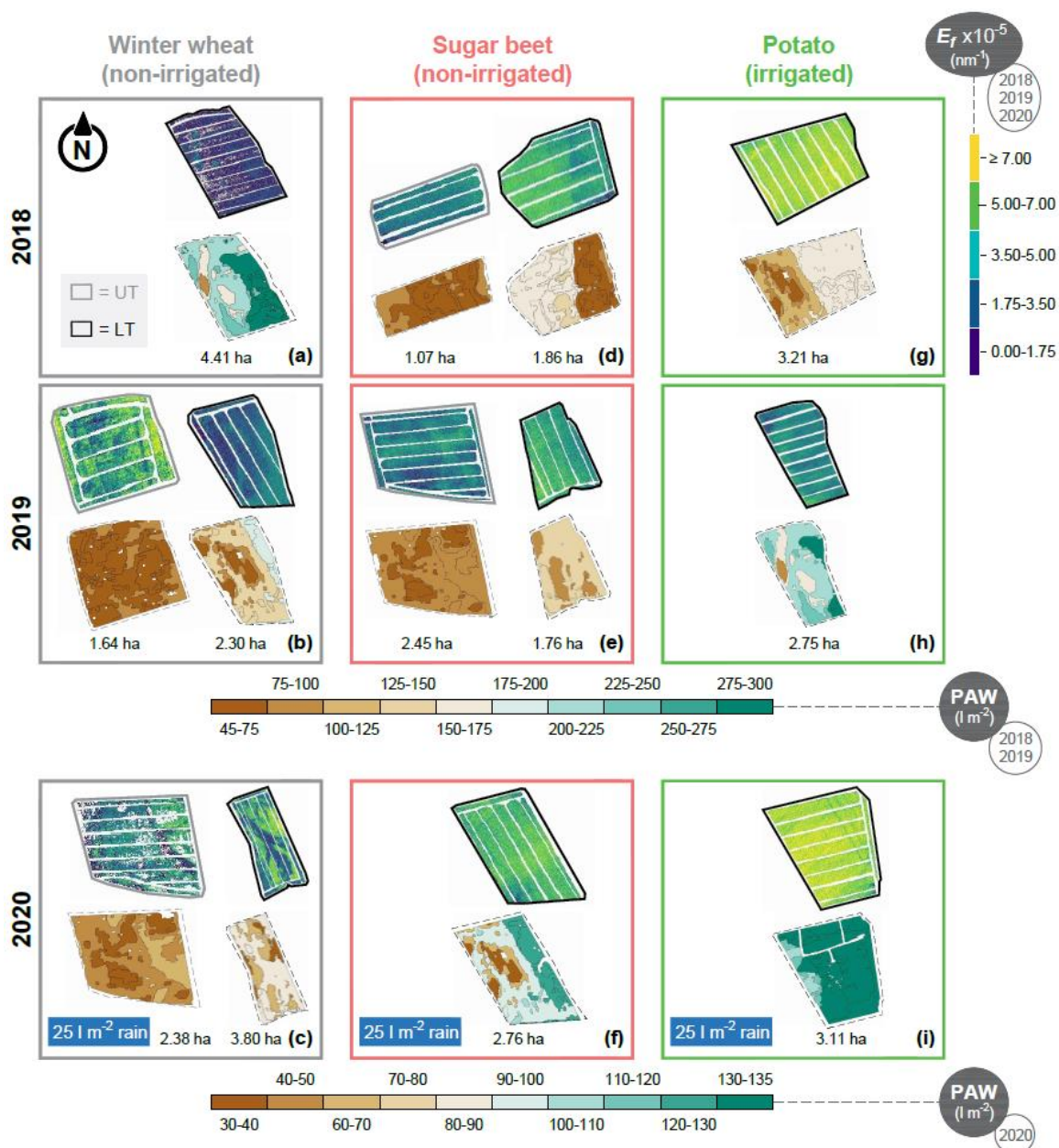


**Figure 1.** Solar-induced chlorophyll fluorescence emission efficiency ( $E_f$ ; upper maps with thick boundaries) and plant available water in the root zone (PAW; lower maps with dashed boundaries)

maps of the non-irrigated winter wheat (a-c, grey charts) and sugar beet (d-f, red charts) fields, as well as irrigated potato (g-i, green charts) fields in 2018 (top row), 2019 (medium row) and 2020 (bottom row) according to their location either in the upper (UT, gray) and lower (LT, back) terrace. Blue labels indicate the scenarios in 2020 where 25 l m<sup>-2</sup> of precipitation were registered in the seven days prior to RS data acquisition.

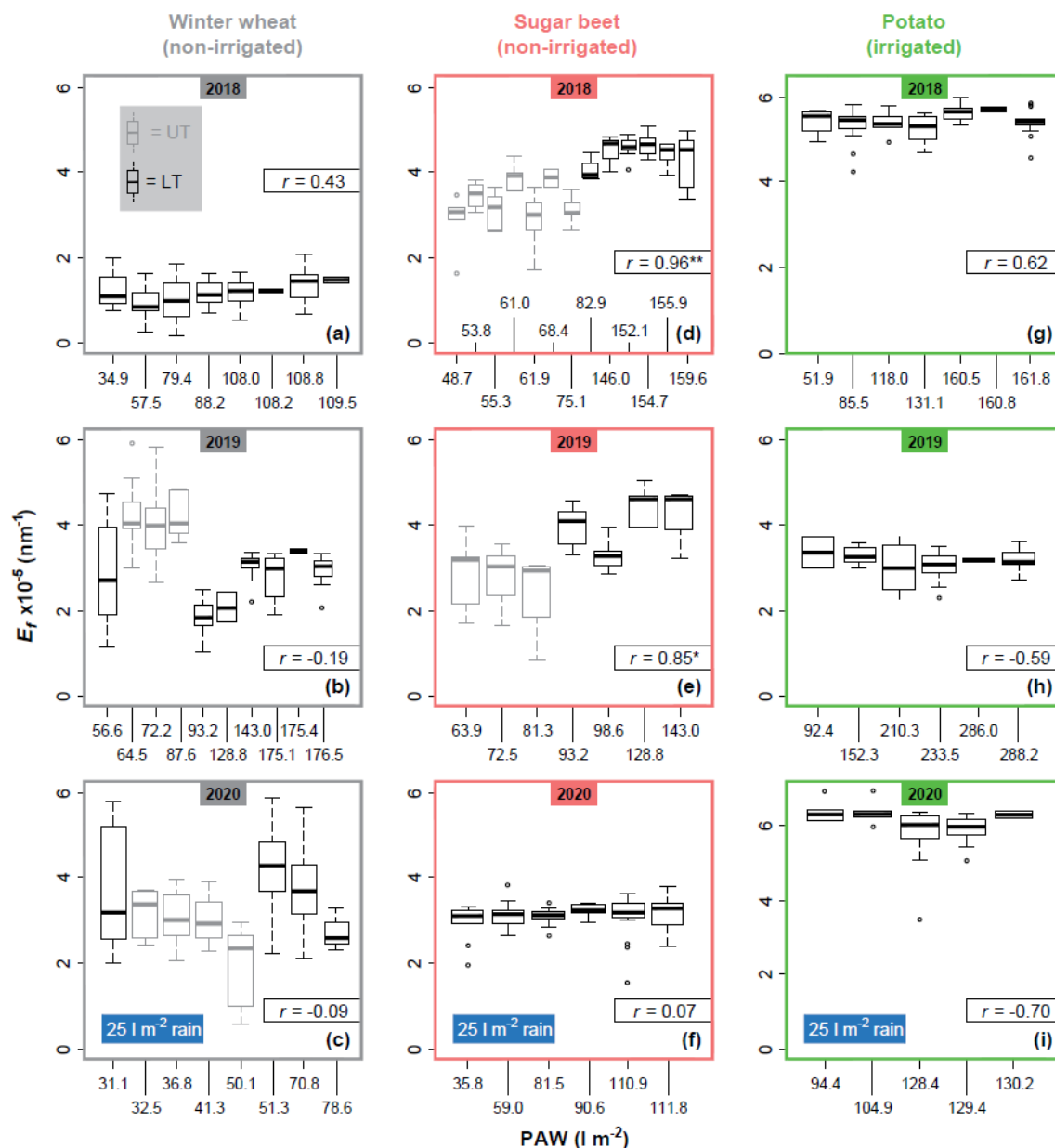


**Figure 2.** Solar-induced Chlorophyll Fluorescence Emission Efficiency ( $E_f$ ) box-plotted with plant available water in the root zone (PAW) for the non-irrigated winter wheat (a-c, grey chart) and sugar beet (d-f, red chart) fields, as well as irrigated potato (g-i, green chart) fields in 2018 (top row), 2019 (medium row) and 2020 (bottom row) according to their location either in the upper (UT, gray) or lower (LT, back) terrace. Blue labels indicate the scenarios in 2020 where 25 l m<sup>-2</sup> of precipitation were registered in the seven days prior to RS data acquisition. \*\* and \* represent significant relations at  $p < 0.01$  and  $p < 0.05$ , respectively.

Of particular interest is the relation of the SIF response to varying PAW levels compared to the response of reflectance-based (i.e., the enhanced vegetation index -EVI-; Huete et al., 2002) and thermal-based (i.e., land surface temperature, LST) products. We contrasted the spatial response of morning SIF (Fig. 3a), LST (Fig. 3b) and EVI (Fig. 3c), and afternoon SIF (Fig. 3d) and LST (Fig. 3e) across a decreasing PAW transect of 147 m in length from X to X' (Fig. 3f) in a non-irrigated winter wheat field located in the UT-LT transition area. The transect crosses fundamentally different soils in the UT-LT division, where the change of PAW is attributed to the presence of coarse alluvial depositions between the terraces. Here, alluvial and aeolian deposits are mixed due to natural depositional processes and anthropogenic management (Brogi et al., 2019). Along this transect, SIF starts decreasing close to the beginning of the lower PAW zone, which is about 45 m before the EVI did. Moreover, SIF yielded a stronger reduction ( $\% \Delta = -22\%$ ) compared to the reduction in EVI ( $\% \Delta = -5\%$ ; Fig. 3g). Remarkably, the stronger decrease in EVI matches with the area where plants suffer the most from low PAW, since most of the shallow soil has conserved its original alluvial characteristics (e.g., presence of rocks and sandy textures). To our knowledge, these results show for the first time evidence of the anticipated higher sensitivity of SIF to mild water stress in the spatial domain compared to the greenness-based EVI. A similar comparison done between morning (~10:30 h) and afternoon (~16:15 h) SIF and LST suggest a ~6 h earlier response of SIF to a lower PAW zone. In the morning, SIF showed a stronger change ( $\% \Delta = |22|$ ) compared with LST ( $\% \Delta = |5|$ ), while in the afternoon the difference is less pronounced ( $\% \Delta = |20|$  in SIF and  $\% \Delta = |13|$  in LST; Fig. 3h). Similarly as observed with the EVI, the LST data show the stronger decrease in soil zones with lower water retention capabilities.

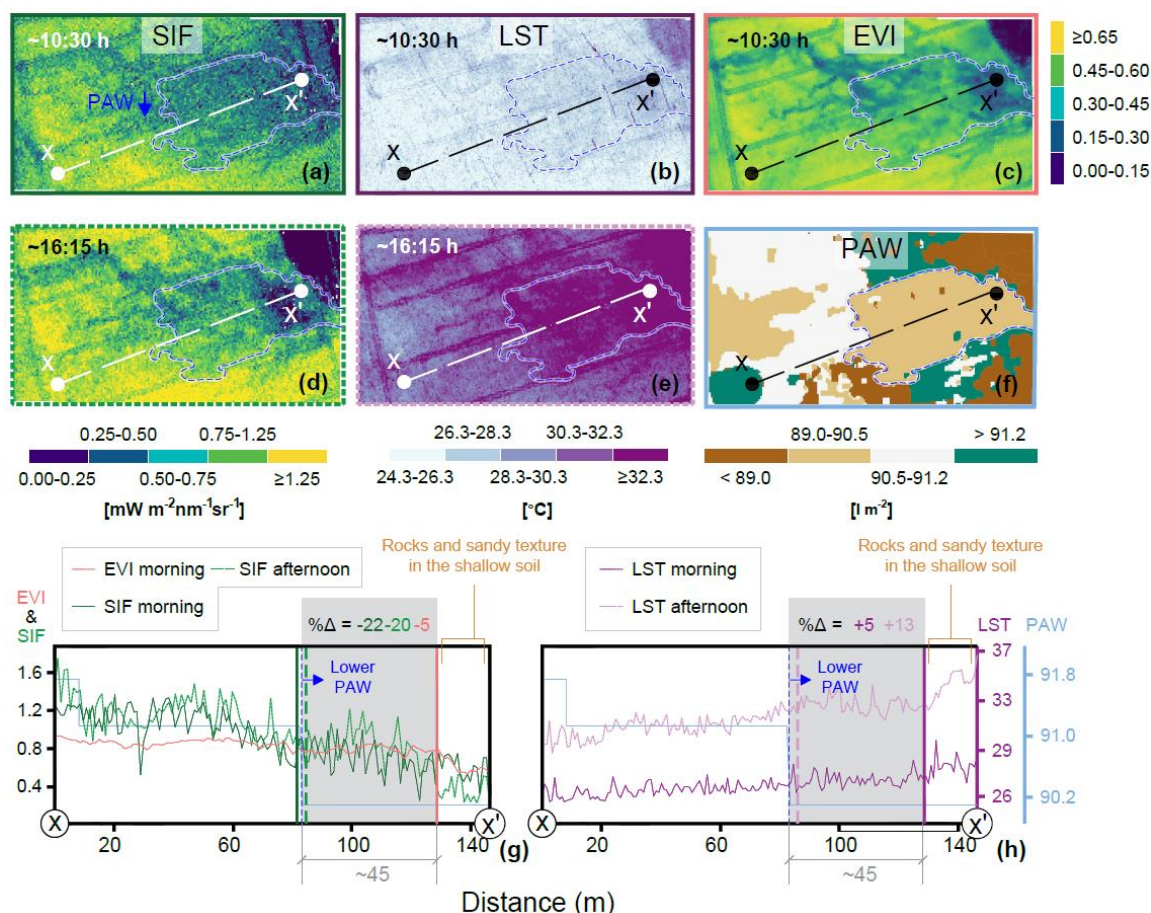


**Figure 3.** Morning solar induced chlorophyll fluorescence (SIF; a), land surface temperature (LST; b) and enhanced vegetation index (EVI; c), and afternoon SIF (d) and LST (e) maps captured on June 23<sup>rd</sup> (2020) in a winter wheat field located in the border between the upper (UT) and lower (LT) terraces. A lower plant available water in the root zone (PAW; f) area is highlighted in all the maps with a dashed blue line. SIF, LST, EVI and PAW values across the X-X' profile are presented in panels (g) and (h), with the respective change percentages ( $\% \Delta$ ) in the lower PAW area. Vertical green, red and purple bars within (g) and (h) represent the approximate response start points of SIF, EVI and LST respectively.

## Discussion

The great difference between the minimum and maximum absolute  $E_f$  values observed in mild water stressed winter wheat and not stressed potato fields, respectively, might be attributed to their contrasting phenological stages. While potato was at an early stage of development with accelerating metabolism, winter wheat was in an opposite situation already approaching senescence. Moreover, significant positive  $E_f$ -PAW relationships detected for mild water stress conditions in sugar beet can be explained by the time of SIF data acquisition in the seasonal and diurnal context. Considering the seasonal context, the strong  $E_f$ -PAW relationship is attributable to the early phenological stage of the crop with actively growing plants (Joiner et al., 2014). In those stages, the constant demand of resources makes plants more sensitive to even slight variations in water supply. Furthermore, the higher water demand of sugar beet (FAO 2012) might additionally

increase its sensitivity for decreasing PAW. Considering the diurnal context, SIF data were collected at ~10:30 h, a time when SIF tends to increase (Siegmann et al., 2021) alongside the photochemical activity (Pinto et al., 2016). Such a positive relation might indicate the greater photosynthetic rate and thus higher SIF signals (van der Tol et al., 2016) in zones with a higher amount of PAW.

In winter wheat, the positive slope observed on the LT field of 2018 may be caused by different degrees of senescence in zones with different PAW. Lower  $E_f$  values in the zones with less PAW can be explained by the shorter growing period in these areas, where senescence and chlorophyll degradation (Chapman et al., 2021) might occurred earlier. On the contrary, slower senescence and higher  $E_f$  values of the analyzed time point are expected in areas with more water available for plants. The discussed results suggest that spatial variations in  $E_f$  of a canopy exposed to homogenous photosynthetically active radiation intensity (i.e., open sky conditions), and free of significant biotic and abiotic stressors, respond to differences in PAW. Nevertheless, such a significant spatial relationship between  $E_f$  and PAW cannot be detected in fields with sufficient rain or artificial water supply. Under those conditions the  $E_f$  spatial dynamics might be determined by other factors like specific poor soil chemical properties of a region, which constitutes an unexplored research field.

The anticipated  $E_f$  response to lower PAW, compared with EVI and LST, can be explained by the higher  $E_f$  sensitivity to subtle changes in plant physiology under the studied mild stress condition. These findings illustrate the importance of integrating high spatio-temporal resolution information (Porcar-Castell et al., 2021) for the early detection of water shortage effects aiming at timely irrigation to improve the water use efficiency (Ač et al., 2015) and avoid crop losses. Moreover, such gradual response of SIF to crop water demands in the spatial domain suggest its potential use for the development of new precision irrigation tools. To our knowledge, these results show for the first time evidence of the anticipated higher sensitivity of SIF to mild water stress compared to the greenness-based EVI and thermal-based LST. Our results complement satellite-based studies (Liu et al., 2021; Shen et al., 2021) by providing a high-spatial-resolution perspective on the sensitivity of SIF to varying soil water content and evolving water limitation. Our results additionally complement satellite-based studies (Liu et al., 2021; Shen et al., 2021) by providing a high-spatial-resolution perspective on the sensitivity of SIF to varying soil water content and evolving water limitation.

Since maintaining water relations is crucial for plant metabolism and growth, plants have developed multiple strategies to structurally and functionally acclimate to limitations in soil water. These acclimatory mechanisms include sensing of water potential by the roots, hormone signaling from the root to the shoot, closure of stomata, adjustments of root and shoot growth, alterations in leaf morphology and anatomy and finally leaf shedding. These mechanisms occur on different time scales, are dynamically adjusted to the severity of drought and are dependent of the ecological plasticity of a species. Thus, it is very complex to causally separate those adaptation mechanisms and to understand their relations to SIF emission intensity, while it can be assumed that SIF emission intensity is primarily determined by the amount of canopy chlorophyll content and the efficiency of photosynthetic light reactions. Nevertheless, the comprehension of the SIF-PAW link involves considering the contribution of plant responses related to specific processes according to the stress severity (Fig. 4a1). For instance, strong changes in the pigments composition, canopy structure and morphology might be visible when the stress intensity has increased over weeks to months. Stomatal closure and reduction of the RuBisCo metabolic efficiency responses are more immediate as they are activated min to

h's after a water supply shortage began. This early reaction can be detected with high spatiotemporal SIF information (Damm et al., 2022), which is indeed one of the major advantages of using SIF data (Fig. 4b).

Additional confounding factors within the SIF-PAW spatial relation can be introduced from the soil carbon content, nutrient status (especially N-content,) and compaction, due to the possible influence of soil properties on crop growth and thus on the SIF spatial heterogeneity. Irrespectively of the influence of those soil properties, the soil profile depth (Fig. 4a2) is likely the most important one in the study region, due to the heterogeneous geology and associated pedology (Rudolph et al., 2015). In general, lowest PAW found in this study area is related to shallow soil depth and those areas also show lower SIF. Here, it has to be mentioned that a smaller soil profile depth will also impact other soil properties alongside PAW, with nutrient availability being the most relevant one. However, nutrient (especially N) availability in the study area might well be artificially homogenized due to the high amounts of mineral fertilizers that are normally applied by farmers. Additionally, the soil organic carbon content was found to be relatively homogeneous across the study area (Reichenau et al. 2020).

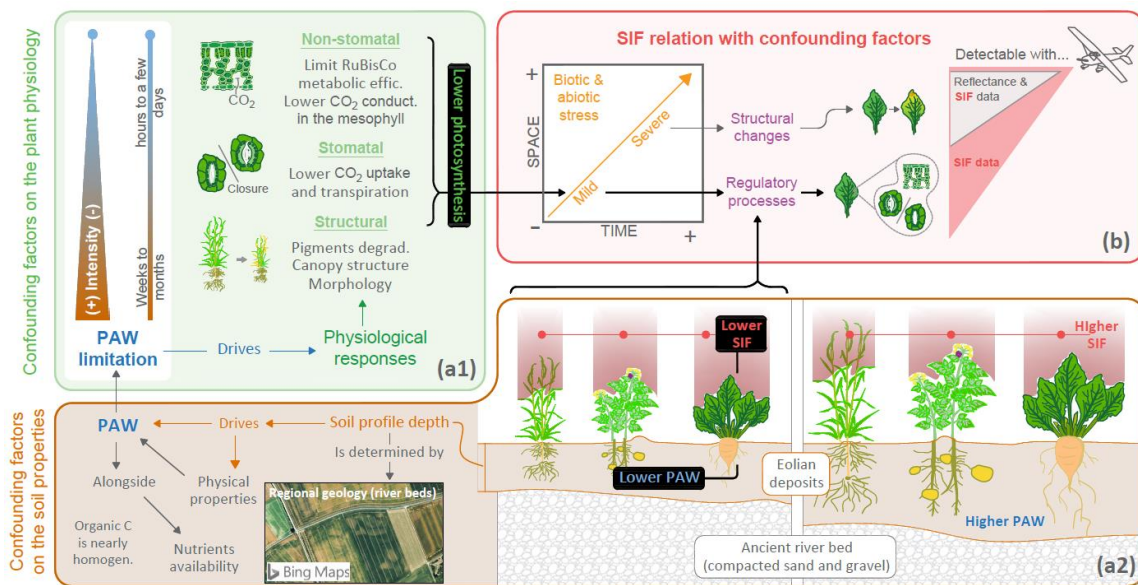


**Figure 4:** Plant physiology- (a1) and soil-related (a2) factors that can confound the solar-induced chlorophyll fluorescence (SIF)-plant available water in the root zone (PAW) relation due to their influence on the spatiotemporal expression of a stress detected in the SIF signal (b). Thick black lines indicate the link between the confounding factors and SIF.

Since soil water limitation provokes numerous different responses in plants, its effect on the spectral properties of vegetation is different and might not only be related to the emission of SIF (Gerhards et al., 2019). Therefore, the complementary use of SIF-with thermal- and reflectance-based information is important to detect the cascade of physiological and structural changes of plants under water stress conditions (Damm et al., 2018). In this context, integrative multi-sensor approaches must be developed and employed for an effective plant water stress monitoring (Panigada et al., 2014). It is worth

mentioning that such complementarity among data sources should account for the type of crop water stress being analyzed, whether it is mild, established, or severe. In this sense, SIF information might be more relevant in detecting mild stress (as herewith addressed), and thus in prescribing irrigation only for selected locations, whereas thermal and reflectance data might play a major role in established and severe stressed environments, respectively.

Since we investigated the  $E_f$ -PAW relation using single  $E_f$  snapshots during an evolving process, a limitation of this study is the lack of higher resolution time series to fully understand how the  $E_f$ -PAW relation would vary considering other times of the day. This motivates further research on a diurnal scale to analyze, e.g., the relation between SIF and PAW during the so-called midday depression and afternoon recovery of photosynthesis. Another limitation of this study was the use of PAW information derived from a geophysics-based soil map, in the absence of actual soil water content information. Although the used PAW data served to provide a first insight into the  $E_f$ -PAW spatial relation in high resolution, future investigations should aim to use either actual soil moisture or more accurately modeled PAW. Within this context, recent advancements in RS technology for soil moisture estimation can support further studies at larger spatial scales. For instance, airborne radar technology like the scanning L-band active passive (SLAP) sensor from NASA (Kim, 2015), or the satellite-based soil moisture passive and active (SMAP) and SMOS (Ma et al., 2019) data sources of NASA and ESA, respectively, have great potential to be comprehensively analyzed together with SIF information.

## **Materials and Methods**

**Study area:** The study site was located near Selhausen, western Germany (50.865228° N, 6.450074° W), a farming area composed of 50 fields, where agricultural investigations in a variety of summer and winter crops are regularly conducted (Simmer et al., 2015). To better understand the influence of contrasting environments (species × phenology × water supply) on the SIF-PAW relation, we analyzed winter wheat (in early ripening phase), as well as sugar beet (vegetative growth phase) and irrigated potato (during tubers formation; Fig. 5a) fields covering a total of 33.50 ha distributed in individual fields captured in 2018 (Fig. 5b), 2019 (Fig. 5c) and 2020 (Fig. 5d). The multiple year comparison was done to add knowledge on the effect of the water supply factor, since each year presents different precipitation regimes. The location of the study site within Germany and the specific location of the individual fields is presented in Fig. 5d and e, respectively. The yellow dashed line in Fig. 5e shows the division between an upper and lower terrace (UT and LT). The UT present shallow soils with a fine loess layer (up to 30-90 cm depth) covering coarse materials; whereas the LT is composed of soils with a thicker loess layer over a generally less coarse material (Brogi et al., 2019). Monthly temperatures were similar within the three observed years (~18 °C). In the two weeks before data acquisition in 2018 and 2019, the low amount of precipitation likely resulted in a reduction of available soil water resources. Especially 2018 is known to have been generally affected by an intense drought period (Graf et al., 2020). We can thus assume that plants had to cope with limited soil water availability in these two years (see also the calculation of plant available water in the root zone, PAW). In 2020, on the contrary, 25 l m<sup>-2</sup> of precipitation was recorded in the seven days before the airborne campaign, and therefore, we consider this year as unaffected by water limitations.

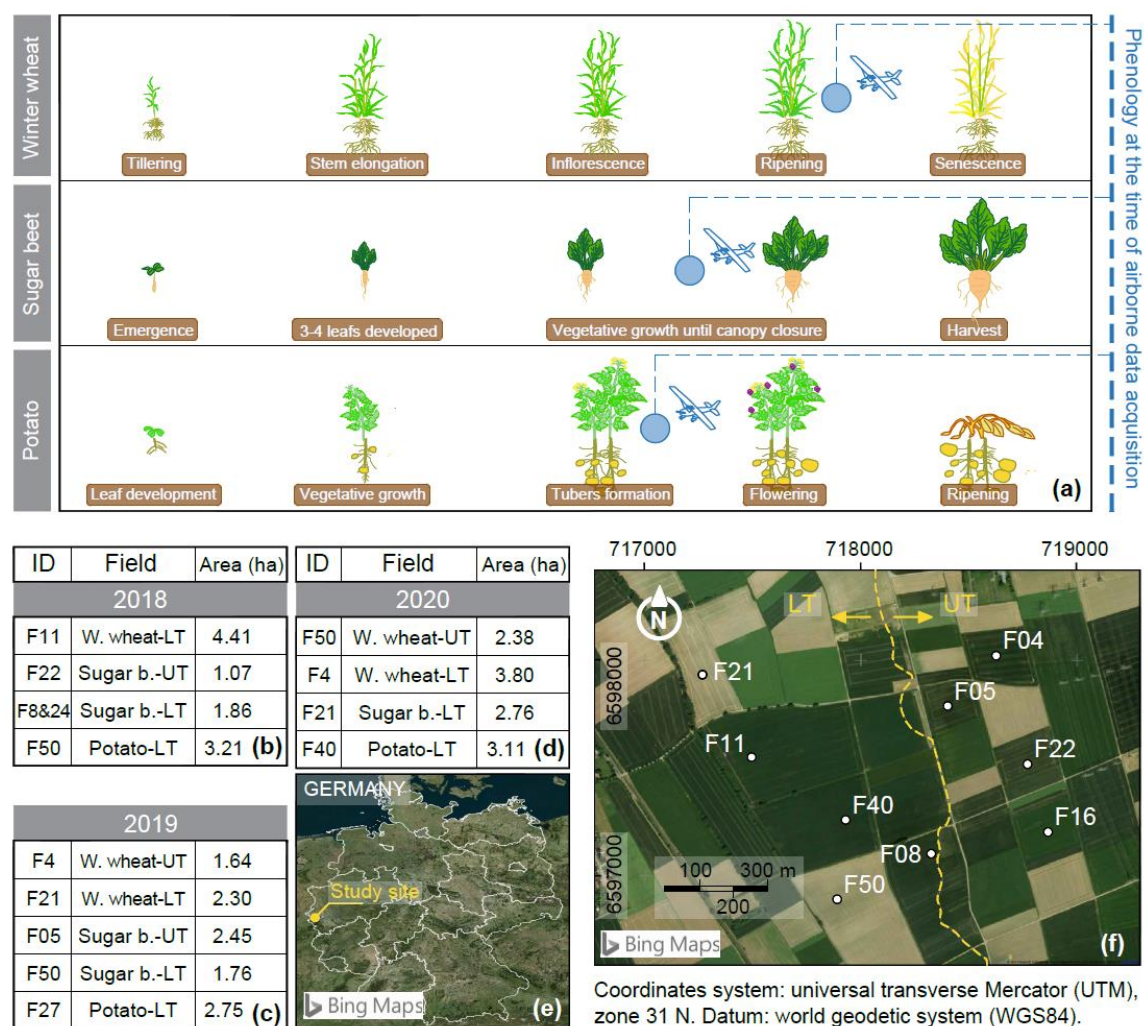


**Figure 5.** Phenologies of the three analyzed crops at the time of the airborne data acquisition (a), and the respective areas and identification (ID) of the analyzed fields (in accordance to Brogi et al., 2019) in June 27<sup>th</sup> 2018 (b), June 26<sup>th</sup> 2019 (c) and June 23<sup>rd</sup> 2020 (d). The location of the study area and the specific fields are presented in panels (e) and (f), respectively. Source of the background images: BingMaps.

**Remote sensing data acquisition:** Airborne SIF data was collected on 2018 (June 27<sup>th</sup>), 2019 (June 26<sup>th</sup>) and 2020 (June 23<sup>th</sup>) late in the morning (~10:30-11:30 h) under cloud free conditions at 600 m above the ground level. Data collection campaigns consisted in six flight lines (~360 m width x ~12 km length) from which high-resolution field-level SIF information was extracted. An additional set of afternoon (~16:00 h) SIF data was collected and used in the comparison between morning and afternoon LST response to low PAW levels in one specific winter wheat field in 2020. The sensor used to acquire the airborne-SIF information was the high-performance airborne imaging spectrometer HyPlant (Siegmann et al., 2019; Rascher et al., 2015), a hyperspectral instrument composed by two modules, the DUAL and the FLUO. The first records data from 400 to 2500 nm, and it is mostly used to compute narrow band vegetation indices (Vis). The FLUO module was built to retrieve SIF, and therefore records high spectral resolution data in the O<sub>2</sub>-B and

O<sub>2</sub>-B oxygen absorption bands, with a Full Width Half Maximum (FWHM) of 0.3 nm. LST information was retrieved from long wave infrared (LWIR, 8000 to 11500 nm spectra) data measured with a push broom line scan spectroradiometer (TASI-600) installed in the same aircraft with HyPlant.

**Remote sensing data processing:** 1 m pixel<sup>-1</sup> SIF was computed (Fig. 6a) using the Spectral Fitting Method (SFM), which retrieves the fluorescence and reflectance signals in adjacent wavelengths over a specific spectral range at both sides of the oxygen absorption bands (Cogliati et al., 2015). Differently from other SIF retrieval methods, the SFM algorithm incorporates radiative transfer theory to correct for atmospheric interferences caused, e.g. by water vapor, aerosols, and surface air pressure. More details about how SIF was retrieved with the SFM approach can be consulted in Siegmann et al. (2021).

Recently, several approaches have been proposed to correct the top-of-canopy SIF for the canopy structural effect; for instance, Zeng et al. (2022) proposed the use of the near-infrared radiance of vegetation, while Yang et al. (2020) proposed the use of the FCVI (Fig. 6b). We used the FCVI-based approach, since its correction for the SIF scattering within the canopy is fully based on the spectral invariant theory, which describes how photons interact with the top canopy surface and the pathways they can follow if not used for photosynthesis (e.g., passing through canopy gaps or continuing towards lower strata). We calculated the FCVI with information from the HyPlant DUAL module as the difference of the averaged reflectance in the near infrared (NIR; from 750 to 900 nm,  $R_{<750-900>}$ ) and visible (VIS; from 400 to 700 nm,  $R_{<400-700>}$ ) regions of the spectrum (eq. 1). As suggested by Yang et al. (2020), only pixels with FCVI higher than 0.18 were considered for the analysis in order to exclude pixels with low fractional cover and thus with a higher influence of the soil background. The FCVI was used as factor in the following equation to derive  $E_f$  (eq. 2; Fig. 6c), accounting for the scattering and PAR absorption effects on the SIF signal, and therefore, providing information about changes in plant physiology.

$$FCVI = R_{<750-900>} - R_{<400-700>} \quad (\text{eq. 1})$$

$$E_f = \frac{\pi * SIF}{iPAR * FCVI} \quad (\text{eq. 2})$$

where iPAR represents the incoming photosynthetically active radiation, obtained from terrestrial environmental observations (TERENO, 2022) and SIF refers to far-red SIF. Since the SIF is retrieved from one single angle, it is multiplied by  $\pi$  as an estimation of the SIF emitted in all directions of the upper hemisphere that is exposed to the sun light. As a reflectance-based greenness index, we chose the enhanced vegetation index (EVI), which was calculated according to eq. 3. The numbers in brackets describe the spectral window on which top-of-canopy reflectance of HyPlant's DUAL module was averaged.

$$EVI = 2.5 * \frac{R_{<795-810>} - R_{<665-680>}}{R_{<795-810>} + 6 * R_{<665-680>} - 7.5 * R_{<475-490>} + 1} \quad (\text{eq. 3})$$

Evapotranspiration (ET) was computed using Sentinel-2 and -3 data through the Sentinels for ET (Sen-ET) approach (Guzinski et al., 2020; Fig. 6d) employing the python modules developed from the Sen-ET plugin for ESA's Sentinel Toolbox Development Platform (SNAP) software (ESA, 2021). Biweekly accumulated ET of each field were

computed during the two and a half months before the airborne campaign, and cubic spline functions were used to interpolate the resulting five Time Points (TPs; Fig. 6e). These ET curves were later used to adjust the water availability maps to specific values for each field; more details are provided in sections below.

For the LST retrieval, first, a radiometric correction is applied to obtain the total radiation measured by the sensor. Subsequently, an atmospheric correction is applied in order to disentangle the surface radiation from the radiation reflected and emitted from the atmosphere. Finally, the corrected data is geo located through a geometric correction process. More details about the standardized TASI-600 data process can be consulted in Hanuš et al. (2016).

**Soil data:** The soil information used in this study has 1 m pixel<sup>-1</sup> resolution (the same as the airborne SIF data) and was derived from the geophysics-based ECa mapping presented by Brogi et al. (2019) (Fig. 6f). The authors published a ~90 ha soil map of the Selhausen area, which includes the investigated fields and differentiates between 18 soil units that are quantitatively described up to 2 m depth. The geophysics based ECa methodology follows the principle that specific physical properties of a soil will determine its capacity to conduct electricity across. Therefore, soil units sharing similar ECa dynamics with depth might share alike soil characteristics, thus belonging to a same soil class. The geometry of the 18 soil units was obtained by analyzing ECa maps with machine learning algorithms, while their specific soil properties were identified with a strategic field sampling directed to 100 representative points. For more information about the methodology and the description of each soil unit properties refer to Brogi et al. (2019) and references therein.

**Generation of the plant available water in the root zone (PAW) maps:** To convert the textural information provided by the geophysics-based soil map into numerical values of PAW capacity (PAW<sub>cap</sub>), the Mualem-van Genuchten model (van Genuchten, 1980) was used (eq 4, Fig. 6g):

$$\theta_w(h) = \theta_r + \frac{\theta_s - \theta_r}{(1 + |\alpha h|^n)^m} \quad (\text{eq. 4})$$

where  $\theta_w$ ,  $\theta_r$ , and  $\theta_s$  (cm<sup>3</sup> cm<sup>-3</sup>) are the actual volumetric, residual, and saturated water content, respectively. The  $h$  (-cm) is the pressure head,  $\alpha$  is the inverse of the air entry pressure (cm<sup>-1</sup>),  $n$  is a dimensionless parameter related to the pore size distribution, and  $m$  a parameter that is set equal to  $1 - 1/n$ . The soil hydraulic parameters to solve eq. 4 were estimated based on textural information from the soil map using the pedotransfer function of (PTF) of Rawls and Brakensiek (1985). The PAW<sub>cap</sub> was calculated as the difference between the  $\theta_w$  obtained at  $h = -100$  cm (field capacity) and  $h = -15000$  (wilting point). This calculation was performed on each soil unit of the geophysics-based soil map.

For each crop, the PAW<sub>cap</sub> was calculated over their rooting depth used in previous studies from the same region (Brogi et al., 2020). Specific root zone depths of sugar beet, potato and winter wheat were: 1.5, 0.6, and 1 m, respectively. Moreover, it was assumed that roots cannot penetrate deep into soils that are characterized by coarse layers composed of compacted sand and gravel materials, as this is generally observed in the study area and proposed by literature (Daddow and Warrington, 1983). Thus, the PAW<sub>cap</sub> in soil units A1a-d, B1b, D1a-d, and D2 was calculated up to the depth of such coarse layers only.

The ratio between the precipitation (as the main year-level water input) and ET (as the main field-level water loss) integrals of the five biweekly time points (TPs) before the airborne campaign was used as a correction factor (CF; Fig. 6h) to convert the PAW<sub>cap</sub> map into the estimated actual PAW (referred just as PAW; eq. 5, Fig. 6i). If no data was available for one specific TP, then it was calculated as the average of the two neighboring TP's. Since CF's account for the field-level ET, there is one specific CF per field. These CF's were then multiplied by the respective individual maps, in order to obtain the field-specific PAW maps (Fig. 6j). In the study region most fields are not irrigated and thus PAW is only determined by natural precipitation and ET, yet, potato fields are irrigated with mobile systems. Therefore, according to standard irrigation practices in the region, 30 l m<sup>-2</sup> were added to the PAW of potato fields accounting for the amount of water irrigated during the week before HyPlant data acquisition.

$$CF = \int_{TP1}^{TP5} f(\text{Prec.}) dP \div \int_{TP1}^{TP5} f(\text{ET}) dET \quad (\text{eq. 5})$$

The CF formula was designed from the sense that 'the higher the water income over the water output, the closer the PAW to reach its maximum (PAW<sub>cap</sub>). In Fig. 7 the precipitation and ET integrals (Fig. 7a-d) and the resulting CF's (Fig. 7e) are presented.

**Data analysis:** The analysis of the data was directed to estimate the spatial relation between PAW and  $E_f$ , i.e., to evaluate how much of the  $E_f$  spatial variability (as dependent variable) can be explained by variations of PAW (as independent variable) in the spatial domain. For that purpose, the  $E_f$  maps from the three study years were overlaid with the respective field-level PAW maps, both with 1 m pixel<sup>-1</sup> resolution (Fig. 6k). Machinery paths were removed from the  $E_f$  imagery since they are not related to the soil moisture spatial patterns of interest. Similarly, polygons smaller than 20 m<sup>2</sup> were removed from the PAW maps. The average  $E_f$  for each soil unit was calculated, and then box-plotted vs. its PAW. In addition, Pearson correlation coefficients ( $r$ ) of the  $E_f$ -PAW relations were calculated in order to understand the strength of the influence that PAW had on the SIF emitted by plants. Since the unit of PAW is l m<sup>-2</sup>, it was not compared to the total but the averaged  $E_f$  m<sup>-2</sup> of a certain soil unit. The results were differentiated by year, crop and geographic location within the study area, whether they were located in the UT (lower PAW) or LT (higher PAW). In order to assess the performance of our PAW estimating method we further compared it with time domain reflectometry (TDR, reported in Mungen et al., 2021) data generated on June 26<sup>th</sup> of 2019 (same day of the HyPlant campaign). In Fig. S1 (supplementary information) we plotted the relation between 1502 field-level averaged TDR-based soil moisture (%) data points and our PAW estimations. The resulting  $r = 0.88$  ( $p < 0.001$ ) relation confirms the reliability of our approach.

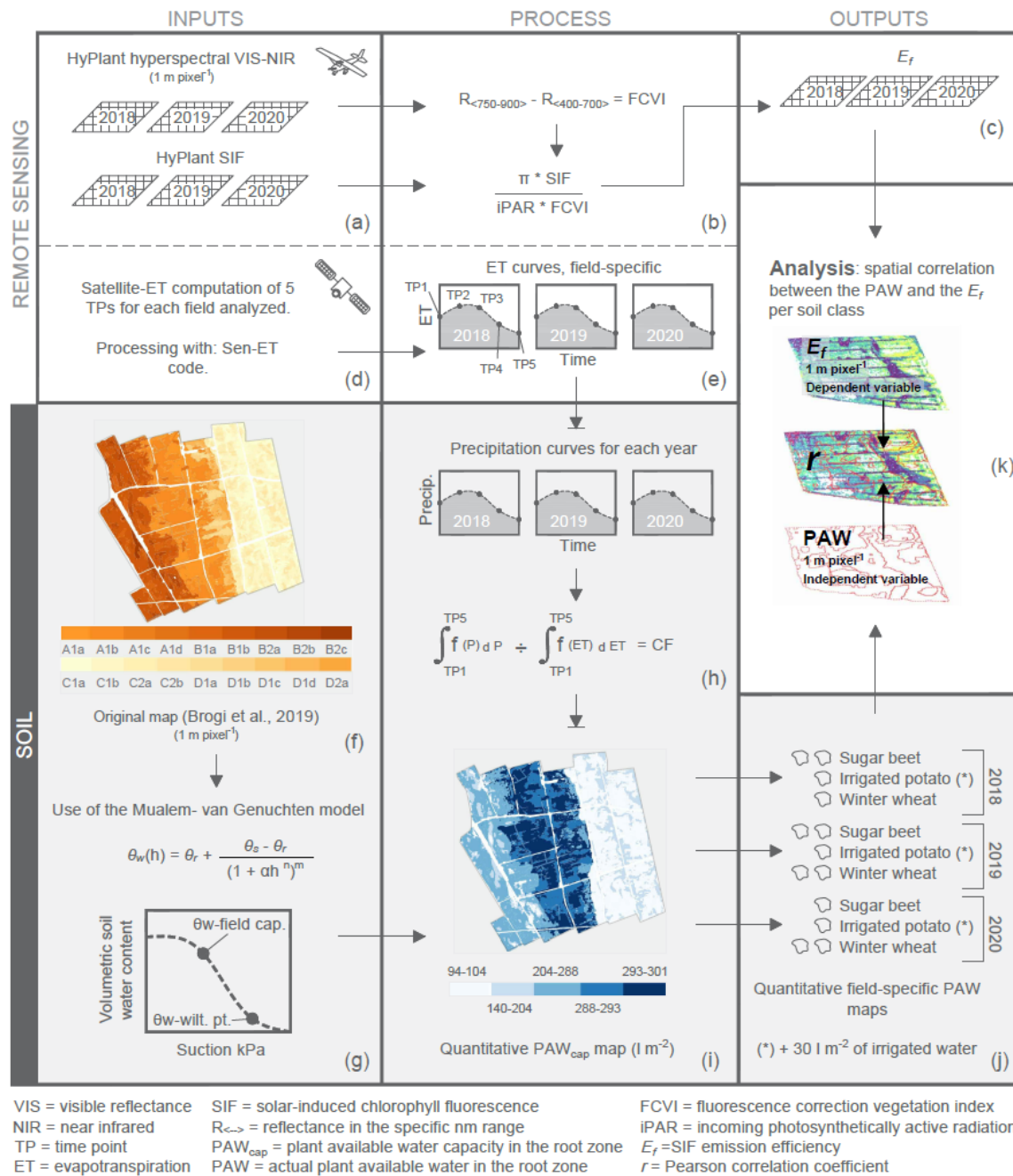


**Figure 6.** Summary of materials and methods separated according to inputs, process and outputs, and analysis done with the airborne (a-c), satellite (d and e) and soil (f-i) datasets. The gray shadow encloses the steps followed with the soil data. The statistical analysis (j) was done with the outputs from the remote sensing and soil data processing. All abbreviations are provided in the bottom.

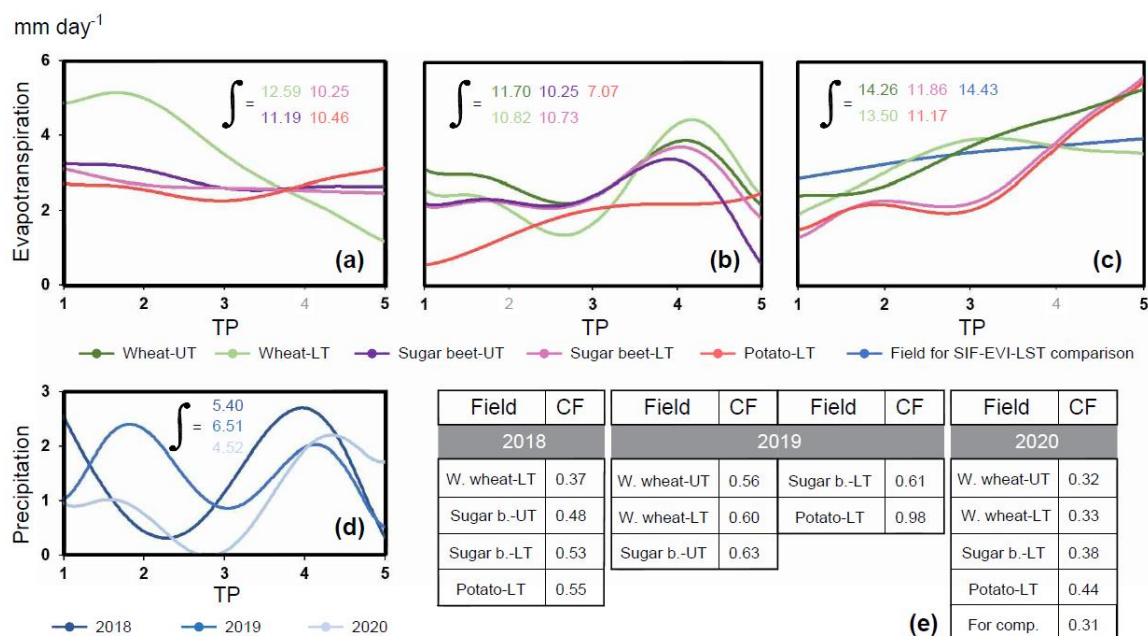


**Figure 7.** Evapotranspiration (ET; a-c) and precipitation (d) curves (in mm day<sup>-1</sup>) interpolated with the cubic splines function between time points (TPs). Grey numbers in the x-axis represent specific TP's with not available data and therefore calculated as the average of the two neighboring TP's. The area under the curve for each field is presented within each panel. The ET information presents an average error of around 30% according to Guzinski et al., 2020. The resulting correction factors (eq. 5) are presented in panel (e).

## Acknowledgments

The authors acknowledge the founding through: (i) the ESA's 'PhotoProxy campaign' project, under the contract no. 4000125731/19/NL/LF, (ii) ESA's FLEXSense campaign (ESA Contract No. 4000125402/18/NL/NA), and (iii) the European Union's (EU's) Training on Remote Sensing for Ecosystem Modelling (TRuStEE) consortium founded through the Horizon 2020 research and innovation program under the Marie Skłodowska-Curie grant agreement no. 721995. Support for data acquisition was provided by the SFB/TR 32 "Patterns in Soil-Vegetation-Atmosphere Systems: Monitoring, Modelling, and Data Assimilation"-subproject D2 ([www.tr32.de](http://www.tr32.de)), funded by the Deutsche Forschungsgemeinschaft (DFG). We also thank the 'Strukturwandel-Projekt Bioökonomie REVIER' funded by the German Federal Ministry of Education and Research project (ID 031B0918A), the Deutsche Forschungsgemeinschaft (DFG, German Research Foundation) under Germany's Excellence Strategy – EXC 2070–390732324, and the support of the ATLAS project funded through the EU's Horizon 2020 research and innovation program under grant agreement No. 857125. The authors also appreciate valuable field measurement data acquired and shared by the HGF initiative TERrestrial ENvironmental Observations (TERENO) and the ICOS project of the European Research Infrastructure programme (ESFRI). We acknowledge as well Prof. Dr. Sergio Cogliati for sharing the SFM code for the retrieval of SIF, and Dr. Héctor Nieto for sharing his python scripts to help process the Sen-ET outputs.

## Data availability statement

The data used in this study is publicly available at the JULICH Data repository through the following DOI: (DOI to be created and added upon acceptance).

## References

- [1] Food and Agricultural Organization of the United Nations (FAO) (2021) AQUASTAT. Available at [fao.org/aquastat](http://fao.org/aquastat). Accessed January 3, 2022.
- [2] A. Damm et al., Remote sensing of plant-water relations: An overview and future perspectives. *J. Plant Physiol.* 277, 3-19 (2018).
- [3] M. Gerhards, M. Schlerf, K. Mallick, T. Udelhoven, Challenges and Future Perspectives of Multi-/Hyperspectral Thermal Infrared Remote Sensing for Crop Water-Stress Detection: A Review. *Remote Sens.* 11(10), 1240 (2019).
- [4] G.-H. Mohammed et al., Remote sensing of solar-induced chlorophyll fluorescence (SIF) in vegetation: 50 years of progress. *Remote Sens. Environ.* 231, 111177 (2019).
- [5] M. Meroni et al., Remote sensing of solar-induced chlorophyll fluorescence: Review of methods and applications. *Remote Sens. Environ.* 113(10), 2037–2051 (2009).
- [6] L. Guanter et al., Global and time-resolved monitoring of crop photosynthesis with chlorophyll fluorescence. *Proc. Natl. Acad. Sci. U.S.A.* 111(14), E1327–E1333 (2014).
- [7] F. Jonard et al., Value of sun-induced chlorophyll fluorescence for quantifying hydrological states and fluxes: Current status and challenges. *Agric. For. Meteorol.* 291, 108088 (2020).
- [8] Y. Zeng, et al., Combining near-infrared radiance of vegetation and fluorescence spectroscopy to detect effects of abiotic changes and stresses. *Remote Sens. Environ.* 270, 112856 (2022).
- [9] A. Damm, et al., Response times of remote sensing measured sun-induced chlorophyll fluorescence, surface temperature and vegetation indices to evolving soil water limitation in a crop canopy. *Remote Sens. Environ.* 273, 112957 (2022).
- [10] S. Xu, Z. Liu, L. Zhao, H. Zhao, S. Ren, Diurnal Response of Sun-Induced Fluorescence and PRI to Water Stress in Maize Using a Near-Surface Remote Sensing Platform. *Remote Sens.* 10(10), 1510 (2018).
- [11] C. von Hebel et al., Understanding Soil and Plant Interaction by Combining Ground-Based Quantitative Electromagnetic Induction and Airborne Hyperspectral Data. *Geophys. Res. Lett.* 45, 7571–7579 (2018).
- [12] J. Quiros et al., Sun Induced Chlorophyll Fluorescence and Vegetation Indices for heat stress assessment in three crops at different geophysics-derived soil units. ESSOAR [Preprint] (2020). <https://doi.org/10.1002/essoar.10504968.1> (accessed 3 January 2022).
- [13] Q. Shen et al., Relationship of surface soil moisture with solar-induced chlorophyll fluorescence and normalized difference vegetation index in different phenological stages: a case study of Northeast China. *Environ. Res. Lett.* 16, 024039 (2021).
- [14] M. Drusch et al., The FLuorescence EXplorer Mission Concept—ESA's Earth Explorer 8. *IEEE Trans. Geosci. Remote Sens.* 55(3), 1273-1284 (2017).
- [15] P. Yang, C. van der Tol, P.-K.-E. Campbell, E.-M. Middleton, Fluorescence Correction Vegetation Index (FCVI): A physically based reflectance index to separate physiological and non-physiological information in far-red sun-induced chlorophyll fluorescence, *Remote Sens. Environ.* 240, 111676 (2020).
- [16] M.T.F. Wong, S. Asseng, Determining the causes of spatial and temporal variability of wheat yields at sub-field scale using a new method of upscaling a crop model. *Plant Soil* 283, 203-215 (2006).
- [17] C. Brogi, et al., Large-scale soil mapping using multi-configuration EMI and supervised image classification. *Geoderma* 335, 133-148 (2019).
- [18] C. Brogi et al., Added value of geophysics-based soil mapping in agro-ecosystem simulations, *SOIL* 7, 125–143 (2021).

- [19] A. Huete et al., Overview of the radiometric and biophysical performance of the MODIS vegetation indices. *Remote Sens. of Environ.* 83, 195–213 (2002).
- [20] J. Joiner et al., The seasonal cycle of satellite chlorophyll fluorescence observations and its relationship to vegetation phenology and ecosystem atmosphere carbon exchange. *Remote Sens. Environ.* 152, 375-391 (2014).
- [21] Food and Agricultural Organization of the United Nations (FAO) (2012) Crop yield response to water. Available at fao.org. Accessed February 4, 2022.
- [22] B. Siegmann et al., Downscaling of far-red solar-induced chlorophyll fluorescence of different crops from canopy to leaf level using a diurnal data set acquired by the airborne imaging spectrometer HyPlant. *Remote Sens. Environ.* 264, 112609 (2021).
- [23] F. Pinto et al., Sun-induced chlorophyll fluorescence from high-resolution imaging spectroscopy data to quantify spatio-temporal patterns of photosynthetic function in crop canopies. *Plant Cell Environ.* 39, 1500-1512 (2016).
- [24] C. Van der Tol et al., A model and measurement comparison of diurnal cycles of sun-induced chlorophyll fluorescence of crops. *Remote Sens. Environ.* 186, 663-677 (2016).
- [25] E.A. Chapman, S. Orford, J. Lage, S. Griffiths, Capturing and Selecting Senescence Variation in Wheat. *Front. Plant Sci.* 12, 638738 (2021).
- [26] A. Porcar-Castell et al., Chlorophyll a fluorescence illuminates a path connecting plant molecular biology to Earth-system science. *Nat. Plants* 7, 998-1009 (2021).
- [27] A. Ač, Z. Malenovský, J. Olejníčková, A. Gallé, U. Rascher, G. Mohammed, Meta-analysis assessing potential of steady-state chlorophyll fluorescence for remote sensing detection of plant water, temperature and nitrogen stress. *Remote Sens. Environ.* 168, 420-436 (2015).
- [28] Y. Liu, C. Dang, H. Yue, C. Lyu, X. Dang, Enhanced drought detection and monitoring using sun-induced chlorophyll fluorescence over Hulun Buir Grassland, China. *Sci. Total Environ.* 770, 145271 (2021).
- [29] S. Rudolph, J. van der Kruk, C. von Hebel, M. Ali, M. Herbst, C. Montzka, S. Pätzold, D.A. Robinson, H. Vereecken, L. Weihermüller, Linking satellite derived LAI patterns with subsoil heterogeneity using large-scale ground-based electromagnetic induction measurements. *Geoderma* 241–242, 262-271 (2015).
- [30] T. G. Reichenau, W. Korres, M. Schmidt, A. Graf, G. Welp, N. Meyer, A. Stadler, C. Brogi, K. Schneider, A comprehensive dataset of vegetation states, fluxes of matter and energy, weather, agricultural management, and soil properties from intensively monitored crop sites in western Germany. *Earth Syst. Sci. Data* 12, 2333–2364 (2020).
- [31] C. Panigada, et al., Fluorescence, PRI and canopy temperature for water stress detection in cereal crops. *Int. J. Appl. Earth Obs. Geoinf.* 30, 167-178 (2014).
- [32] E. Kim, “Scanning L-Band Active Passive (SLAP) - Recent Results from an Airborne Simulator for SMAP” in *Proceedings of the IEEE International Geoscience and Remote Sensing Symposium (IGARSS, Milan, Italy, 2015)*.
- [33] H. Ma, et al., Satellite surface soil moisture from SMAP, SMOS, AMSR2 and ESA CCI: A comprehensive assessment using global ground-based observations. *Remote Sens. Environ.* 231, 111215 (2019).
- [34] C. Simmer, et al., Monitoring and modeling the terrestrial system from pores to catchments – the Transregional Collaborative Research Center on Patterns in the Soil-Vegetation-Atmosphere System. *Bull Am Meteorol Soc* 96, 1765-1787 (2015).
- [35] A. Graf, Altered energy partitioning across terrestrial ecosystems in the European drought year 2018. *Philos Trans R Soc Lond B Biol Sci* 375(1810), 20190524 (2020).
- [36] B. Siegmann et al., The high-performance airborne imaging spectrometer HyPlant—From raw images to top-of-canopy reflectance and fluorescence products: Introduction of an automatized processing chain. *Remote Sens.* 11(23), 2760 (2019).
- [37] U. Rascher et al., Sun-induced fluorescence – a new probe of photosynthesis: First maps from the imaging spectrometer HyPlant. *Glob. Change Biol.* 21(12), 4673–4684 (2015).
- [38] S. Cogliati et al., Retrieval of sun-induced fluorescence using advanced spectral fitting methods. *Remote Sens. Environ.* 169, 344–357 (2015).

- [39] Terrestrial Environmental Observations (TERENO) (2022) Data Discovery Portal. Available at [ddp.tereno.net/](http://ddp.tereno.net/). Accessed January 3, 2022.
- [40] R. Guzinski, H. Nieto, I. Sandholt, G. Karamitlios, Modelling High-Resolution Actual Evapotranspiration through Sentinel-2 and Sentinel-3 Data Fusion. *Remote Sens.* 12(9), 1433 (2020).
- [41] European Space Agency (ESA) (2021) STEP - Scientific Toolbox Exploitation Platform. Available at [step.esa.int/main](http://step.esa.int/main). Accessed January 3, 2022.
- [42] J. Hanuš, T. Fabiánek, L. Fajmon, “potential of airborne imaging spectroscopy at Czechglobe” in *Proceedings of The International Archives of the Photogrammetry, Remote Sensing and Spatial Information Sciences (XXIII ISPRS Congress, Prague, Czech Republic, 2016)*, pp. 15-17.
- [43] Mengen et al., The Sarsense Campaign: Air- and Space-Borne C- and L-Band SAR for the Analysis of Soil and Plant Parameters in Agriculture. *Remote Sens.* 13, 825 (2021).
- [44] M.T. van Genuchten, A Closed-form Equation for Predicting the Hydraulic Conductivity of Unsaturated Soils, *Soil Sci Soc Am J* 44(5), 892–898 (1980).
- [45] W.J. Rawls, D. Brakensiek, “Prediction of soil water properties for hydrologic modeling” in *Watershed management in the eighties*, E.B. Jones, T.J. Ward, Eds. (American Society of Civil Engineers –ASCE–, 1985), pp. 293–299. Reston, VA: American Society of Civil Engineers.
- [46] C. Brogi et al., Simulation of spatial variability in crop leaf area index and yield using agroecosystem modeling and geophysics-based quantitative soil information. *Vadose Zone J.* 19, e20009 (2020).
- [47] R.L. Daddow, G. Warrington, “Growth-limiting soil bulk densities as influenced by soil texture”, (United States Department of Agriculture –USDA- Forest Service, 1983) 17 pp.

## SUPPLEMENTARY INFORMATION: “Spatial relation between solar-induced chlorophyll fluorescence and plant available water in the root zone”

Juan Quiros-Vargas<sup>1,\*</sup>, Cosimo Brogi<sup>2</sup>, Alexander Damm<sup>3,4</sup>, Bastian Siegmann<sup>1</sup>, Patrick Rademske<sup>1</sup>, Vicente Burchard-Levine<sup>5</sup>, Vera Krieger<sup>1</sup>, Marius Schmidt<sup>2</sup>, Jan Hanuš<sup>6,7</sup>, Lutz Weihermüller<sup>2</sup>, Onno Muller<sup>1</sup>, Uwe Rascher<sup>1</sup>

<sup>1</sup>Institute of Bio- and Geosciences, Plant Sciences (IBG-2), Forschungszentrum Jülich GmbH, Jülich, Germany, 52425; <sup>2</sup>Institute of Bio- and Geosciences, Agrosphere (IBG3), Forschungszentrum Jülich GmbH, Jülich, Germany, 52425; <sup>3</sup>Department of Geography, University of Zurich, Zurich, Switzerland, CH-8057; <sup>4</sup>Eawag, Swiss Federal Institute of Aquatic Science & Technology, Surface Waters – Research and Management, Dübendorf, Switzerland, CH-8600; <sup>5</sup>Environmental Remote Sensing and Spectroscopy Laboratory (SpecLab), Spanish National Research Council (CSIC), Madrid, Spain; <sup>6</sup>Global Change Research Institute of the Czech Academy of Sciences, Brno, Czech Republic, 603 00; <sup>7</sup>Czech Technical University, Faculty of Civil Engineering, Department of Geomatics, Czech Republic

\*Juan Quiros-Vargas

Email: [j.quiros@fz-juelich.de](mailto:j.quiros@fz-juelich.de)

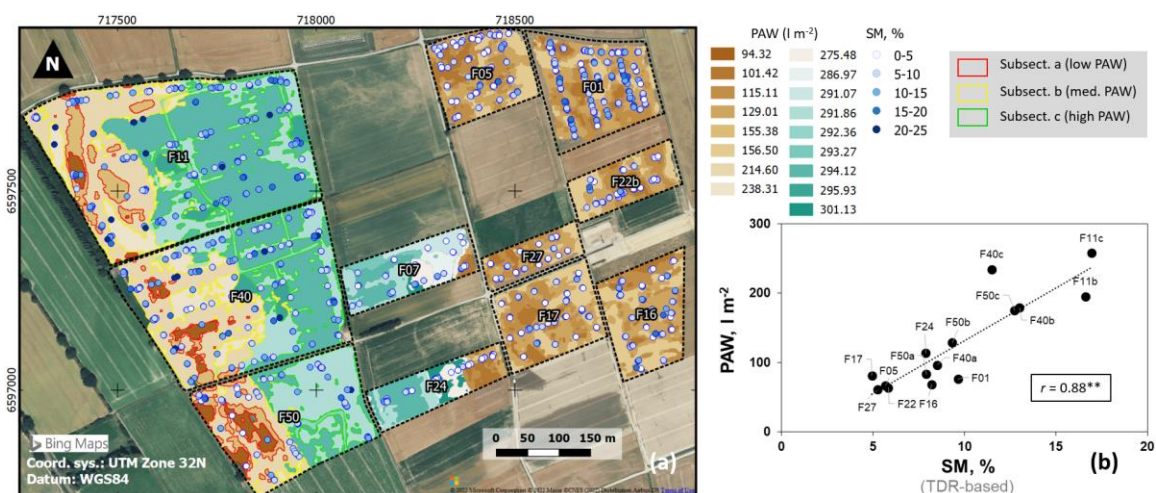


**Figure S1.** Comparison between 1502 time-domain reflectometry (TDR)-based soil moisture (SM, % at 5 cm depth collected the same day of the HyPlant campaign in 2019 –June 26<sup>th</sup>–; Mengen et al., 2021) data points and the plant available water (PAW) estimated with the methods used in the present manuscript (a). Both data were averaged at field level and their respective correlation ( $r$ ) and significance ( $p$ ) were estimated (b). \*\* represent the significant relation at  $p < 0.01$ . Source of the background images: BingMaps.

4.1.3 Third publication (Quiros-Vargas et al., 2022)

“Fractal Geometry and the Downscaling of Sun-Induced Chlorophyll Fluorescence Imagery”

<b>Authors (country):</b>	<b>Book:</b> Encyclopedia of Mathematical Geosciences
J. Quiros-Vargas (GE)	<b>Editorial:</b> Springer Nature
B. Siegmann (GE)	<b>Status:</b> Published
Alexander Damm (CH)	<b>Contribution of the doctorate candidate:</b>
Ran Wang (US)	• Conceptualization: 80%
John Gamon (US)	• Data analysis: 80%
Vera Krieger (GE)	• Writing: 100%
B. S. Daya Sagar (IN)	• Field work: 0%
Onno Muller (GE)	
Uwe Rascher (GE)	

DOI: [10.1007/978-3-030-26050-7\\_120-1](https://doi.org/10.1007/978-3-030-26050-7_120-1)

# F

## Fractal Geometry and the Downscaling of Sun-Induced Chlorophyll Fluorescence Imagery



Juan Quiros-Vargas<sup>1</sup>, Bastian Siegmann<sup>1</sup>, Alexander Damm<sup>2,3</sup>, Ran Wang<sup>4</sup>, John Gamon<sup>4,5</sup>, Vera Krieger<sup>1</sup>, B. S. Daya Sagar<sup>6</sup>, Onno Muller<sup>1</sup> and Uwe Rascher<sup>1</sup>

<sup>1</sup>Institute of Bio- and Geosciences, IBG-2: Plant Sciences, Forschungszentrum Jülich GmbH, Jülich, Germany

<sup>2</sup>Department of Geography, University of Zurich, Zürich, Switzerland

<sup>3</sup>Eawag, Swiss Federal Institute of Aquatic Science & Technology, Surface Waters – Research and Management, Dübendorf, Switzerland

<sup>4</sup>Center for Advanced Land Management Information Technologies, School of Natural Resources, University of Nebraska–Lincoln, Lincoln, NE, USA

<sup>5</sup>Department of Earth and Atmospheric Sciences and Department of Biological Sciences, University of Alberta, Edmonton, AB, Canada

<sup>6</sup>Systems Science and Informatics Unit, Indian Statistical Institute-Bangalore Centre, Bangalore, India

### Synonyms

[Geometry of nature](#)

### Definition

The fractal geometry is a young branch of mathematics that studies the configuration of complex shapes and phenomena formed by the repetition of patterns.

### Introduction

“Clouds are not spheres, mountains are not cones, coastlines are not circles, and bark is not smooth, nor does lightning travel in a straight line” (Mandelbrot 1982). The fractal geometry was developed by Benoît Mandelbrot in the 1970s to describe those and all other chaotic geometries observed in nature. The theory states that natural phenomena can be characterized as a repetition of self-similar (isotropic) or self-affine (anisotropic) patterns with dimensions, not limited to the Euclidean 1-, 2-, and 3-D planes. Thus, the complexity of fractal geometries is described by the so-called Fractal Dimensions (FDs), real numbers within the [1, 4] interval. This means that the more complex a line, a polygon, or a prism is, the higher to 1 (but lower than 2), 2 (but lower than 3), and 3 (but lower than 4) its dimension is, respectively.

Applications of the fractal geometry in science are nearly as many as natural phenomena exist. One example is the Remote Sensing (RS)-based investigation of scale dependencies of dynamic processes in vegetation, especially between individual leaves and the ecosystem. Since such dynamic processes are composed by nonlinear phenomena, the implementation of linear methods for its analysis might lead to local approaches with limited applicability beyond specific circumstances. The use of the fractal geometry, instead, can greatly contribute to RS of vegetation and help understanding image features as interconnected and scale-independent spatiotemporal patterns.

### Fractal Geometry and the Power Law (PL) Distribution of Sun-Induced Chlorophyll Fluorescence (SIF)-Emitting Objects

Several approaches exist to mathematically prove the existence of fractal geometry in the distribution of RS-measured objects; the computation of universal Power Laws (PLs), also known as scaling laws, is one of them (Nagajothi et al. 2021).

A PL distribution indicates the presence of fractal geometry composed by patterns where few occurrences of large magnitudes and numerous occurrences of small magnitudes are observed regardless the scale. The function of a PL distribution is described with the following equation:

$$y = \alpha x^\beta$$

where  $\alpha$  is a constant representing the scale, and  $\beta$  is the exponent which represents the dimension of the function (closely related to the fractal dimension). Examples of PL distribution can be found almost in any area of research. For instance, in economics, a PL can describe how the richness in a country is distributed in few individuals holding huge amounts of money and many individuals with scarce monetary resources. Another example can be found in linguistics, where the frequency of words in a text follows a PL as well, with few words repeated thousands of times, and many words used only in few occasions.

Hypothetically, PLs can be used to describe the distribution of RS-measured properties of vegetation like the emitted SIF signal, since: (i) Its heterogeneity is related to spatial patterns defined by factors like canopy structure, shape, and size of agricultural fields or the organization of tree species in a forest; and (ii) SIF, as a red light emitted from vegetation, is more clearly aggregated across spatial scales (pixel sizes) than other more uniform signals like reflectance. Therefore, this chapter focusses on the analysis of the distribution of SIF emitting objects in an agricultural field to confirm whether they present a PL distribution (fractal geometry) or not, and how the scaling and dimension factors behave across spatial scales.

## Case Study: “Fractal Geometry for SIF-Downscaling”

**Context:** The world is confronted with substantial socioeconomic challenges. Agricultural production must ensure food security for a growing population, while it is imperative to protect and sustainably manage natural resources. Cropland expansion at the cost of natural ecosystems is not an option; therefore, large-scale farming must employ technology and advanced management to improve yields. RS offers possibilities to contribute making this possible. Recently available RS platforms equipped with SIF sensors constitute a powerful tool, since SIF shows large sensitivity to actual photosynthetic efficiency of crops (Mohammed et al. 2019). Such information is complementary to commonly used Vegetation Indices (VIs) and offers new pathways to assess plant health and, thus, optimize crop management. The forthcoming Fluorescence Explorer (FLEX) satellite mission of the European

Space Agency (ESA) was planned within this context. Its relatively coarse resolution of 300 m, however, limits applicability for small field sizes and to investigate inter-field heterogeneity of croplands. Thus, downscaling satellite SIF products (understood as the increase of the spatial resolution) is currently a research subject of utmost importance.

Previous studies have addressed the SIF-downscaling considering its physical relation with explanatory variables like the land surface temperature (Duveiller et al. 2020), and using machine learning-based statistical relations with VIs (Zhang et al. 2020). Another approach with applications on plant phenotyping was presented by Krämer et al. (2021), who analyzed the potential use of aggregated SIF pixel to extract representative values for crop plots representing few m<sup>2</sup>. Despite the great relevance of these contributions, a more versatile downscaling approach capable to run in a diversity of ecosystems is still not available but needed. We hypothesize that the flexibility of the fractal theory as a complexity measure together with the discontinuity of self-similar geometries captured in RS data (Sun et al. 2006) enables new strategies to advance downscaling approaches of SIF.

**Aims:** This study aims (i) to analyze if the aggregation of SIF over vegetation objects follows a universal PL distribution (i.e., representing fractal geometry) across spatial scales, and (ii) to evaluate how the scaling and dimension components of the PLs behave across spatial scales.

**Analysis:** We analyze the fractal geometry vegetation (SIF-emitting) objects through the computation of PLs at 1.5, 5, 10, and 15 m pixel<sup>-1</sup> resolutions. Far red SIF at 740 nm (hereafter named “SIF”) in a 65 ha soybean field was retrieved from an imaging fluorometer (IBIS, Specim, Oulu Finland) with the Spectral Fitting Method (SFM, Cogliati et al. 2015; Fig. 1a). Only vegetation pixels were considered and afterward segmented into individual homogeneous objects through unsupervised classification (Fig. 1b). For the first aim, the total SIF (SIF<sub>TOT</sub>) of each object was calculated and its distribution plotted in order to identify the presence of a PL distribution. For the second aim, the scaling and dimension factors of the PLs from the different spatial resolutions were compared in order to understand if they follow scale-independent patterns.

**Results:** Besides the high intrafield variability observed in Fig. 1, the distribution of the SIF<sub>TOT</sub> information aggregated by objects follows the PL distribution at all analyzed scales (Fig. 2a). Such order, characterized in the function equations, describes how the data is arranged in patterns of few occurrences of objects with high SIF<sub>TOT</sub>, and numerous occurrences of objects with low SIF<sub>TOT</sub> emission. For downscaling purposes, the information about known variables related to the analyzed feature, like the object area (Fig. 2b), could potentially be used to infer the SIF<sub>TOT</sub> of the polygons. Furthermore, the linear increase of the scaling factor and the nearly constant dimension factor for 1.5 to 15 m

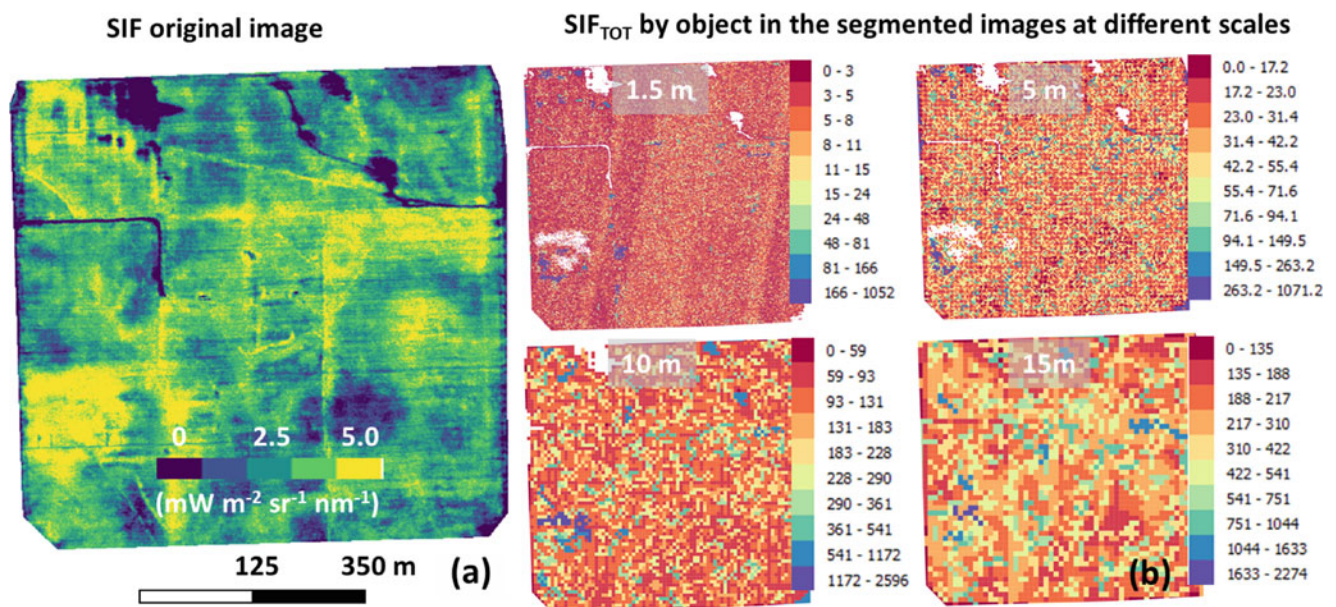
pixel<sup>-1</sup> sizes (Fig. 2c) might indicate the scale-invariant property of the SIF signal aggregation patterns within the range of analyzed resolutions.

## Summary

Our results indicate that the distribution of the SIF<sub>TOT</sub> information aggregated by object follows the PL distribution for 1.5 to 15 m pixel<sup>-1</sup> resolutions, i.e., the fractal geometry is present in the distribution of individual SIF-emitting objects at all analyzed scales. Moreover, the linear ( $R^2 = 0.998$ ) increase of the PL-scaling component, and the nearly constant dimension across the scales, might be an indicator of the

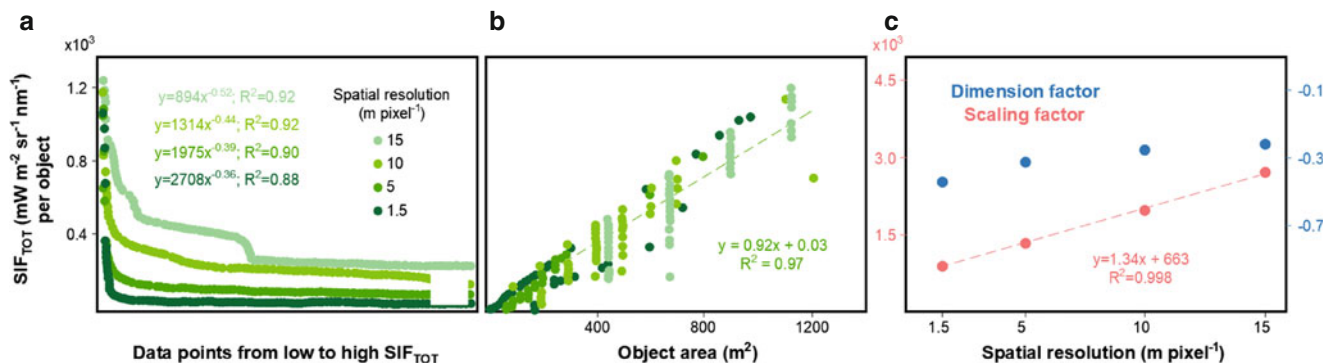
scale-invariant property of the SIF signal aggregation patterns within the range of analyzed resolutions.

In theory, similar PL characterizations of high resolution SIF-explanatory variables could help to understand how to spatially disentangle SIF<sub>TOT</sub> represented in a coarse pixel (e.g., measured by FLEX) in the SIF<sub>TOT</sub> contributions of individual vegetation objects within the measurement footprint. Further studies might address that subject across diverse ecosystems to provide more evidence on the suitability of this proposed approach to downscale and link coarse-scale-retrieved SIF<sub>TOT</sub> with field-level SIF<sub>TOT</sub> information.



**Fractal Geometry and the Downscaling of Sun-Induced Chlorophyll Fluorescence Imagery, Fig. 1** Sun-Induced chlorophyll Fluorescence (SIF) image (a) and the respective segmented images

considering individual aggregation scales, i.e., 1.5, 5, 10, and 15 m pixel<sup>-1</sup> (b)



**Fractal Geometry and the Downscaling of Sun-Induced Chlorophyll Fluorescence Imagery, Fig. 2** Power Law (PL) distributions of the total Sun-Induced chlorophyll Fluorescence (SIF<sub>TOT</sub>) data observed

at 1.5, 5, 10, and 15 m pixel<sup>-1</sup> scales (a), and the linear relation of SIF<sub>TOT</sub> with respect to the object area (b). The dimension and scaling factors of the PLs equations at all scales are present in (c)

## Cross-References

- ▶ [Fractal Dimension](#)
- ▶ [Fractal Geometry in Geosciences](#)
- ▶ [Fractal Landscapes](#)
- ▶ [Fractals](#)
- ▶ [Multifractals](#)
- ▶ [Power-Laws](#)
- ▶ [Remote Sensing](#)
- ▶ [Scaling and Scale Invariance](#)

## Bibliography

- Cogliati S, Verhoef W, Kraft S, Sabater N, Alonso L, Vicent J, Moreno J, Drusch M, Colombo R (2015) Retrieval of sun-induced fluorescence using advanced spectral fitting methods. *Remote Sens Environ* 169: 344–357
- Duveiller G, Filippini F, Walther S, Köhler P, Frankenberg C, Guanter L, Cescatti A (2020) A spatially downscaled sun-induced fluorescence global product for enhanced monitoring of vegetation productivity. *Earth Syst Sci Data* 12:1101–1116
- Krämer J, Siegmann B, Thorsten K, Onno M, Rascher U (2021) The potential of spatial aggregation to extract remotely sensed sun-induced fluorescence (SIF) of small-sized experimental plots for applications in crop phenotyping. *Int J Appl Earth Obs Geoinf* (in press)
- Mandelbrot B (1982) *The fractal geometry of nature*. Freeman, San Francisco, p 1982
- Mohammed GH, Colombo R, Middleton EM, Rascher U, van der Tol C, Nedbal L, Goulas Y, Pérez-Priego O, Damm A, Meroni M, Joiner J, Cogliati S, Verhoef W, Malenovsky Z, Gastellu-Etchegorry JP, Miller JR, Guanter L, Moreno J, Moya I, Berry JA, Frankenberg C, Zarco-Tejada PJ (2019) Remote sensing of solar-induced chlorophyll fluorescence (SIF) in vegetation: 50 years of progress. *Remote Sens Environ* 231:111177
- Nagajothi K, Rajashekara HM, Sagar DBS (2021) Universal fractal scaling laws for surface water bodies and their zones of influence. *IEEE Geosci Remote Sens Lett* 18(5):781–785
- Sun W, Xu G, Gong P, Lliang S (2006) Fractal analysis of remotely sensed images: a review of methods and applications. *Int J Remote Sens* 20(22):4963–4990
- Zhang Z, Xu W, Qin Q, Long Z (2020) Downscaling solar-induced chlorophyll fluorescence based on convolutional neural network method to monitor agricultural drought. *IEEE Trans Geosci Remote Sens* 59(2):1012–1028

## 4.2 First author conference peer reviewed study and posters

#### 4.2.1 Fourth publication (Quiros-Vargas et al., 2021)

“Response of Bean (*Phaseolus vulgaris* L.) to Elevated [CO<sub>2</sub>] in Yield, Biomass and Chlorophyll fluorescence”

**Conference:** IEEE International Geoscience and Remote Sensing Symposium (IGARSS, Brussels, Belgium, 2021)

<b>Authors (country):</b>  J. Quiros-Vargas (GE) Rafael D. Caldeira (PT) N.Z. dos Santos (GE) L. Zimmermann (GE) B. Siegmann (GE) Thorsten Kraska (GE) M.W. Vasconcelos (PT) Uwe Rascher (GE) Onno Muller (GE)	<b>Journal:</b> Proceedings of the IEEE International Geoscience and Remote Sensing Symposium (IGARSS, Brussels, Belgium)  <b>Status:</b> Published  <b>Contribution of the doctorate candidate:</b> <ul style="list-style-type: none"><li>• Conceptualization: 80%</li><li>• Data analysis: 100%</li><li>• Writing: 95%</li><li>• Field work: 85%</li></ul>
--	--

DOI: [10.1109/IGARSS47720.2021.9554347](https://doi.org/10.1109/IGARSS47720.2021.9554347)

# RESPONSE OF BEAN (*Phaseolus vulgaris* L.) TO ELEVATED [CO<sub>2</sub>] IN YIELD, BIOMASS AND CHLOROPHYLL FLUORESCENCE

Juan Quirós-Vargas<sup>1,\*</sup>, Rafael Diogo Caldeira<sup>2</sup>, Nicolas Zendonadi dos Santos<sup>1</sup>, Lars Zimmermann<sup>1</sup>, Bastian Siegmann<sup>1</sup>, Thorsten Kraska<sup>3</sup>, Marta W. Vasconcelos<sup>2</sup>, Uwe Rascher<sup>1</sup>, Onno Muller<sup>1</sup>

<sup>1</sup> Institute of Biogeosciences, IBG2: Plant Sciences, Forschungszentrum Jülich GmbH, 52425 Jülich, Germany

<sup>2</sup> Universidade Católica Portuguesa, CBQF—Centro de Biotecnologia e Química Fina—Laboratório Associado, Escola Superior de Biotecnologia, Rua Diogo Botelho 1327, 4169-005 Porto, Portugal

<sup>3</sup> Field Lab Campus Klein-Altendorf, University of Bonn, 53359 Rheinbach, Germany

\*Presenter: j.quirós@fz-juelich.de

## ABSTRACT

The impact of elevated [CO<sub>2</sub>] (e[CO<sub>2</sub>]) in on yield, biomass (BM) and chlorophyll fluorescence (ChlF) was analyzed in three genotypes of common beans (*Phaseolus vulgaris* L.), a key food-security crop. Active- and passive-sensed ChlF traits acquired by the Light-Induced-Fluorescence-Transient (LIFT), Moni-Pulse-Amplitude-Modulation (MoniPAM), and Fluorescence Box (FloX) instruments were compared. Total biomass increased for all genotypes under e[CO<sub>2</sub>], but their biomass partitioning significantly differed. The highest yielding genotype under e[CO<sub>2</sub>] also showed the highest photosynthetic activity according to different active-sensed ChlF methods. Furthermore, e[CO<sub>2</sub>] resulted in earlier senescence, which was detected by either satellite- or FloX-derived Normalized Difference Vegetation Index (NDVI). Moreover, we observed a significant agreement between MoniPAM- and LIFT-measured ChlF data ( $R^2 = 0.89$ ,  $p = 0.02$ ), as well as between SIF and FloX measurements ( $R^2 = 0.62$ ,  $p = 0.03$ ).

**Index Terms**— LIFT, FloX, MoniPAM, FACE, biomass, yield, grain quality

## 1. INTRODUCTION

Free air CO<sub>2</sub> enriched (FACE) experiments have been implemented to understand the impact of the increasing levels of atmospheric CO<sub>2</sub> in plants. Legumes, are among the most sensitive species to e[CO<sub>2</sub>] [1,2]. For instance, at -150-200 ppm higher [CO<sub>2</sub>], [2] estimated an augment of 24% in bean yield, and [3] reported an increase in the leaf area and a reduction in the stomata density in leaves. However, [4] found no yield increase in bean plants grown under e[CO<sub>2</sub>], despite an increment in photosynthesis rates and dry matter production. Furthermore, growth at e[CO<sub>2</sub>] was shown to impact the mineral elements concentrations,

where the response in legumes differed depending on the intensity and duration of the imposed stress, plant genotype and developmental stage [5]. Fluctuations on mineral elements concentrations stand as an important concern, since dietary deficiencies of both macro and, particularly, micronutrients are a major global public health problem. Thus, e[CO<sub>2</sub>] may severely impact the whole agroecosystem through both positive and negative effects of crop adaption.

Due to its close relationship to photosynthetic activity chlorophyll Fluorescence (ChlF) allows a deeper understanding of plant physiology at leaf and canopy level, which is important in crop adaptation. ChlF provides useful information to assess the response of crops in a FACE experiment, e.g., by comparing the photosynthetic efficiency of genotypes when the [CO<sub>2</sub>] is elevated. ChlF can be estimated on the basis of active and passive methods using light induced fluorescence transients (LIFT; [6]) and solar-induced ChlF (SIF) [7] measurement, respectively. The yield of photosystem II (PSII,  $Fq'/Fm'$ ) can also be obtained from LIFT data. An alternative active sensing method is the pulse amplitude modulate (PAM) fluorometry used to estimate steady-state ChlF. The comparison of ChlF metrics from different sensors is a topic of great research interest aiming at comprehending how the data from several sources can be integrated to better understand ChlF spatio-temporal variations. In addition, such knowledge can contribute to the forthcoming 'FLuorescence EXplorer' (FLEX) satellite mission of the European Spatial Agency (ESA) [8].

In this context we analyzed the response of three bean genotypes to e[CO<sub>2</sub>] in (i) yield and biomass (BM), as well as in (ii) the diurnal ChlF and photosynthetic efficiency of three genotypes during the pod-filling stage. Moreover, (iii) sensor metrics were compared; SIF was correlated with the active-sensed ChlF data, whereas the yield of photosystem II from LIFT ( $Fq'/Fm'$ ) was compared with the one of MoniPAM (YII).

### 3. MATERIAL AND METHODS

**3.1. Study site and experiment:** The study area was located at Campus Klein Altendorf, which is affiliated with the University of Bonn, Germany (50°37'29.39"N, 6°59'11.33"E). The so called 'BreedFACE' operated by Forschungszentrum Jülich consisted of an octagon of ~7.25 m steel pipes (~254 m<sup>2</sup>) with tiny openings each 20-30 cm for the ejection of CO<sub>2</sub>. CO<sub>2</sub> was automatically controlled to be 600 ppm in the center of the ring. The system was activated on July 29 and stayed working until August 29 with some gaps between July 31 to August 8, August 12 and August 19. The experiment was a complete randomized block design, with 2-4 repetitions of eleven genotypes, planted in 1.2x2.6 m plots at e[CO<sub>2</sub>] and ambient CO<sub>2</sub> (a[CO<sub>2</sub>]) conditions. The present study focuses on three genotypes, henceforth named: G1, G2 and G3, with three repetitions of G1 and G2, and two repetitions of G3.

**3.2. Instruments and data acquisition:** The fluorescence box (FloX; JB Hyperspectral, Dusseldorf, Germany) and LIFT were mounted on the 'field-snake', an automated platform for field phenotyping with Real Time Kinematics (RTK) accuracy (~2 cm) in the horizontal (X-Y) and vertical (Z) axes. From the FloX the SIF measured at 760 nm in the O<sub>2</sub>-A band (SIF-A) was correlated with LIFT and MoniPAM information. LIFT and FloX data were collected at the beginning (Bpf) and end of pod filling (Epf) at different hours from 08:30 to 16:30. Bpf measurements were taken on July 30, July 31 and August 1, while Epf ones were collected on August 23 and August 27. MoniPAMs constantly recorded ChlF and the YII information from the same leaf during 29 days, from July 30 to August 27, 2019.

**3.3. Data processing:** Quantum GIS (QGIS, version 2.18.22), an open source Geographic Information System (GIS), was used to extract the LIFT and FloX data points. The extracted LIFT data was then processed with an R script in order to extract ChlF and  $Fq'/Fm'$  information [9]. The FloX data was processed with an R-script developed by the manufacturer, and furtherly filtered according to a quality indicator called 'E-stability'. The latter was done to remove unreliable data points under unstable light conditions. FloX SIF yield was estimated as the ratio of SIF-A to incoming photosynthetic active radiation (PAR) at 750nm. The MoniPAM ChlF and YII information was processed and readout with the WinControl commercial software (Heinz Walz GmbH, Germany).

**3.4. Estimation of BM and yield:** above-ground BM samples were destructively collected on August 27. Ten plants per plot were uprooted. Leaves+stem, grains and pods were weighed after being dried at 60° during 5 days. The weights were converted to percentages of leaves+stem, pods and grains (i.e., yield) from the total BM.

### 4. RESULTS AND DISCUSSION

**4.1. Changes in vegetative and reproductive Biomass:** At e[CO<sub>2</sub>], genotypes 1, 2 and 3 accumulated more BM, with 74, 119 and 64 g more of total (leaf, stem, grains and pods) BM compared with the ambient experiment (Fig. 1a). This difference was significant for G1 and G2, but not for G3. Besides such general BM increase, the way plants divide the gained BM into vegetative and reproductive organs is counted to analyze genotypic response to e[CO<sub>2</sub>]. Remarkably, in comparison with the a[CO<sub>2</sub>] environment, G1 allocated 7% more BM in grains under e[CO<sub>2</sub>] (Fig. 1b and c). G2, in turn, allocated 8% more BM to leaves+stem, while decreased its grain and pod BM by 5% and 3%, respectively. Furthermore, G3 BM partitioning stayed similar for both [CO<sub>2</sub>] conditions, with a marginal increase of 1% in leaves+stem and decreased of 1% in grains at e[CO<sub>2</sub>].

Potentially, the impact of the e[CO<sub>2</sub>] on the BM of G1 and G2 can be explained by the following factors (and their interactions): i) higher photosynthetic efficiency; ii) the short time that the e[CO<sub>2</sub>] was active (3-4 weeks) may have reduced the stomatal density, which has been reported in long term experiments. Thus, higher gas exchange may have occurred to maintain the higher photosynthetic efficiency at e[CO<sub>2</sub>]; iii) the late application of e[CO<sub>2</sub>] may have contributed to avoid the impact of downregulation during most of the pod-filling. Thus, possibly keeping high photosynthetic rates during that stage; and iv) the balanced sink-source interaction, due to the presence of active sinks during the e[CO<sub>2</sub>] treatment.

Lastly, an apparent earlier senescence was observed in the field. Firstly, this was shown for the complete FACE ring with a diameter of 17.5 meter by the seasonal normalized difference vegetation index (NDVI) curve computed with high resolution (3 m) satellite information (Fig. 2; Planet Labs, San Francisco, CA, USA), Secondly, at plot level, the FloX-derived NDVI similarly suggest how the loose of greenness occurred faster in the e[CO<sub>2</sub>] experiment towards Epf (Fig. 2).

**4.2. Diurnal ChlF at a[CO<sub>2</sub>] and e[CO<sub>2</sub>] environments:** A higher SIF yield in the morning, and a subsequent rise after the noon decay was observed at Bpf, as it was likewise observed by [7] at early corn senescence. A similar behavior, despite less pronounced, is detected in the e[CO<sub>2</sub>] still at Epf (Fig. 3a); at the time the a[CO<sub>2</sub>] constantly decreased after the morning. SIF yield variations obey to the diurnal PAR cycle, however, the link between both parameters is not the same along the day; thus additional physiological mechanisms might play a key role modulating this relation [11].

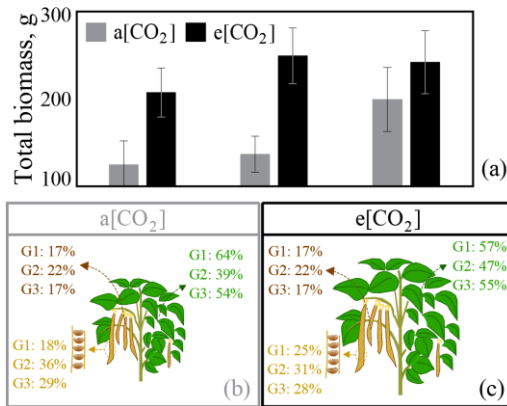


**Fig. 1.** Total biomass accumulation at both [CO<sub>2</sub>]'s (a), and genotypes biomass partitioning at a[CO<sub>2</sub>] (b) and e[CO<sub>2</sub>] (c).

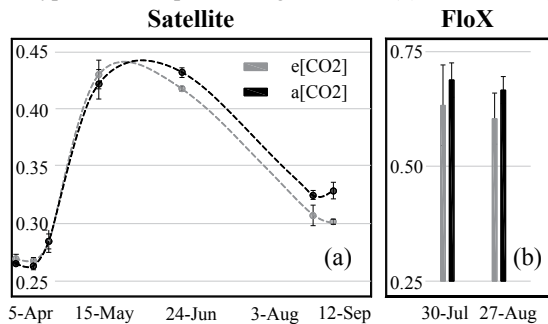


**Fig. 2.** Seasonal (April to September) satellite-NDVI curve (a), and FloX-NDVI at Bpf (July 30) and Epf (August 27).

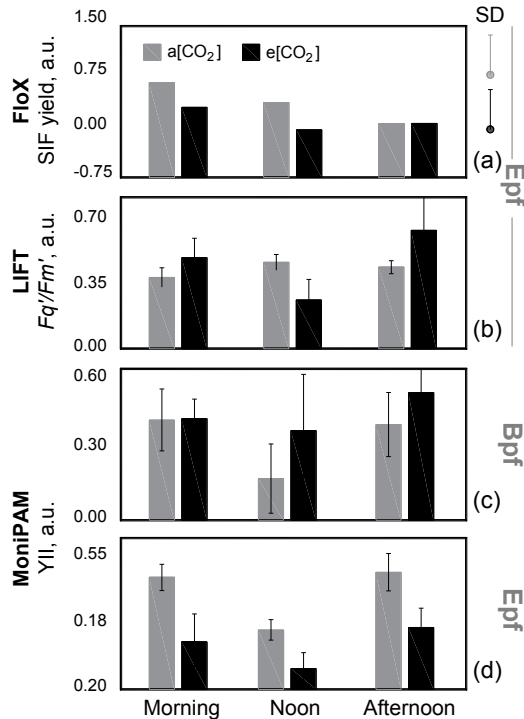


**Fig. 3.** FloX-derived SIF yield (a) and LIFT-derived  $Fq'/Fm'$  (b) averaged for the three genotypes at Epf. And MoniPAM-derived YII for G3 at Bpf (c) and Epf (d). Results are presented per [CO<sub>2</sub>] condition during the morning (8:30-11:00h), noon (12:00-13:00h) and afternoon (14:00-16:30h).

The  $Fq'/Fm'$  was higher under e[CO<sub>2</sub>] at Bpf in the noon and afternoon, while at Epf it was higher in the morning and afternoon, but significantly lower than the one measured at noon in the a[CO<sub>2</sub>] plots (Fig. 3b). The latter is comparable with the diurnal yield of PSII reported by [8] at late corn senescence, with the difference that in their study the decay is dimmer and occurred around 2 hours later. In another study, [12] identified a similar pattern of the  $Fq'/Fm'$  estimated from LIFT and MoniPAM instruments, with this characteristic decay in the quantum efficiency of PSII at noon, being clearer in the MoniPAM data (Fig. 3 c and d). The least productive genotype, G3, presented the lower photosynthetic efficiency at Epf, conversely to G1 (the most yield responsive). G2, in particular, showed a higher  $Fq'/Fm'$  in the morning at e[CO<sub>2</sub>] in Epf, which could be associated to its larger increase in total BM compared with G1 and 3. The response observed in the three analyzed genotypes may not be a rule of thumb for beans. Indeed, considering all the eleven genotypes included in the same FACE experiment (eight of which are not included in the present study) the accumulation in vegetative and reproductive BM at e[CO<sub>2</sub>] of G1-G2-G3 is above the average.

**4.3. Comparison of instruments metrics:** A significant ( $p = 0.03$ ) correlation ( $R^2 = 0.62$ ) was found between FloX-derived SIF-A and the ChIF estimation derived from MoniPAM in the a[CO<sub>2</sub>]; a similar relation ( $R^2 = 0.64$ ) was observed in the e[CO<sub>2</sub>] with the SIF-A, although with a lower significance ( $p = 0.12$ ; Fig. 4a). On the contrary, regarding the photosynthetic efficiency-related parameters, only the LIFT measurements ( $Fq'/Fm'$ ) in the e[CO<sub>2</sub>] did correlate with the SIF-A ( $R^2 = 0.98$ ,  $p = 0.13$ ; Fig. 4b). Following a similar goal, [13] found a lower  $R^2$  (0.32) in avocado leaves but more significant ( $p < 0.001$ ) correlation between SIF and LIFT-derived yield of PSII. The comparison between the active sensing methods showed a high correlation ( $R^2 = 0.88-0.89$ ,  $p = 0.02$ ) of ChIF data (Fig. 4c), but no link between the YII (MoniPAM) and  $Fq'/Fm'$  (LIFT; Fig. 4d).

## 5. CONCLUSIONS

The response to e[CO<sub>2</sub>] in BM and yield varied for the different genotypes. While G1 increased 7% the BM at e[CO<sub>2</sub>], G2 destined 8% more BM to leaves+stems. G3 BM partitioning was similarly in both [CO<sub>2</sub>] environments. The effect of e[CO<sub>2</sub>] was associated earlier senescence, which was detected from satellite- and FloX-derived NDVI. Higher photosynthetic rates, derived from LIFT-  $Fq'/Fm'$  and MoniPAM-YII, at Bpf, may be related to the higher yield-response of G1. Moreover, significant agreements were

observed between MoniPAM ChlF estimation and the respective data from LIFT ( $R^2 = 0.89$ ,  $p = 0.02$ ), as well as with SIF measured with the Flox ( $R^2 = 0.62$ ,  $p = 0.03$ ).

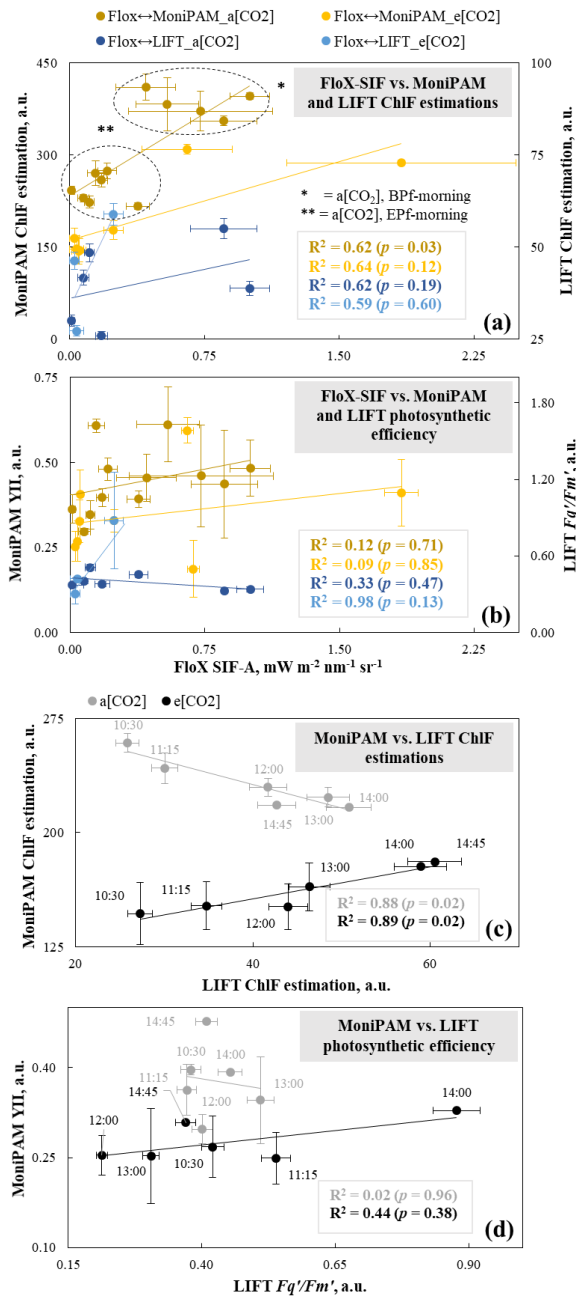


**Fig. 4.** Correlation between the FloX SIF (a.u.) and MoniPAM and LIFT ChlF (a) and photosynthetic efficiency (b) estimations at both timepoints and [CO<sub>2</sub>] concentrations, and the comparison between MoniPAM and LIFT ChlF (c) and photosynthetic efficiency (d) at Epf under both [CO<sub>2</sub>] conditions. Error bars for LIFT ChlF correspond to the 5% of the value; the remaining error bars correspond to the SD.

**Acknowledgements:** Authors would like to thank the scientific support of National Funds from FCT - Fundação para a Ciência e a Tecnologia through project

UID/Multi/50016/2019, and EPPN through project #53. This work was supported by the European Union's Horizon 2020 Research and Innovation program EPPN2020 (grant agreement: 731013) and under the Marie Skłodowska-Curie grant agreement no. 721995 (within the Training on Remote Sensing for Ecosystem Modelling –TRuStEE- consortium). The BreedFACE is established in the German-Plant-Phenotyping Network funded by the German Federal Ministry of Education and Research (project identification number: 031A053).

## 7. REFERENCES

- [1] E.A. Ainsworth, S.P. Long, "30 years of free-air carbon dioxide enrichment (FACE): What have we learned about future crop productivity and its potential for adaptation?" *Glob. Change Biol.*, pp. 27-49, 2020.
- [2] A. Rogers, E.A. Ainsworth, and A.D.B. Leakey, "Will Elevated Carbon Dioxide Concentration Amplify the Benefits of Nitrogen Fixation in Legumes?," *Plant Physiol.*, pp.1-151, 2009.
- [3] P. Sánchez-Espino, A. Larqué-Saavedra, T. Nava-Sánchez, and C. Trejo. "Maize and bean plants response to CO<sub>2</sub> enrichment," *Agricencia*, pp. 311-320, 1999.
- [4] J.B.L. da Silva, P.A. Ferreira, L.C. Pires, E.G. Pereira, and J.E.S. Carneiro, "Influences of two CO<sub>2</sub> concentrations and water availability on bean crop," *Eng. Agric.*, pp. 730-738, 2013.
- [5] J.C. Soares, et al., "Preserving the nutritional quality of crop plants under a changing climate: importance and strategies," *Plant and Soil*, pp. 1-26, 2019.
- [6] Z. Kolber, et al., "Measuring photosynthetic parameters at a distance: laser induced fluorescence transient (LIFT) method for remote measurements of photosynthesis in terrestrial vegetation," *Photosynthesis Research.*, pp. 121-129, 2005.
- [7] G.H. Mohammed, R. Colombo, E.M. Middleton, U. Rascher, et al., "Remote sensing of solar-induced chlorophyll fluorescence (SIF) in vegetation: 50 years of progress," *Remote Sens. Environ.*, pp. 1-39., 2019.
- [8] T.K.E. Campbell, K.F. Huemmrich, E.M. Middleton, et al., "Diurnal and Seasonal Variations in Chlorophyll Fluorescence Associated with Photosynthesis at Leaf and Canopy Scales," *Remote Sens.*, pp. 1-27, 2019.
- [9] B. Keller, S. Matsubara, U. Rascher, R. Pieruschka, A. Steier, T. Kraska, O. Muller, "Genotype Specific Photosynthesis x Environment Interactions Captured by Automated Fluorescence Canopy Scans Over Two Fluctuating Growing Seasons," *Front. Plant Sci.*, 1482, 2019.
- [10] P. Sánchez-Espino, A. Larqué-Saavedra, T. Nava-Sánchez, C. Trejo, "Maize and bean plants response to CO<sub>2</sub> enrichment," *Agricencia*, pp. 311-320, 1999.
- [11] F. Pinto, et al., "Sun-induced chlorophyll fluorescence from high-resolution imaging spectroscopy data to quantify spatio-temporal patterns of photosynthetic function in crop canopies," *Plant Cell Environ.*, pp. 1500-1512, 2016.
- [12] A.R. Raesch, et al., "Field Observations with Laser-Induced Fluorescence Transient (LIFT) Method in Barley and Sugar Beet," *Remote Sens.*, pp. 159-169, 2014.
- [13] R. Wyber, Z. Malenovsky, M.B. Ashcroft, et al., "Do Daily and Seasonal Trends in Leaf Solar Induced Fluorescence Reflect Changes in Photosynthesis, Growth or Light Exposure?," *Remote Sens.*, pp. 1-19, 2017.

#### 4.2.2 Fifth publication (Quiros-Vargas et al., AGU-2020)

### “Solar Induced Chlorophyll fluorescence and Vegetation Indices for Heat Stress Assessment in Three Crops at Different Geophysics-Derived Soil Units”

**Conference:** American Geophysical Union (AGU Fall Meeting, online, 2020)

**Authors:** Juan Quiros-Vargas (GE), Cosimo Brogi (GE), Vera Krieger (GE), B. Siegmann (GE), Marco Celesti (IT), Micol Rossini (IT), Sergio Cogliati (IT), L. Weihermüller (GE), Uwe Rascher (GE)

**Abstract:** Remotely-sensed Solar Induced chlorophyll fluorescence (SIF) is a novel promising tool to retrieve information on plants' physiological status due to its direct link with the photosynthetic process. At the same time, narrow band Vegetation Indices (VIs) such as the MERIS Terrestrial chlorophyll index (MTCI), and the Photochemical Reflectance Index (PRI), as well as broad band VIs like the Normalized Difference Vegetation Index (NDVI), have been widely used for crop stress assessment. A match between these remote sensing products and the spatial distribution of soil units is expected; nevertheless, an in-depth analysis of such relationship has been rarely performed so that additional studies are required. In this contribution, we aimed at the comparison in the use of normalized SIF ( $SIF = SIF/PAR$ ; computed with the Spectral Fitting Method, SFM) and VIs (MTCI, PRI and NDVI) for heat stress assessment in corn, sugar beet and potato at the beginning and towards the end of a heatwave occurring in Selhausen, Germany, 2018. Data were acquired with the HyPlant airborne sensor, which is a high performance imaging spectrometer with around 0.30 nm of spectral resolution in the Oxygen absorption bands. We compared different plots located in the upper (poorer soil characteristics for agriculture such as water holding capacity and content of coarse sediments) or lower landscape terraces; we also evaluated the different remote sensing products in comparison with site specific geophysics-based soil maps. At the beginning of the heat wave we found that, compared with VIs, SIF data showed a clearer differentiation of the stress conditions at a terrace level in potato and sugar beet. However, towards the end of the wave a significant decrease of MTCI and NDVI contrasted with higher SIF in sugar beet and corn. Nonetheless, those crops (sugar beet and corn) did not show significant SIF differences between terraces. A significant spatial match was found between SIF and geophysics-derived soil spatial patterns ( $p = 0.004-0.030$ ) in fields where NDVI was more homogeneous ( $p = 0.028-0.499$ , respectively). This suggests the higher sensitivity of SIF to monitor heat stress compared with common VIs.

DOI: [10.1002/essoar.10504968.1](https://doi.org/10.1002/essoar.10504968.1)

#### 4.2.3 Sixth publication (Quiros-Vargas et al., EGU-2022)

“Spatial dependency of Solar-induced Chlorophyll fluorescence (SIF)-emitting objects in the footprint of a FLuorescence EXplorer (FLEX) pixel: a SIF-downscaling perspective”

**Conference:** European Geosciences Union (EGU, Vienna, Austria, 2022)

**Authors:** Juan Quiros-Vargas (GE), B. Siegmann (GE), A. Damm (CH), Vera Krieger (GE), Onno Muller (GE), Uwe Rascher (GE)

**Abstract:** The assessment of large-scale vegetation functioning is essential to improve cropland productivity and monitor natural ecosystem health. The development of remote sensing (RS) technologies over decades made such assessments possible from field- to global-scale. Nevertheless, commonly used reflectance-based RS methods are often not sensitive enough to timely inform preventive or corrective actions. Recent advances on the RS of solar-induced chlorophyll fluorescence (SIF) have opened opportunities for novel approaches of earlier stress detection since SIF was found to be closely linked to photosynthesis. The forthcoming FLuorescence EXplorer (FLEX) satellite mission of the European Space Agency (ESA, to be launched) will offer timely non-aggregated global-scale SIF data at 300 m spatial resolution. Such pixel size, even though unique and accurate enough to monitor processes at biome level, may not be suitable to assess field scale processes. Therefore, the development of methodologies to downscale satellite-SIF information is currently of utmost interest since allowing to increase the spatial resolution of origin observations. A first step to comprehend the characteristics that possible approaches must meet is to understand the magnitude of the spatial variability within a coarse pixel footprint across representative vegetation types. Our study consequently aims to understand the spatial variability within the footprint of a FLEX pixel. We particularly analyze the spatial dynamics of SIF via the near infrared reflectance of vegetation (NIRv) data derived from Sentinel 2, World View- and Geo Eye- (10.0 m, 0.30, 0.40 m pixel<sup>-1</sup>, respectively) that was suggested as proxy for SIF in absence of environmental stress. With Sentinel 2 based NIRv we focus on four ecosystems, including small and large scale agriculture, pampa and savannah, with World View- and Geo Eye based NIRv, we investigate rain and coniferous forests. The very high resolution of World View- and Geo Eye was required to compute the variograms of forests since they were affected by a nugget effect when using Sentinel-2 images. Investigated ecosystems represent the most abundant vegetation types that the FLEX mission will cover. We also assessed the relation between the spatial dependencies (approximated by the lag of calculated semi-variograms) and the average object size in all the ecosystems. We found largest spatial dependencies (400-600 m) in large-scale agriculture, pampa and savannah and contrasting lower (<10 m) in forests. Spatial dependencies of small-scale agricultural scenes were in a middle position with approximately 100 m. Moreover, the spatial dependencies were found to be significantly ( $p = 0.023$ ) linked to the average object size of the ecosystems. This demonstrates the importance of flexible downscaling methods, e.g. in a fractals-based direction (Quiros-Vargas et al., in press).

DOI: [10.5194/egusphere-egu22-12671](https://doi.org/10.5194/egusphere-egu22-12671)

#### 4.2.4 Seventh publication (Quiros-Vargas et al., LPS-2022a)

### “Spatial relation between Sun-induced Chlorophyll fluorescence (SIF) and the Plant Available Water (PAW) in the root zone”

**Conference:** Living Planet Symposium (LPS, Bonn, Germany, 2022)

**Authors:** Juan Quiros-Vargas (GE), Cosimo Brogi (GE), A. Damm (CH), B.Siegmann (GE), P. Redemske (GE), V. Burchard (ES), Vera Krieger (GE), L. Weihermueller (GE), Onno Mueller (GE), Uwe Rascher

**Abstract:** All life on earth depends on the availability of water. Climate change and wasting customs threat to limit its access to a large part of the population. Inefficient water management systems makes agriculture one of the activities that contribute most to such an alarming situation. Thus, the need of new ideas for a better efficiency in the use of water constantly grows, which implies the use of remote sensing (RS) techniques to cover large areas. Reflectance-based RS products, such as vegetation indices, have shown low sensitivity to detect the effects of water limitation on vegetation before the stress has impacted canopy structural properties. Thermal information is more closely related to water stress in plants, but is also affected by other factors not related to soil water limitations, e.g. wind speed and humidity. Recently, the use of sun-induced chlorophyll fluorescence (SIF) for water stress assessments has gained interest, since it is directly related to the photosynthetic activity that dynamically responds to limitations in the availability of water. Nevertheless, it is not clear yet how the spatial relation between SIF and soil water content behaves according to specific vegetation and soil characteristics. Therefore, in the present study we analyzed the link between airborne-SIF and geophysics-based plant available water (PAW) in the root zone of three crops (winter wheat, summer non-irrigated sugar beet and irrigated potato) during three growing seasons (2018, 2019 and 2020). We found a strong positive correlation ( $r = 0.92$ ;  $p < 0.01$ ) when water was a limiting factor, i.e., in the non-irrigated summer crop (sugar beet). The relation disappeared when the level of PAW is sufficient to meet the crops water need, i.e. in irrigated crops or years with precipitation events ( $25 \text{ l m}^{-2}$ ) accumulated a few days before data acquisition. An unclear pattern in the relation of winter wheat and PAW might be explained to the advanced growth stage of winter wheat (ripening), when variations on SIF might be influenced by other physiological processes like chlorophyll degradation rather than the PAW in the root zone. Moreover, an expected response of SIF to a low PAW zone in the spatial and the temporal domains compared with the enhanced vegetation index (EVI) and the surface temperature, respectively, is reported in our study for the first time. The presented results contribute to the development of new methodologies for a better efficiency in the use of water by providing new insights on the role of SIF for real-time assessment of crop water stress. Besides, the current availability of global SIF and soil moisture satellite datasets such as the TROPospheric Monitoring Instrument (TROPOMI)-SIF and the Soil Moisture Active/Passive (SMAP) products, respectively, enables further analysis to improve our understanding of the SIF-soil water content relation on larger scales. A brief insight on this relation will be presented on the example of the European heat wave in summer 2018. For this event the relationship between SIF and soil moisture for forests was characterized by high soil water content and low SIF values while crop lands showed an opposite trend.

#### 4.2.5 Eighth publication (Quiros-Vargas et al., LPS-2022b)

### “Sun-induced Chlorophyll fluorescence (SIF)-downscaling from the fractal geometry perspective”

**Conference:** Living Planet Symposium (LPS, Bonn, Germany, 2022)

**Authors:** Juan Quiros-Vargas (GE), B. Siegmann (GE), A. Damm (CH), Ran Wang (US), John Gamon (US), Vera Krieger (GE), B.S. Daya Sagar (IN), Onno Muller (GE), Uwe Rascher (GE)

**Abstract:** Agriculture has to guarantee food security for a constantly growing population by increasing crop productivity with minimized environmental impact. Remote Sensing (RS) for large scale vegetation assessment is one of the most important tools to overcome this challenge. For years the implementation of RS techniques for crop assessment has been mainly based on the use of reflectance-based information, e.g. Vegetation Indices (VIs), which indicate crop stress after its effect has impacted plant structural properties. It is suggested that the use of Sun-induced Chlorophyll fluorescence (SIF) possibly allows earlier crop stress detection, since being in direct relation with photosynthetic activity, thus, making it possible to detect smooth (pre-visual) changes in the functioning of vegetation. RS of SIF has gained interest of researchers thanks to the recent development of algorithms and models to compute SIF from airborne and satellite sensors. The FLuorescence EXplorer (FLEX) satellite mission of the European Space Agency (ESA) will provide SIF data at global scale with a spatial resolution of 300 m. Despite the great value of such data to track large-scale vegetation functional dynamics, there is high interest to study possible ways to increase its resolution to an intra- or inter-field level. Recent studies have addressed that subject using VIs, evapotranspiration and land surface temperature as explanatory variables. Yet, a more flexible method capable to work in multiple ecosystems and spatiotemporal scales is needed. Our hypothesis is that the versatility of the fractal geometry, present in numerous spatial and temporal phenomena in nature, allows fractal approaches to address that need. With this study, we aim to first evaluate the existence of fractal geometry in the spatial distribution of SIF emitting objects based on the presence of the universal Power Law (PL) and, second, to evaluate whether the aggregation of the SIF signal in SIF emitting objects across spatial resolutions is scale invariant. For that purpose we used airborne SIF data retrieved over a ~60 ha soybean field in Nebraska, USA (summer 2018). The image was resampled from its original resolution of 1.5 m to 5, 10 and 15 m pixel size. The resampled images were segmented into individual objects, and for each object the total SIF ( $SIF_{TOT}$ ) was calculated. We found: (i) presence of fractal geometry in the distribution of  $SIF_{TOT}$  objects, since they followed the PL in all the analyzed scales; and (ii) evidence of scale invariance in the SIF aggregated signal. The second was concluded based on the linear increase of the scale factor and the nearly invariant behavior of the dimension factor of the PL equations across spatial resolutions. Both findings constitute the first step towards the use of the fractal geometry for SIF-downscaling, understood as the fragmentation of coarse resolution SIF data into the  $SIF_{TOT}$  of individual vegetation objects under its footprint. The above described study was accepted for publication as the ‘fractal geometry’ chapter in the Springer-Nature Encyclopedia of Mathematical Geosciences, and it was ‘in production’ status by the time of this abstract’s submission. Additionally, we investigated possible bi-variate PL’s where a second variable could explain variations in  $SIF_{TOT}$ . Interestingly, we found in numerous datasets that the inverse of the (SIF emitting) object size fits the PL function with  $SIF_{TOT}$  at  $R^2 > 0.95$ . This finding opens the possibility for practical SIF-downscaling approaches using the fractal theory.

#### 4.2.6 Ninth publication (Quiros-Vargas et al., EARSeL-2022)

“Solar-induced chlorophyll fluorescence (SIF) relation with soil moisture (SM) and gross primary productivity (GPP) at European scale in a heat wave”

**Conference:** European Association of Remote Sensing Laboratories (EARSeL, Potsdam, Germany, 2022)

**Authors:** Juan Quiros-Vargas (GE), B. Siegmann (GE), A. Damm (CH), Cosimo Brogi (GE), Philipp Köhler (US), Roel Van Holst (BE), David Martini (GE), Onno Muller (GE), Uwe Rascher (GE)

**Abstract:** Advancement in the development of imaging spectroscopy methods and instruments have a great impact on the assessment of vegetation functioning. In particular, the retrieval of Solar-Induced chlorophyll fluorescence (SIF) from satellite spectroscopic data attracted attention from the scientific community in recent years. Initially, missions like the Global Ozone Monitoring Experiment 2 (GOME-2), from the European Space Agency (ESA), and the Orbiting Carbon Observatory 2 (OCO-2) from the National Aeronautics and Space Administration (NASA) were used for the retrieval of SIF at satellite scale. Nevertheless, subsequently the unprecedented combination of the spectral resolution, signal-to-noise ratio, and spatial coverage of the Tropospheric Monitoring Instrument (TROPOMI) motivated novel approaches for global scale SIF assessment. The  $\sim 7 \times 3.5$  km pixel<sup>-1</sup> (at nadir) daily SIF data provided by the TROPOMI-SIF product (Köhler et al., 2018), alongside the high resolution in the temporal domain as well (daily revisit time), has large potential to advance our knowledge on large scale ecosystem dynamics. Especially when integrated with other ecosystem variables such as Soil Moisture (SM) and Gross Primary Productivity (GPP), it is possible to advance interpreting the response of ecosystems to stress conditions. In this study we analyze the relationship of SIF with subsurface soil moisture (from the NASA’s soil moisture active/passive –SMAP- mission) and GPP (generated within the ESA’s Scientific Exploitation of Operational Missions -SEOM- Terra-P project) during the European Heat Wave (HW) in 2018, aiming to understand the continental scale response of vegetation to abnormally high temperatures. Therefore, in this study we classified the averaged soil moisture maps from June to early August into eight groups (from  $\sim 50$  l m<sup>-3</sup> to 300 l m<sup>-3</sup>) and analyzed their relation with the corresponding SIF and GPP data. We also analyzed the behavior of SIF in each soil moisture class with special attention to HW peaks in the fourth week of June and the third of July. We found a strong positive SIF- soil moisture relation ( $r = 0.91$ ,  $p < 0.01$ ) and a lower, but more heat sensitive, SIF pattern across time in the lower soil moisture classes. Moreover, our results suggest that a positive SIF-GPP relation is uncoupled and even becomes negative during the heat wave (as reported by Martini et al., 2021) in regions with soil moisture below 130 l m<sup>-3</sup>, but remains positive in areas with higher soil water content. Our results provide the first insight of the SIF-GPP relation contextualized in the frame of the soil water content. Furthermore, motivates future deeper analyses of this three-variate (SIF, SM, and GPP) relation within the specific lowest and highest soil moisture classes.

#### 4.2.7 Tenth publication (Quiros-Vargas et al., EMS-2022)

“Vegetation and climate: initial concepts about the relation between the sun-induced chlorophyll fluorescence (SIF) and the soil water content (SWC)”

**Conference:** European Meteorological Society (EMS, Bonn, Germany, 2022)

**Authors:** Juan Quiros-Vargas (GE), Bastian Siegmann (GE), Alexander Damm (CH), Uwe Rascher

**Abstract:** Climate conditions directly impact on vegetation growth, this is quite clear; yet, “how vegetation functioning alters climate?” is an open query rising many questions. Understanding the impact of vegetation functioning on climate is important to better comprehend climatological processes and thus to improve models, due to the influence of plants on the carbon and water cycles. For decades it was impossible to have information about plant functioning in the (regional to global) scale of climatological models, nevertheless, the advent of satellite-based remote sensing (RS) methods for the retrieval of sun-induced chlorophyll fluorescence (SIF, as a proxy of photosynthesis) made it feasible. For instance, using satellite SIF and precipitation data, Green et al. (2017; DOI 10.1038/ngeo2957) recently provided one of the first contributions in such direction. The authors reported that regional biosphere-atmosphere feedbacks can explain up to 30% of precipitation variance, mainly because of the role of plants in the regulation of the water flux from the soil towards the atmosphere. As a complement to such studies with focus on the vegetation-atmosphere link, in two recent studies we analyzed the relation that SIF has with the soil water content (SWC) at airborne and satellite scales. At airborne scale we found that (i) the SIF-SWC relation is crop- and growth stage-dependent, and that (ii) SIF showed a faster response to water limitations compared to conventional (reflectance-based) RS products. On the satellite level we found a strong impact of the SIF-SWC relation on the gross primary productivity (GPP) during a heat wave at European scale. With these contributions from the RS area, we aim to provide novel information that can help the meteorological research community to better understand how vegetation functioning can alter climatological processes, with potential applications in the improvement of climate models.

DOI: [10.5194/ems2022-612](https://doi.org/10.5194/ems2022-612)

### 4.3 Co-authored peer-reviewed articles (only listed)

- [1] B. Siegmann, M.P. Cendrero-Mateo, S. Cogliati, A. Damm, J. Gamon, D. Herrera, C. Jedmowski, L.V. Junker-Frohn, T. Kraska, O. Muller, P. Rademske, C. van der Tol, **J. Quiros-Vargas**, P. Yang, U. Rascher, Downscaling of far-red solar-induced chlorophyll fluorescence of different crops from canopy to leaf level using a diurnal data set acquired by the airborne imaging spectrometer HyPlant. *Remote Sens. Environ.* 264, 112609 (2021).
- [2] B. Siegmann, L. Alonso, M. Celesti, S. Cogliati, R. Colombo, A. Damm, S. Douglas, L. Guanter, J. Hanuš, K. Kataja, T. Kraska, M. Matveeva, J. Moreno, O. Muller, M. Píkl, F. Pinto, **J. Quiros-Vargas**, P. Rademske, F. Rodriguez-Morene, N. Sabater, A. Schickling, D. chüttemeyer, F. Zemek, U. Rascher, The high-performance airborne imaging spectrometer HyPlant—From raw images to top-of-canopy reflectance and fluorescence products: Introduction of an automatized processing chain. *Remote Sens.* 11, 2760 (2019).

### 4.4 Main not co-authored discussed studies (only listed)

- [3] C. Brogi et al., Simulation of spatial variability in crop leaf area index and yield using agroecosystem modeling and geophysics-based quantitative soil information. *Vadose Zone J.* 19, e20009 (2020).
- [4] A. Damm, S. Cogliati, R. Colombo, L. Fritsche, A. Genangeli, L. Genesio, J. Hanus, A. Peressotti, P. Rademske, U. Rascher, D. Schuettemeyer, B. Siegmann, J. Sturm, F. Miglietta, Response times of remote sensing measured sun-induced chlorophyll fluorescence, surface temperature and vegetation indices to evolving soil water limitation in a crop canopy. *Remote Sens. Environ.* 273, 112957 (2022).
- [5] A. Mac Arthur, I. Robinson, M. Rossini, N. Davis, K. MacDonald, A dual-field-of-view spectrometer system for reflectance and fluorescence measurements (Piccolo Doppio) and correction of etaloning. In *Proceedings of the 5th International Workshop on Remote Sensing of Vegetation Fluorescence* (Paris, France, 2014).
- [6] D. Martini, K. Sakowska, G. Wohlfahrt, J. Pacheco-Labrador, C. van der Tol, A. Porcar-Castell, T.S. Magney, A. Carrara, R. Colombo, T.S. El-Madany, R.

- Gonzalez-Cascon, M. Pilar Martín, T. Julitta, G. Moreno, U. Rascher, M. Reichstein, M. Rossini, M. Migliavacca, Heatwave breaks down the linearity between sun-induced fluorescence and gross primary production. *New Phytol.* (2021).
- [7] K. Nagajothi, H.M. Rajashekara, D.B.S. Sagar, Universal fractal scaling laws for surface water bodies and their zones of influence. *IEEE Geosci Remote Sens Lett* 18(5), 781–785 (2021).
- [8] C. von Hebel, M. Matveeva, E. Verweij, P. Rademske, M.S. Kaufmann, C. Brogi, H. Vereecken, U. Rascher, J. Van der Kur, Understanding Soil and Plant Interaction by Combining Ground-Based Quantitative Electromagnetic Induction and Airborne Hyperspectral Data. *Geophys. Res. Lett.* 45, 3 (2018).
- [9] P. Yang, C. van der Tol, P.-K.-E. Campbell, E.-M. Middleton, Fluorescence Correction Vegetation Index (FCVI): A physically based reflectance index to separate physiological and non-physiological information in far-red sun-induced chlorophyll fluorescence. *Remote Sens. Environ.* 240, 111676 (2020).

## 5 Other contributions of the author since 2019 (only listed)

## 5.1 Co-authored conferences related to the topic of the thesis

- [1] V. Krieger, [...] **J. Quiros-Vargas** [...], et al., “Winter wheat case study in a field in Germany on the suitability of optical remote sensing parameters to track GPP dynamics from sub-diurnal to seasonal scale” in *Proceedings of the European Association of Remote Sensing Laboratories* (EARSeL, Postdam, Germany, 2022).
- [2] B. Siegmann, J. Bendig, **J. Quiros-Vargas**, O. Muller, S. Cogliati, A. Damm, U. Rascher, “Downscaling of Far-red Solar-induced Fluorescence from Canopy to Leaf Level – A Necessary Step to Derive Physiological Information of Plants from Remote Sensing Data,” in *Proceedings of the European Association of Remote Sensing Laboratories* (EARSeL, Postdam, Germany, 2022).
- [3] U. Rascher, K. Acerbon, J. Bendig, J. Krämer, V. Krieger, **J. Quiros-Vargas**, B. Siegmann, O. Muller, "Measuring and Understanding the Dynamics of Solar-Induced Fluorescence (SIF) and its Relation to Photochemical and Non-Photochemical Energy Dissipation - Scaling Leaf Level Regulation to Canopy and Ecosystem Remote Sensing," in *Proceedings of the IEEE International Geoscience and Remote Sensing Symposium* (IGARSS, Brussels, Belgium, 2021), pp. 203-206.
- [4] U. Rascher, [...] **J. Quiros-Vargas** [...], et al., “Measuring and understanding solar-induced fluorescence (SIF) across plant functional types and different scales – Synthesizing three years of FLEX campaign activities to quantitatively understand the dynamics in SIF observations from the leaf to the satel” in *Proceedings of the Living Planet Symposium* (LPS, Bonn, Germany, 2022).
- [5] V. Krieger, [...] **J. Quiros-Vargas** [...], et al., “On the potential of optical remote sensing parameters to track GPP dynamics from sub-diurnal to seasonal scale – A case study in a winter wheat field in Germany” in *Proceedings of the Living Planet Symposium* (LPS, Bonn, Germany, 2022).
- [6] O. Knopf, [...] **J. Quiros-Vargas** [...], et al., “Effects of Free-Air Carbon Dioxide Enrichment (FACE) on Photosynthesis and Growth of Winter Wheat” in *Proceedings of the 7th International Plant Phenotyping Symposium* (IPPS, Wageningen, 2022).

## 5.2 First author and co-authored articles not directly related to the topic of the thesis

- [1] **J. Quiros-Vargas**, T.L. Romanelli, U. Rascher, J. Agüero, Sustainability Performance through Technology Adoption: A Case Study of Land Leveling in a Paddy Field. *Agronomy* 10(11), 1681 (2020).
- [2] **J. Quiros-Vargas**, L.R. Khot, R.T. Peters, A.K. Chandel, B. Molaei, Low Orbiting Satellite and Small UAS-Based High-Resolution Imagery Data to Quantify Crop Lodging: A Case Study in Irrigated Spearmint. *IEEE Geoscience and Remote Sensing Letters* 17(5), 755-759 (2020b).
- [3] **S. Sankaran\***, **J. Quiros-Vargas\***, P.N. Miklas, Unmanned aerial system and satellite-based high resolution imagery for high-throughput phenotyping in dry bean. *Comput. Electron. Agric.* 165, 104965 (2019).
- [4] **J. Quiros-Vargas**, R.J. McGee, G.J. Vandemark, T. Romanelli, S. Sankaran, Field phenotyping using multispectral imaging in pea (*Pisum sativum* L) and chickpea (*Cicer arietinum* L). *Eng. Agric. Environ. Food.* 12(4), 404-413 (2019).
- [5] **J. Quiros-Vargas**, C. Zhang, J.A. Smitchger, R.J. McGee, S. Sankaran, Phenotyping of Plant Biomass and Performance Traits Using Remote Sensing Techniques in Pea (*Pisum sativum*, L.). *Sensors* 19, 2031 (2019).
- [6] B. Molaei, A. Chandel, R.T. Peters, L.R. Khot, **J. Quiros-Vargas**, Investigating lodging in spearmint with overhead sprinklers compared to drag hoses using entropy values from low altitude VIS-imagery. *Inf. Process. Agric.* Vol, pp (2021).
- [7] C. Zhang, S. Serra, **J. Quiros-Vargas**, W. Sangjan, S. Musacchi, S. Sankaran, Non-invasive sensing techniques to phenotype multiple apple tree architectures. *Inf. Process. Agric.* Vol, pp (2021).
- [8] R. Sinha, **J. Quiros-Vargas**, S. Sankaran, L.R. Khot, High resolution aerial photogrammetry based 3D mapping of fruit crop canopies for precision inputs management. *Information Processing in Agriculture. Inf. Process. Agric.* Vol, pp (2021).
- [9] J. Sanaz, S. Sankaran, A. Marzougui, S. Kostick, Y. Si, **J. Quiros-Vargas**, K. Evans, High-Throughput Phenotyping of Fire Blight Disease Symptoms Using Sensing Techniques in Apple. *Front. Plant Sci.* 10, 56 (2019).

## 6 Additional activities (deliverables, talks, proposals and field campaigns)

**Table 1:** Deliverables, talks, proposals and field campaign contributions from 2019 to 2022.

Deliverables
<p><b>For the TRuStEE consortium:</b></p> <ul style="list-style-type: none"> <li>→ Title of deliverable 1: <i>"Small Unmanned Aerial Systems- (sUAS) based platforms and methods developed within the TRuStEE consortium for Solar Induced Chlorophyll fluorescence (SIF) retrieval"</i>.</li> <li>→ Title of deliverable 2: <i>"Dataset of diurnal passive and active Chlorophyll fluorescence measurements on a bean face"</i></li> <li>→ Title of deliverable 3: <i>"Solar Induced Chlorophyll fluorescence (SIF) for Heat Stress Assessment in Three Crops Growing at Different Geophysics-Derived Soil Classes in Two Edaphic Regions"</i>.</li> </ul> <p><b>For ESA:</b> support in the Flexsense 2018 and 2019 campaign reports.</p> <p><b>For Photoproxy:</b> contribution on the second and third versions of the project report.</p>
Talks
<p><b>For the 'Svalbard Integrated Arctic Earth Observing System (SIOS) Training course on Hyperspectral Remote Sensing':</b></p> <ul style="list-style-type: none"> <li>→ Title of talk 1: <i>"Vegetation spectroscopy"</i>.</li> <li>→ Title of talk 2: <i>"Up/Down Scaling of FLux-measurements to UAV-, aircraft- and spaceborne-sensors"</i>.</li> <li>→ Title of talk 3: <i>"Spatial relation between airborne-SIF and the water available for plants in the root zone"</i></li> </ul> <p><b>For the 'Del Monte Global Conference on Smart Farming':</b></p> <ul style="list-style-type: none"> <li>→ Title of the talk: <i>"Hyperspectral remote sensing of Sun-induced Chlorophyll fluorescence (SIF)"</i>.</li> </ul>
Proposals
<p><b>Submitted to ESA</b> for the acquisition of high resolution (sub m) satellite imagery [accepted]</p> <ul style="list-style-type: none"> <li>→ Title of the PROPOSAL: <i>"Understanding the optimal pixel-size to downscale satellite coarse-resolution products"</i>.</li> </ul> <p><b>Submitted to NASA</b> to participate in the 'Summer School on Satellite Observations and Climate Models' [rejected]</p> <ul style="list-style-type: none"> <li>→ Title of the PROPOSAL: <i>"Satellite-based vegetation functioning assessment for the improvement of climate models"</i>.</li> </ul>
Field campaigns support
<ul style="list-style-type: none"> <li>→ <b>2019:</b> Flexsense HyPlant Campaign.</li> <li>→ <b>2020:</b> IBG-2 stakeholder HyPlant Campaign.</li> <li>→ <b>2021:</b> Land surface Interactions with the Atmosphere over the Iberian Semi-arid Environment (LIAISE).</li> <li>→ <b>2022:</b> Cassava Source-Sink project.</li> </ul>